THE UNIVERSITY OF
WARWICK

A Generalised Approach to Active Pedestrian Safety Testing

by

Igor Doric

A Doctoral Thesis
submitted in partial fulfilment of the
requirements for the award of

Doctor of Philosophy

of the University of Warwick
Department: Warwick Manufacturing Group (WMG)

August 2017

Contents

Acknowledgements ii

Declaration iii

Abstract v

List of Figure vi

List of Table vii

1. Introduction 1

1.1. Motivation 1

1.2. Research Objective 3

2. Literature 6

2.1. Introduction 6

2.2. Pedestrian Protection Systems 6

2.3. Automotive Sensors 8

2.4. Testing 13

2.5. Characteristic Features of a Pedestrian 18

2.5.1. Anthropometric Measures and Joint Range of Motion 18

2.5.2. Crossing Behaviour (Macroscopic Motion) 20

2.6. Objectives for a Novel Active Pedestrian Safety Test System 22

3. Research on Pedestrian Kinematics (Microscopic Motion) 24

3.1. Introduction 24

3.2. Group 1 - Continuous Motion Pattern 25

3.3. Group 2 - Gait Transitions 27

3.4. Group 3 - Direction Transitions 28

3.5. Group 4 - Combined Transitions 29

3.6. Conclusion 30

4. Test System Approach **35**
4.1. Introduction . . . 35
4.2. Positioning Apparatus . . . 36
4.3. Pedestrian Dummy Device . . . 40
4.3.1. Necessary Degrees Of Freedom . . . 40
4.3.2. Comparison of Drive Principles . . . 41
4.3.3. Mechatronic Setup and Modeling . . . 43
4.3.4. Control . . . 50
4.3.5. Conclusion . . . 53

5. Test System Optimisation **55**
5.1. Introduction . . . 55
5.2. Usability and Robustness . . . 57
5.3. Shape Design and Variation . . . 63
5.4. Replication of Thermal and Radar Signature . . . 65
5.5. Conclusion . . . 67

6. Consideration of Athmospheric Disturbances **69**
6.1. Introduction . . . 69
6.2. Influence on Automotive Sensors . . . 70
6.3. Conclusion . . . 74

7. Consideration of Natural Human Behaviour **75**
7.1. Introduction . . . 75
7.2. Technical Design . . . 76
7.3. Conclusion . . . 77

8. Generalised Active Pedestrian Safety Test Methodology **80**
8.1. Introduction . . . 80
8.2. Active Pedestrian Safety Test Methodology . . . 81
8.3. Conclusion . . . 84

9. Integrated Test Approach **86**
9.1. Introduction . . . 86
9.2. Combination of Virtual and Indoor Tests . . . 87
9.3. Conclusion . . . 93

10. Conclusions and Recommendations for Further Work **94**
10.1. Scientific Contributions 94
10.2. Recommendations for Further Work 99

Appendix **101**
A. List of IEEE Journal Publications 101
B. List of Conference Publications (Peer Reviewed) 102
C. List of Conference Presentations 104
D. List of Automotive Patents 105

References **106**

Acknowledgements

The author wishes to thank:

Professor Robert Harrison for his guidance and supervision.

Dr Emma Rushforth and Professor Tony McNally for their helpful feedback.

Dr Stewart Birrell and Professor Hermann Steffan for their valuable comments and discussions.

Professor Thomas Brandmeier for his trust, support and encouragement.

Mr Peter Mayer, Mr Andreas Reitberger, Mr Sebastian Wittmann, Mr Tran Duy Giap and Mr Sinan Hasirlioglu for their technical assistance, interest and friendship.

Ms Amela Dizdarevic for the support and motivation.

Marlin for the countless inspiring walks and runs together.

My parents, sister and grandparents. Thank you for making me who I am today.

Declaration I

I declare that this thesis was composed by myself, that the work contained herein is my own except where stated otherwise in the text, by reference or acknowledgement, and that this thesis has not been submitted for a degree at another university.

Declaration II

I am proud to declare that parts of this thesis have already been published in the *IEEE Transactions on Intelligent Transportation Systems*, which is based on google scholar, currently the world leading scientific journal in the area of Transportation:

I. Doric, A. Reitberger, S. Wittmann, R. Harrison and T. Brandmeier, *A Novel Approach for the Test of Active Pedestrian Safety Systems*, in IEEE Transactions on Intelligent Transportation Systems, doi: 10.1109/TITS.2016.2606439, http://ieeexplore.ieee.org/document/7581089/, © 2017 IEEE

Abstract

Active pedestrian safety systems can help to significantly increase pedestrian road safety, but must be tested very carefully before used in series application. Since there is usually a very small amount of time to prevent the collision, the activation of an emergency brake is always a critical decision. On the other hand, of course, false triggerings must be prevented.

Aiming to increase pedestrian and vehicle safety, this thesis presents a novel approach for the test of active pedestrian safety systems.

From the question "What is needed to test and compare future active pedestrian safety systems?" are resulting the following questions:

1. What are the significant characteristics of real pedestrians?
2. How can this features be mapped to a test system?

This thesis presents characteristic features of pedestrians from the perspective of automotive surround sensors and introduces a novel test system approach including a realistic pedestrian dummy which is able to replicate those characteristics. Furthermore it introduces a novel active pedestrian safety test methodology, based on the variation of target characteristics, environmental conditions and driver behaviour.

The proposed pedestrian dummy was set up in real size and tested on the test track in vehicle tests. A video of the described test and the novel pedestrian dummy can be seen here: `https://youtu.be/eF5IkqsknBE`

List of Figure

1.1. Replication r of the features of a pedestrian B to a dummy C under the condition of identical ADAS significant characteristics A [10] © 2017 IEEE. 4

2.1. Simulated pedestrian AEB scenario in IPG CarMaker 6.0.1. 8
2.2. Pedestrian detection system with emergency braking tested by the ADAC with a stuntman, photo: ADAC e.V. [37]. 15
2.3. Rotatable bridge system. 15
2.4. Overrunable platform robot beside test vehicle. 15
2.5. Current test system design: (a) portal rig, (b) moveable platform, (c) pulled platform [10] © 2017 IEEE. 16
2.6. Phases of crossing the street: (a) walking to the curb: curb can be reached from various directions, (b) waiting at the curb: decision about crossing speed is made; gap acceptance determines start of crossing, (c) crossing the street: various crossing pattern (1-5) [10] © 2017 IEEE. 21

3.1. Definition of specific groups of motion pattern and transitions for research on indicators for path prediction. Group 1: a) continuous walking, b) continuous running; Group 2: c) standing - walking - running - standing, d) standing - running - walking - standing; Group 3: e) walking 90°, f) walking 45°, g) running 90°, h) running 45°; Group 4: i) walking - running 90°, j) walking - running 45°, k) running - walking 90°, l) running - walking 45° [10] © 2017 IEEE. 26
3.2. Definition of the coordinate system [10] © 2017 IEEE. 27
3.3. Representative sensor data during continuous locomotion [10] © 2017 IEEE. 31
3.4. Representative sensor data during gait transitions C1, C2 and C3 [10] © 2017 IEEE. 32

3.5. Representative sensor data during gait transitions D1, D2 and D3 [10] © 2017 IEEE. 33
3.6. Representative sensor data of a test person during direction transition G: running 90° [10] © 2017 IEEE. 33
3.7. Representative sensor data of a test person during combined transition I:walking to running 90° and combined transition K: running to walking 90° [10] © 2017 IEEE. 34

4.1. Concepts for the positioning apparatus: (a) basic model, (b) advanced model [10] © 2017 IEEE. 37
4.2. Model of the positioning apparatus installed on a test track (construction: MESSRING Systembau MSG GmbH) [10] © 2017 IEEE. . 39
4.3. Simplified models of relevant DOF: (a) basic requirement for human locomotion: 4 + 6 DOF, (b) additional consideration of arm motion and orientation of the head 9 + 6 DOF, (c) replication of complex motion pattern: 21 + 6 DOF [10] © 2017 IEEE. 41
4.4. Antagonistic muscle setup for the actuation of one DOF [10] © 2017 IEEE. 44
4.5. Relation between $F_{PAM1,2}$, $P_{1,2}$, $\varepsilon_{1,2}$ and ϑ in antagonistic configuration [10] © 2017 IEEE. 45
4.6. Functional principle of a McKibben PAM: (a) relaxed, (b) inflated [10] © 2017 IEEE. 45
4.7. Comparison between the ideal model $F_{PAM,ideal}$ and measured values; Validation of $F_{PAM,real}$ at constant pressure of 300 kPa [10] © 2017 IEEE. 48
4.8. Preprocessing of motion capture data to joint angles per robot joint per time and pressure data per muscle per time. 48
4.9. Real time control of the Pedestrian Dummy Device. 49
4.10. Structure of the fuzzy control circuit for PAM j of joint i [10] © 2017 IEEE. 49
4.11. Validation of the fuzzy control algorithm - phase 1: initialisation; phase 2: smooth step from 0 to 60 degree; phase 3: keeping position [10] © 2017 IEEE. 52
4.12. Skeleton and muscle apparatus of the Pedestrian Dummy Device (head: Human Solutions GmbH / RAMSIS model; joints: igus®robolink®) [10] © 2016 IEEE. 54

4.13. Photo of the skeleton and muscle apparatus of the Pedestrian Dummy Device: (a) front perspective static, (b) side perspective static, (c) side perspective running, (d) side/back perspective static [10] © 2017 IEEE. 54

5.1. Modular concept of the 10D Pedestrian Dummy Device divided into its main components. 58
5.2. Upper part of the 10D torso a) front perspective, b) 45° perspective, c) 90° perspective. 59
5.3. Lower part of the 10D torso a) front perspective, b) 45° perspective, c) 90° perspective. 59
5.4. Arm and leg units of the 10D Pedestrian Dummy Device a) right arm front perspective, b) right arm 45° perspective, c) right arm 90° perspective, d) right leg front perspective, b) right leg 45° perspective, c) right leg 90° perspective. 60
5.5. Right foot model of the 10D Pedestrian Dummy Device a) front perspective, b) 45° perspective, c) 90° perspective. 61
5.6. Perspective and three side view of the butterfly shaped connecting component with predetermined breaking point. 62
5.7. 3D scanned body of human test subject. 63
5.8. Shape of the test subject integrated in the head part of the dummy. . 64
5.9. Technical concept for thermal and radar signature variation [75]. . . . 66
5.10. 10D Pedestrian Dummy Device mounted on an overrunable platform robot. 67

6.1. Radar cross section of a static EVT depending on the number of activated rain layers [77] © 2016 IEEE. 71
6.2. Relative intensity of a laser signal depending on the number of activated rain layers [77] © 2016 IEEE. 72
6.3. Histogram of images of a static EVT depending on the number of activated rain layers [77] © 2016 IEEE. 73

7.1. Technical design of the developed Pedestrian Simulator. 78
7.2. Pedestrian Simulator ego perspective [80]. 79
7.3. Birdview of the virtual scenario. 79

8.1. Generalised active pedestrian safety test methodology. 83

9.1. Combination of recorded motion capture trajectories to one motion tree. 88
9.2. Possible combination of motion trees. 88
9.3. Combination of extended motion trees to a more complex motion sequence. 89
9.4. Combination of extended motion trees considering standing rotation. 90
9.5. Combination of extended motion trees considering a variable path length of motion capture recordings and variation of waiting times. . 91
9.6. Combination of virtual variation of relevant parameters and reproducible full vehicle indoor tests. 92

10.1. Self training algorithm in virtual AEB training considering variation of target characteristics and environmental conditions. 100

List of Table

2.1. Overview on key sensor systems used for pedestrian detection including the functional principle and detectable target characteristics [18], [19], [20], [21]. Table published in [10] © 2017 IEEE 10
2.2. Anthropometric data of adult men [40].
Table published in [10] © 2017 IEEE 18
2.3. Degrees of freedom and ranges of motion of human joints [41].
Table published in [10] © 2017 IEEE 19

4.1. Survey and evaluation of drive concepts for a pedestrian dummy.
Evaluation: + positive, o neutral, - negative.
Table published in [10] © 2017 IEEE 42

1. Introduction

The WHO global status report on road safety indicates that 22 percent of all traffic fatalities worldwide are pedestrians [1]. Supporting technologies, such as active and passive pedestrian safety systems, can help to reduce the total number of those fatalities. Passive systems, like a reversible pop-up hood [2] or approaches based on a pedestrian airbag [3], can reduce the severity of the injury but do not prevent the collision itself. Active systems, like an Autonomous Emergency Brake (AEB), can detect critical driving situations and assist the driver in order to prevent an imminent collision. However, the activation of an AEB is a critical driving decisions and must be tested very responsibly with a corresponding test system.

1.1. Motivation

Advanced Driver Assistance Systems (ADAS) can help to prevent accidents involving vulnerable road users. According to [4] there are two main reasons for pedestrian accidents regarding the driver. The first one is 'No action,' the second one 'Late action'. Forward-looking safety systems, like Pedestrian Detection Systems (PDS) can support the driver in those critical situations. If a pedestrian is detected by the PDS and the situation is classified as critical an accident can be prevented by a simple warning or, if the driver does not respond to the warning, by the activation of an AEB.

Since 2009 pedestrian protection is an evaluation criteria in the rating of the European New Car Assessment Programme (Euro NCAP). Until 2015 only passive pedestrian protection systems were rated. However passive systems can only lower the consequences of an accident but not prevent the collision. Consequently from 2016 first test scenarios for AEB systems for pedestrians are part of the rating. Due to this progress, it can be expected that in near future also the test of more complex

pedestrian scenarios will become part of the rating and relevant in order to achieve the full NCAP rating score.

Based on the 2017 Euro NCAP test protocol for pedestrian AEB systems, currently the following pedestrian scenarios are defined:

- CPFA-50: In this scenario, an adult pedestrian runs from the farside in front of an approaching vehicle under test. The crossing direction of the pedestrian is 90° to the vehicle driving direction. If the vehicle under test applies no braking, the collision point is at 50% of the vehicle width. CPFA-50 is the abbreviation for Car-to-Pedestrian Farside Adult 50%. [5]
- CPNA-25 and CPNA-75: In this scenario, an adult pedestrian walks from the nearside in front of an approaching vehicle under test. The crossing direction of the pedestrian is 90° to the vehicle driving direction. If the vehicle under test applies no braking, the collision point is at 25%, respectively at 75% of the vehicle width. CPNA-25 and CPNA-75 are the abbreviations for Car-to-Pedestrian Nearside Adult 50%, respectively Car-to-Pedestrian Nearside Adult 75%. [5]
- CPNC-50: In this scenario, a child pedestrian runs from behind a parked vehicle from the nearside in front of an approaching vehicle under test. The crossing direction of the child pedestrian is 90° to the vehicle driving direction. If the vehicle under test applies no braking, the collision point is at 50%, of the vehicle width. CPNC-50 is the abbreviations for Car-to-Pedestrian Nearside Child 50%. [5]
- CPLA-25 and CPLA-50: In this scenario, an adult pedestrian walks longitudinal in the same direction of the vehicle driving direction. If the vehicle under test applies no braking, the collision point is at 25%, respectively at 50% of the vehicle width. CPLA-25 and CPLA-50 are the abbreviations for Car-to-Pedestrian Longitudinal Adult 25%, respectively Car-to-Pedestrian Longitudinal Adult 50%. [5]

Based on the test protocol the tests must be performed, beside further requirements, at dry weather conditions and temperatures between 5°C and 40°C, at wind speeds below 10 m/s and natural homogenous illumination above 2000 lux. [5]

For the tests the Euro NCAP Pedestrian Target and the Euro NCAP Child Target are used. Both are defined wearing a black long sleeved t-shirt and blue trousers and

have static arms and articulated legs. For the articulation of the legs, one electric motor per body side is integrated in the hips. The motion of the lower legs is passive oscillating, based on the motion of the hips. Both targets provide defined visible, infrared and radar properties. [5], [6]

Standardised pedestrian scenarios and defined properties of the target are necessary for standardised testing. However, for non-standard and development-related tests of new vehicle prototypes, a test system and pedestrian target providing further variation of the pedestrian scenarios and target characteristics are required. Especially for the test of advanced detection algorithm approaches, considering pre-indicators and pedestrian path prediction, like the viewing direction of the pedestrian or the chest angle inclination, as can be seen in [7], a test system which enables the replication of natural human velocity and direction transitions and a variation of significant pedestrian characteristics is required. Furthermore, based on studies in [8], only 35% of the pedestrian cross the street in a linear pattern, while 65% use a more complex crossing pattern. Consequently, more complex pedestrian crossing pattern, including velocity and direction changes, should also be considered in the development-related test of new vehicle prototypes.

Furthermore, especially in the context of autonomous driving, it can be expectet that also pedestrian to vehicle interaction in complex traffic scenarios will be tested in non-standard tests using realistic pedestrian dummies in future.

The main focus of this research is the development of a novel test system for active pedestrian safety, which enables the test of complex pedestrian scenarios, considering the variation of relevant pedestrian characteristics.

1.2. Research Objective

In active pedestrian safety testing, pedestrian characteristics are usually replicated by a pedestrian dummy which should be visible for the automotive sensor systems, while further test equipment should be invisible for the vehicle sensors [9]. The expected results of this research are the specification of ADAS significant characteristics of a real pedestrian and a concept on how this characteristics can be mapped to a realistic test system. This test system should replicate a human being and enable the reproducible test and comparison of advanced pedestrian detection systems, considering pre-indicators and human path prediction.

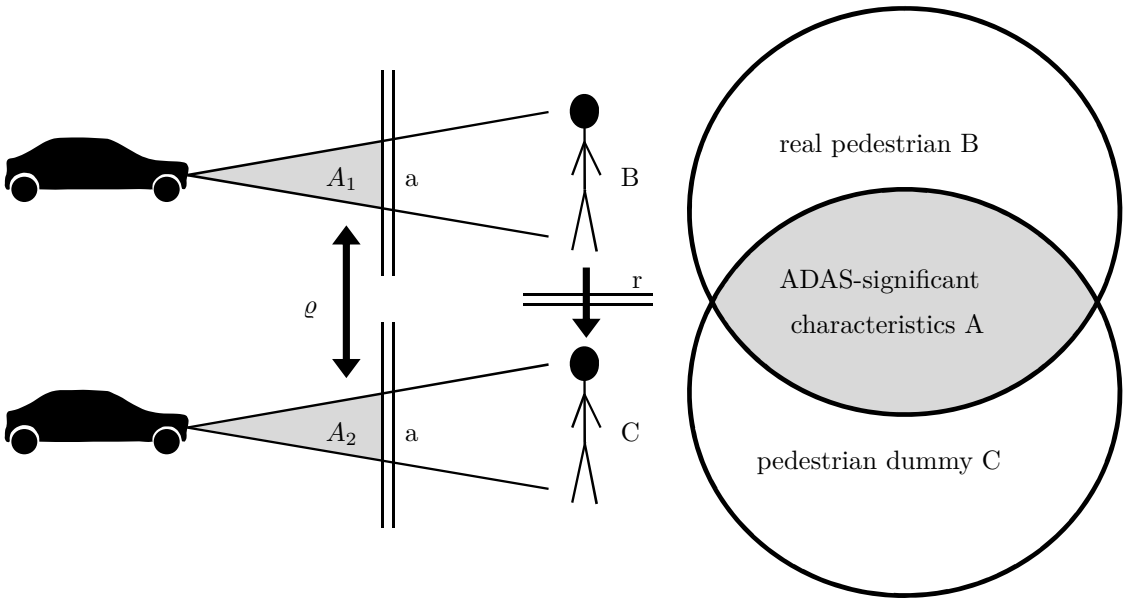

Fig. 1.1.: Replication r of the features of a pedestrian B to a dummy C under the condition of identical ADAS significant characteristics A [10] © 2017 IEEE.

Focus of this research is the replication r of human features B to a pedestrian dummy C under the condition of identical ADAS sensor signals A_1 and A_2. This research intention is visualized by Fig. 1.1.

$$A_1 = a(B) \tag{1.1}$$

$$A_2 = a(C) \tag{1.2}$$

The ADAS filter function of the vehicles sensor system is represented by a. A_1 represents the signal of ADAS significant characteristics of a real pedestrian B. A_2 stands for the corresponding signal of ADAS characteristics of a pedestrian dummy C. This relation is represented by Eq. 1.1 and 1.2.

$$\varrho = corr(A_1, A_2) \tag{1.3}$$

The correlation of signal A_1 and A_2 is represented by ϱ in Eq. 1.3. For ϱ is equal to 1 signal A_1 is identical to signal A_2.

$$C = r\left(B\right)\big|_{\varrho=1+\varepsilon} \tag{1.4}$$

Equation 1.4 summarises the research approach of Fig. 1.1 mathematically. The intention of this research is to create a novel test system C with a minimized ε, while ε represents the deviation from an ideal test system where ϱ is 1.

$$\varepsilon = corr(A_1, A_2) - 1 \tag{1.5}$$

The determination of ε, based on Eq. 1.5, could be used in future work to compare a novel test system approach with real pedestrians and existing test systems.

2. Literature

2.1. Introduction

Pedestrian fatalities have a clear maximum during the winter months [11]. Possible root causes are early darkness combined with bad weather and visibility conditions. Predictive driver assistance systems are able to support the driver in this case, but need to be further developed. The goal is to reduce pedestrian accidents to a minimum. One step to achieve this, is to improve the test systems for the pedestrian detection.

This chapter gives an overview on pedestrian protection systems, automotive sensors, the corresponding test systems and characteristic features of a pedestrian, like anthropometric measures, joint range of motion and pedestrian crossing behaviour.

2.2. Pedestrian Protection Systems

Pedestrian Protection Systems can be divided into active and passive systems. Passive pedestrian protection systems can mitigate the consequences of the collision, by e.g. the activation of a pedestrian airbag, as can be seen in [3]. Another example can be seen in [2], where a reversible pop-up hood is presented, which can help to protect the head of pedestrians, where the deformation space beneath the hood is increased by lifting it up. Of course this procedure is very time-critical. In [12] an optimised design for the inner panel of the hood is shown which can lower the stiffness of the collision area.

Active pedestrian safety systems focus on the predictive pedestrian detection and collision avoidance, by e.g. activation of a pedestrian AEB. If the AEB is activated in time, the pedestrian collision can be avoided entirely. In order to achieve this,

systems for pedestrian detection are required, which are based on different sensor approaches, as for example camera, automotive radar or lidar.

Of course also other approaches, like the optimisation of road layout designs, by reducing the amount of pedestrian to vehicle conflict situations, could help to reduce pedestrian fatalities. However, in existing and historical grown cities, the correction of all pedestrian to vehicle conflict potential would be very complex and the construction work would be very expensive and time consuming.

Other technological approaches, like V2X based pedestrian warnings, as shown in [13], could also help to reduce pedestrian fatalities in future.

However, since pedestrian AEB tests were recently considered in the Euro NCAP protocol, it can be expected that pedestrian AEB systems will incrementally be further developed by the vehicle manufacturers and achieve a wide spread on the global market in near future.

Since the activation of an pedestrian AEB is usually a very time-critical decision, these systems must operate fast and reliable and consequently be tested in detail using an adequate test system during development. Therefore, this thesis is mainly focused on the test of active pedestrian safety systems.

Fig. 2.1 shows the top view, side view and perspective of a simulated pedestrian AEB scenario in IPG CarMaker, where an adult pedestrian is running in front of an approaching vehicle. As illustrated in the figure, the simulated vehicle is equipped with two object detection sensors, which is a camera sensor and a front radar sensor. The field of view of the camera sensor is represented by the yellow area, while the field of view of the front radar is represented by the light blue area.

In this example, the field of view of the camera sensor is 45 degree in horizontal direction and 45 degree in vertical direction, while the field of view of the radar sensor in this example is 16 degree in horizontal direction and 10 degree in vertical direction. It must be considered, that this are only example values, as set by default in this simulation example, and that the sensor field of view and also the sensor resulution can vary, depending on the sensor manufacturer and used sensor type.

In the following section, different automotive sensor approaches, which are used for the activation of pedestrian AEB systems are considered.

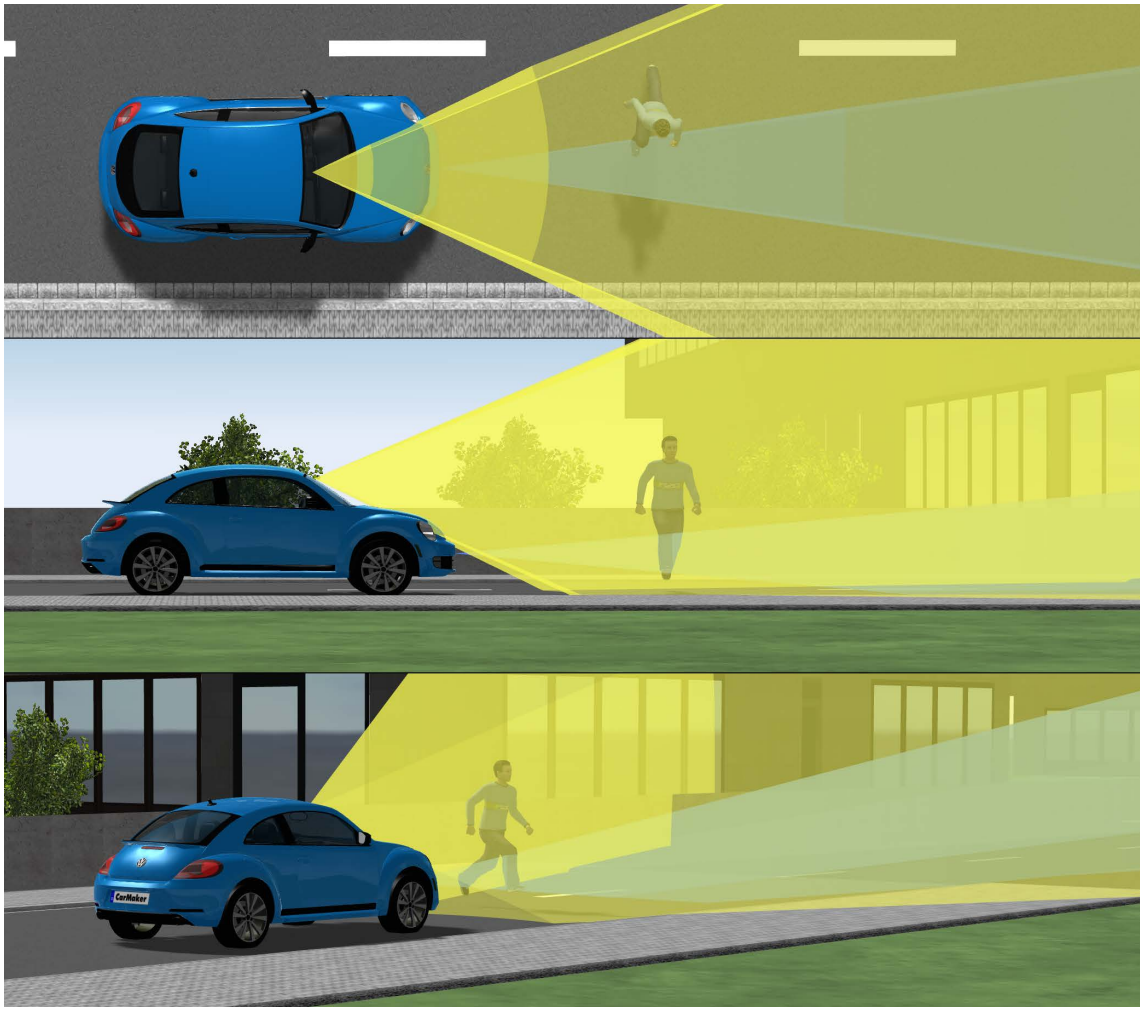

Fig. 2.1.: Simulated pedestrian AEB scenario in IPG CarMaker 6.0.1.

2.3. Automotive Sensors

Pedestrian detection is based on sensor systems, which measure various physical characteristics of the target. For the development of a novel test system it is mandatory to know which sensor systems are commonly used and which physical characteristics can be measured by those systems. Table 2.1, was published in [10], and shows sensor systems used in pedestrian detection, their technical detection principle and the detectable target characteristics.

While sensors based on a passive principle, like mono cameras, stereo cameras and far infrared (FIR) systems consist only of a reveicing unit, sensors based on an active principle, like radar, lidar, near infrared (NIR) systems and photonic mixing devices (PMD) are based on a transmitting and a receiving unit, which measures the

electromagnetic waves which are reflected by the object. A pedestrian dummy must provide the same reflecting, characteristics as a real pedestrian, and in addition also offer the possibility to increase or decrease the reflecting properties between test runs, in order to test the functional borders of the AEB system.

In order to ensure robustness and reliability, multiple sensor systems based on different technical principles can be combined for pedestrian detection [14]. An example for this data fusion for pedestrian detection is shown in [15], where passive far infrared and radar is combined to one multi sensor system. Common combinations are image sensors combined with distance sensors, like radar or lidar [16], [17]. The advantage of this combinations is, that image sensors provide visual information for image processing of the environment, while radar or lidar provide the distance information. If for example a pedestrian is detected based on image processing, the distance information for the area in which the pedestrian was detected can be extracted from the radar or lidar sensor. Consequently, with image processing and distance information combined, a detailed model of the vehicle environment can be generated. Disadvantages of multi sensor systems are the higher costs and the higher amount of data processing.

The shape and dimension of objects can theoretically by determined by every sensor principle depending on the sensor resolution. Distance information can be gathered by measuring of signal time between sending and receiving or by stereoscopic arrangements. The temperature of an object can be measured by a FIR sensor that captures the emitted electromagnetic radiation in the far infrared spectrum with a wavelength of 8 to 14 μm [22]. For radar based systems, also the material of the target is relevant. The ratio between the transmitted and received energy is defined as the radar cross section (RCS) of an object [23]. Generally, good electrical conductors own a high re-radiation rate of radar waves [24].

In summary, Table 2.1, shows that a wide range of sensor systems based on different technical principles and focusing on different target characteristics are used for pedestrian detection. In order to design a novel test system and advanced pedestrian dummy the consideration of those characteristics is a mandatory requirement.

Enzweiler and Gavrila show in [25] a detailed overview of mono camera systems. They demonstrate that the tested systems tend to make similar mistakes, as typical false positives occur in regions with vertical structures. It is demonstrated that stereo compared to mono camera systems have a reduced false positive rate by a factor

Table 2.1.: Overview on key sensor systems used for pedestrian detection including the functional principle and detectable target characteristics [18], [19], [20], [21]. Table published in [10] © 2017 IEEE

Sensor	**Principle**	**Target characteristics**
Mono Camera	Captures visible light reflected by objects	Dimension, clothing, shape
Stereo Camera	Captures visible light reflected by objects; By the second camera distance information are obtained	Dimension, clothing, shape, distance
Far Infrared (FIR)	Captures far infrared electromagnetic waves emitted by objects	Temperature, clothing, dimension, shape
Radar	Transmits electromagnetic waves in the radio frequency range; Measures time between transmission and reception of the radar echo and the radar cross section (RCS)	Material, dimension, surface, shape, distance
Lidar	Transmits laser impulses in the NIR range; Measures time between transmission and reception of laser impulses (distance information)	NIR- reflectivity of surface, dimension, shape, clothing
Near Infrared (NIR)	Transmits near infrared electromagnetic waves; Captures the waves reflected by objects	NIR-reflectivity of surface, clothing, dimension, shape
Photonic Mixing Device (PMD)	Transmits NIR electromagnetic waves; Measures the time of light to obtain distance information for each pixel [21]	Dimension, shape, clothing, surface, distance

of 4-5 [26]. Unfortunately, these vision based systems have similar problems in the pedestrian detection as in the automatic traffic sign detection. The visibility of the objects can be influenced by light conditions, as shown in [27]. The simplest example for the influence of light conditions on camera sensors is the difference of visibility between day and night time, but also during day time the visibility of objects can vary depending on the driving direction and the position of the sun, e.g. when the sensor is blended by the sun.

A sensor system, based on automotive radar, which is robust in all light conditions, is shown in [28]. It detects walking humans by analysing the Doppler spectrum, which is completely different than, for example, the spectrum of a driving car. In [29] the necessary requirements for automotive radar systems, like the field of view, the range or the cycle duration are specified. On the other hand radar has a lower field of view and a lower angular resolution than conventional camera systems, as shown in [30].

Lidar sensors are also used for pedestrian detection. For example [31] shows an approach where a sensor is integrated in the front bumper and can predict in combination with a defined region of no escape an upcoming collision up to 300 ms before the first contact. This allows for instance the already described pop-up hood to lower the consequences of the collision more efficient than contact based systems.

There are also sensor systems in the infrared spectrum used for pedestrian detection, as can be seen in [32]. In general, infrared sensors can be divided in Far Infrared (FIR) and Near Infrared (NIR). While FIR detects the far infrared waves which are emitted by an object, NIR transmits and receives near infrared waves, which are reflected by an object. Consequently, NIR can be used to measure the NIR-reflectivity, while FIR can be used to measure the temperature of an object.

Furthermore, the used algorithms are often focused on different characteristics of a pedestrian. As an example [33] is concentrating on the detection of shoes and legs to detect a pedestrian. A very detailed survey of sensors is shown in [17], where approaches in the visible spectrum, the infrared spectrum and also combinations of different systems like thermal infrared with radar or a mono camera in combination with a lidar is presented.

In summary, there are a lot of different approaches in the area of pedestrian detection. According to [17] currently pedestrian detection lacks well-established databases and benchmarking protocols, which means that it became very hard to compare

different sensor systems and to determine which system in combination with what kind of algorithm is currently the best.

According to the high research activities it can be assumed that in near future advanced detection algorithms in combination with higher resolution sensors are used for pedestrian detection. Also sensor technologies from other research areas could be used. For example, [34] is presenting a system for the remote detection of human vital signs. This radar based technology makes it possible to measure contactless, within a distance of two meters, the heart and breath rate of humans, even if they are wearing a winter jacket. If it would be possible to increase the distance and adapt the technology to moving objects that would mean a new approach in the detection of pedestrians. A probably nearer technology is to predict the behaviour of pedestrians by the automatic analysis of specific indicators. In patent application [7], various pre-indicators are listed, which imply a future change in the speed or direction of a pedestrian. Examples are a modification of the center of gravity, which indicates an acceleration/deceleration or the viewing direction, which could lead to a change of the moving direction.

2.4. Testing

The validation of ADAS functions usually begins with a virtual test. Virtual test approaches like [35] enable tests of safety systems especially during the development. The environment and traffic participants are simulated in scene-based specifications. If, for example, the sensor position changes during the development process, the position of the sensor can be changed easily in the simulation and the test runs can verify if the new sensor position has an influence on the scene based test runs. This procedure helps to achieve high quality algorithms already at early development stage at lower cost.

For ADAS testing, simulation based methods like Model in the Loop (MiL), Software in the Loop (SiL) and Hardware in the Loop (HiL) can be used to test models, the generated algorithms or hardware components, especially during development. However, simulation based approaches usually require detailed models, the used algorithms or for hardware tests expert knowledge of the used communication protocols. Consequently, simulation based methods are most suitable for test driven development and an efficient variation of test parameters, but require sensible data which is usually strictly confidential.

In [36] the 3xD driving simulator was presented, which enables the simulation based test of ADAS and various levels of autonomous driving. The main contribution of the presented approach is, that it enables to drive in any vehicle prototype in the Warwick 3xD driving simulator and test new vehicle functions in a safe simulation environment, while the simulator enables bidirectional interaction between the vehicle prototype and the simulation environment. [36]

Although simulation based approaches can reduce the number of real test runs and improve the quality of algorithms at an early development stage, vehicle tests on the test track can not be replaced completely, because it must be ensured that the used models, algorithms and hardware components also work robust and realiable in an vehicle or vehicle prototype. Also, it would be very difficult to use a virtual approach for the comparison of different systems, because detailed sensor raw data and detection algorithms are needed, which are typically strictly confidential.

Beside pedestrian AEB, also further technological approaches, like V2X based pedestrian warnings, as can be seen for example in [13], have potential for future

application in pedestrian collision avoidance. However, based on the latest consideration of pedestrian AEB in standardised Euro NCAP tests, it can be expected that pedestrian AEB systems will achieve a wide spread and acceptance on the market and will incrementally be further developed in future.

Therefore, this thesis is focused on active pedestrian safety systems and the test of advanced pedestrian detection systems, including pre-indicators and pedestrian path prediction.

In order to test and compare AEB systems, they can be examined at the most outlying interface, which means to test the complete system in a vehicle or vehicle prototype on a test track. As can be seen in Fig. 2.2, a vehicle equipped with a pedestrian AEB, was tested by the General German Automobile Club (ADAC) with a stuntman, wearing protective clothing, and published online in a technical report and video in [37].

Pedestrian dummies, respectively pedestrian targets, can replace this dangerous task. In order to move a pedestrian dummy in front of an approaching test vehicle, the target is usually attached to a bridge system, an overrunable platform robot or a pulled platform.

Fig. 2.3 shows a rotatable bridge system, installed at the DEKRA test track in Klettwitz, moving an attached pedestrian dummy. In order to avoid a possible collision, the bridge system can shoot the dummy upwards into a safe area, which is usually triggered by a light barrier.

Fig. 2.4 shows an ultraflat overrunable platform robot at the CARISSMA test track in Ingolstadt, which can also be used in AEB tests to move a pedestrian dummy in front of an approaching vehicle. These platform robots enable flexible motion on the test track and consequently a wider range of test scenarios compared to linear motion systems.

In order to create a test system for full vehicle test runs with moving dummies, two subsystems are necessary. The first subsystem enables the macroscopic motion within the test area, e.g. moving across the street. The second subsystem is the dummy itself, which is designed to replicate a pedestrian.

Within the EU project AsPeCSS existing pedestrian dummies and their macroscopic motion systems were assessed [19]. Macroscopic motion system enable pedestrian

Fig. 2.2.: Pedestrian detection system with emergency braking tested by the ADAC with a stuntman, photo: ADAC e.V. [37].

Fig. 2.3.: Rotatable bridge system.

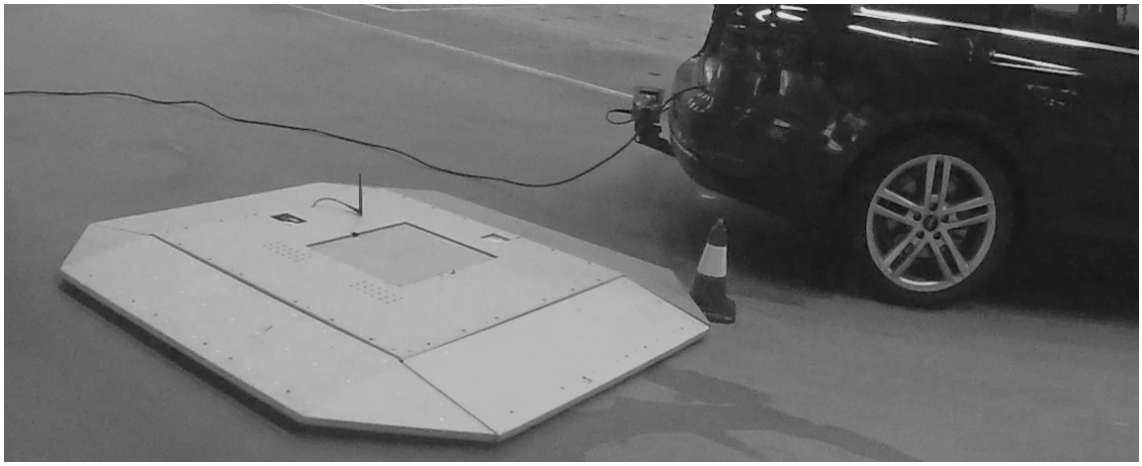

Fig. 2.4.: Overrunable platform robot beside test vehicle.

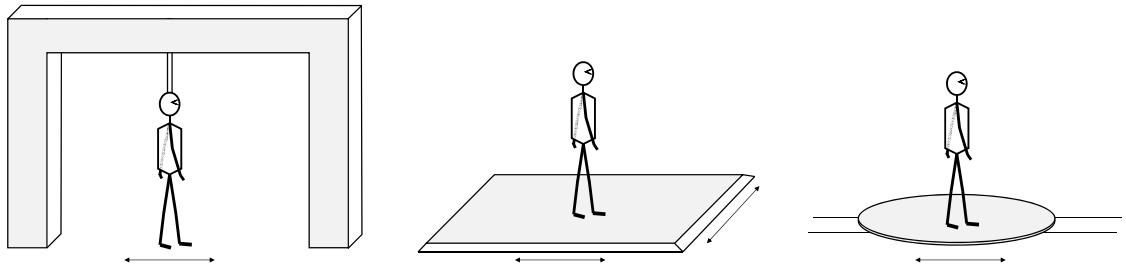

Fig. 2.5.: Current test system design: (a) portal rig, (b) moveable platform, (c) pulled platform [10] © 2017 IEEE.

dummies to move on the road. These systems can be distinguished according to their construction. There are portal rigs, moving platforms and pulled platforms.

Portal rig systems provided by Continental [38], Frontone and 4a engineering enable linear motion of the dummy. An advanced system based on this concept was built in the project "Objective Tests for Forward Looking Pedestrian Crash Avoidance/Mitigation Systems" [39]. Some of the systems provide a test cancel sequence which safes the dummy and the vehicle prototype in case of an incorrect detection. However, they are not able to replicate direction changes.

Movable platforms provided by DSD or TRL are electrical driven platforms. They can be moved manually via remote control or automatically. These systems enable flexible movements and can replicate various scenarios.

4a engineering developed an ultra flat platform which is pulled by a flat belt running over the road. The system is very thin, so it is currently not detected by PMD, and furthermore the system achieves good radar results [19]. Though, only linear motion is possible.

Fig. 2.5 illustrates the concepts of the described systems, where a pedestrian dummy is moved by a portal rig, a movable robot platform, or a pulled plaftorm.

Similar to the macroscopic motion, AsPeCSS also evaluated pedestrian dummies. These can be distinguished regarding their ability to move their limbs. The dummy provided by IDIADA and those of TRL are able to move their feet in order to replicate a walking person. Other dummies, like the vFSS adult and the NHTSA adult are not able to move their limbs. The posture of static dummies was generally positioned in the midstance phase. This posture was defined during the AsPeCSS project. Dummies with no realistic posture could not be detected well by video based systems. [19]

Within the project “Objective Tests for Forward Looking Pedestrian Crash Avoidance/Mitigation Systems“ dummies with joints were developed in order to enable a manual modification of the dummy posture [39].

Furthermore, 4active systems developed an articulated pedestrian dummy with simplified motion of the arms and legs. For the motion of the upper legs, two electric actuators were integrated in the hip of the pedestrian dummy. The lower legs are actuated only passively by the motion of the upper legs.

2.5. Characteristic Features of a Pedestrian

2.5.1. Anthropometric Measures and Joint Range of Motion

For detection, respectively classification of humans, typical measures and proportions of the human body are necessary. In this subsection, an overview on anthropometric measurements of average adult men is given and the ranges of motion (ROM) of human joints are summarised.

Table 2.2 shows the anthropometric data of average adult men in the age group between 18 and 65 and in the age group between 18 and 25 in a percentile of 50 [40].

Table 2.2.: Anthropometric data of adult men [40].
Table published in [10] © 2017 IEEE

age group	**18-65**	**18-25**
shoulder breadth (biacromial)	405	410
shoulder breadth (bideltoid)	480	470
hip breadth	360	355
sitting shoulder height	625	640
chest depth	225	205
body height	1750	1790

Table 2.3 summarises the degrees of freedom (DOF) and ROM of human joints. Finger and toe joints are not considered because of missing relevance for pedestrian detection. In total, 38 DOF are shown in the table.

Table 2.3.: Degrees of freedom and ranges of motion of human joints [41].
Table published in [10] © 2017 IEEE

joint	**DOF**	**motion**	**ROM**
head	3	flexion / extension	65°/ 40°
		lateral flexion left / right	35°/ 35°
		rotation left / right	50°/ 50°
trunk	3	flexion / extension	85°/ 60°
		lateral flexion left / right	40°/ 40°
		rotation left / right	40°/ 40°
shoulder girdle	2x2	elevation / depression	40°/ 10°
		protraction / retraction	30°/ 25°
shoulder	2x3	flexion / extension	170°/ 40°
		abduction / adduction	180°/ 40°
		inward / outward rotation	70°/ 60°
elbow	2x2	flexion / extension	150°/ 10°
		pronation / supination	90°/ 90°
hand	2x2	flexion / extension	80°/ 60°
		radio / ulnar abduction	20°/ 40°
hip	2x3	flexion / extension	140°/ 20°
		abduction / adduction	50°/ 30°
		inward / outward rotation	40°/ 30°
knee	2x2	flexion / extension	150°/ 10°
		inward / outward rotation	10°/ 40°
foot	2x2	flexion / extension	50°/ 30°
		eversion / inversion	30°/ 60°

2.5.2. Crossing Behaviour (Macroscopic Motion)

In this thesis the term macroscopic motion is defined as the variation of a single pedestrians position during the process of crossing a roadway. This process is divided into three phases [8, 42]:

- **Phase 1: Walking to the curb** (Fig. 2.6(a))

  This phase can be described by various pedestrian movement models, for example social force model [43, 44], discrete choice model [45, 46] and cellular automata models [47–49] which are referred as examples in [8]. In general, it must be assumed that a pedestrian can reach the start point of crossing from different directions, as it can be seen in Fig. 2.6(a). The point can be reached parallel, perpendicular and in oblique angles to the driving direction.

- **Phase 2: Waiting at the curb** (Fig. 2.6(b))

  This phase can be described by gap acceptance based models [50, 51]. During this phase, pedestrians wait for a suitable gap to cross and choose their estimated crossing velocity [52]. The decision for crossing the street at unsignalised areas depends on three factors which are near-side traffic gap, pedestrians age and number of pedestrians in a group crossing the street [53].

- **Phase 3: Crossing the street** (Fig. 2.6(c))

  Based on studies in [8] there are five main crossing patterns. In pattern (1), pedestrians walk perpendicularly to the road toward the destination (26%). The pedestrians on pattern (2) walk perpendicularly to the road and then turn to their destination (31%). Pattern (3) describes a way were pedestrians walk directly toward their destination in a specific angle (9%). In pattern (4) pedestrians walk to the middle line, walk along the road and then walk to the destination (16%). The path shown in the last pattern (5) is perpendicular to the road in the start and end point and oblique between them (18%). According to the study most pedestrians cross the street as shown in pattern 2. Only very few pedestrians cross the street linear in a specific angle. Hence, about 35% of the pattern correspond to a linear crossing pattern (pattern 1 and 3), while 65% of the pedestrian cross streets in a more complex pattern.

  The speed of crossing depends on various factors. A field study shows the dependence of speed on age. Older pedestrians (65+) cross streets with an

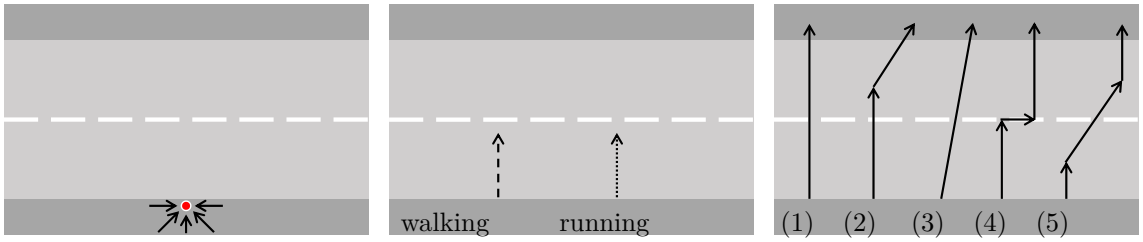

(a) (b) (c)

Fig. 2.6.: Phases of crossing the street: (a) walking to the curb: curb can be reached from various directions, (b) waiting at the curb: decision about crossing speed is made; gap acceptance determines start of crossing, (c) crossing the street: various crossing pattern (1-5) [10] © 2017 IEEE.

average value of 0.97 $\frac{m}{s}$, younger pedestrians (14 to 64 years) in average with 1.25 $\frac{m}{s}$. [54]

The norm value for walking speed, independent of traffic situations is 1.20 to 1.50 $\frac{m}{s}$. The value depends on step length and step frequency. Both are proportional to the walking speed. [55]

It also has to be considered, that in over 12% of all fatal pedestrian accidents the main cause is darting or running into road [56]. Refered to studies in [57] the velocity of walking persons is 1.34 $\frac{m}{s}$, of running persons 5.36 $\frac{m}{s}$ and for a sprinting person 7.7 $\frac{m}{s}$.

2.6. Objectives for a Novel Active Pedestrian Safety Test System

Currently available test systems and pedestrian dummies have only limited suitability for the test of advanced pedestrian detection algorithms, especially focused on pre-indicators and pedestrian path prediction. Therefore, a novel pedestrian dummy and test system approach will be presented in the following chapters, which is focused on the replication of natural human motion pattern and pre-indicators for pedestrian path prediction.

The objectives for the novel pedestrian dummy and test system approach can be summarised as follows:

- Objective 1: The novel pedestrian dummy, developed as part of this research, will have the ability to replicate a dynamic pedestrian and spontaneuously accelerate from standing to running under the consideration of natural human motion pattern and pre-indicators like the chest angle inclination.
  - Darting or running into road is the main cause in over 12% of all fatal pedestrian accidents [56].
  - Advanced pedestrian detection algorithms can detect pre-indicators like the chest angle inclination for pedestrian path prediction [7].
- Objective 2: The novel pedestrian dummy will have the ability to change its walking and running directions and viewing angle of the head.
  - Only 35% of pedestrian cross the street in a linear pattern, while 65% cross streets in a more complex pattern, including direction changes [8].
  - The viewing direction of the head is an indicator for possible direction changes and can be used as pre-indicator for pedestrian path prediction [7].
- Objective 3: The novel pedestrian dummy will have the ability to replicate natural human motion of its arms and legs.
  - The natural motion of the arms and legs can be detected based on radar technology [28].

  - Ground contact of the feet is important for some detection algorithms [33].

- Objective 4: The novel pedestrian dummy will enable a variation of the sensor visibility between test runs.
  - In order to test the functional borders of the pedestrian AEB systems, a variation of the sensor visibility between test runs must be considered.
  - Generally, good electrical conductors provide a high re-radiation rate of radar waves [24].
  - To provide a low inital radar signature, the amount of metal components will be a design criteria for the dummy material and for the actuator concept of the dummy.

This objectives will enable non-standard tests during development in order to test and optimise the functional borders of new detection algorithm approaches and pedestrian AEB systems. Furthermore, providing natural human motion of the arms and legs and head rotation, the novel pedestrian dummy will enable the test of pedestrian to vehicle interaction, especially in the context of autonomous driving.

3. Research on Pedestrian Kinematics (Microscopic Motion)

3.1. Introduction

This chapter shows the analysis of pedestrian kinematics during continuous walking, continuous running, velocity transitions, direction transitions and combined velocity and direction transitions. The main focus of this chapter is to prove that pre-indicators like the chest angle modification or the variation of pedestrian leg frequencies and amplitudes can indicate a near-future velocity or direction transition of a pedestrian.

Consequently, this significant pedestrian characteristics can be used for pedestrian path prediction and advanced pedestrian detection algorithms, as was also proposed in [7].

In order to test advanced detection algorithms considering pre-indicators, features like the realistic and controlled variation of leg frequencies and a realistic modification of the chest angle must also be considered in the corresponding test systems. Hence, the motion capture data recorded in this chapter is also used as input for the Pedestrian Dummy Device presented in Ch. 4 and Ch. 5.

In order to replicate pedestrian kinematics they need to be studied in detail. In the following the term microscopic motion describes the variation of a pedestrians arm and leg motion and frequency, the modification of a pedestrians center of gravity, inclination angle of the body and the orientation of a pedestrians head. This kind of microscopic motion pattern are important indicators for the prediction of a pedestrians near future behaviour and crossing path [7].

In order to understand this microscopic motion pattern and their indication for a pedestrians macroscopic motion a study was performed with several subjects. In this study four groups of motion pattern are distinguished. First one are continuous motion pattern (continuous walking, continuous running). Second are velocity transitions (e.g. transition between walking and running). Third one are direction transitions (e.g. 90° and 45° transitions). The last and most complex are combined direction and velocity transitions.

Wearing a motion capture system based on inertial measurement units, the subjects had to perform a set of sequential movements. To ensure the repeatability and the equality between the experimental procedures and the different subjects, specific trajectories were defined. Fig. 3.1 shows the top view of the defined trajectories, while Fig. 3.2 defines the measured roll, pitch, and yaw angles.

The motion capture data was recorded using a Xsens motion capture system based on small and leightweight inertial sensors which were applied to the test subjects. The sensor measurements were compared between ten male test subjects, aged between 21 and 30. The figures in this section show representative sensor data of a single test subject during continuous walking, continuous running, velocity transitions, direction transitions and combined transitions.

The key sensor values analysed in this chapter are:

- the pitch angle of the upper leg sensors, representing hip flexion/extension,
- the pitch angle of the lower leg sensors, representing knee flexion/extension,
- the pitch angle of the chest sensor, representing trunk flexion/extension,
- the yaw angle of the chest sensor, representing trunk rotation left/right,
- the roll angle of the chest sensor, representing trunk abduction/adduction.

3.2. Group 1 - Continuous Motion Pattern

Focus of this section is the investigation of microscopic motion during continuous locomotion. First the subjects were asked to walk (Fig. 3.1(a)) and then to run (Fig. 3.1(b)) a straight line.

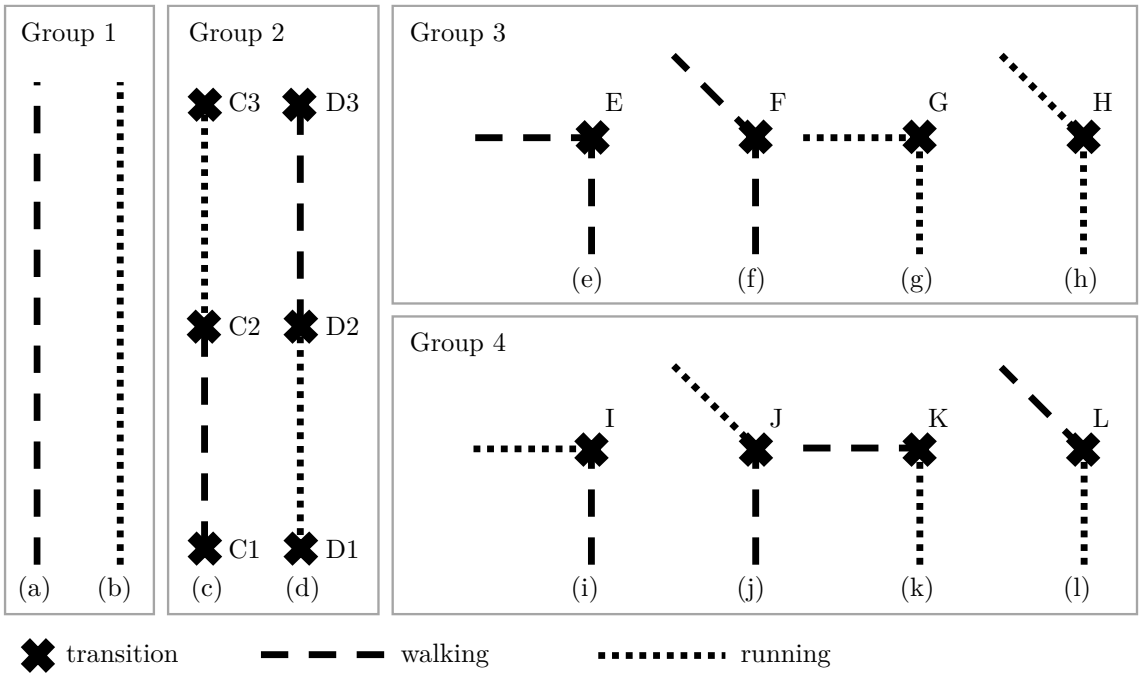

Fig. 3.1.: Definition of specific groups of motion pattern and transitions for research on indicators for path prediction. Group 1: a) continuous walking, b) continuous running; Group 2: c) standing - walking - running - standing, d) standing - running - walking - standing; Group 3: e) walking 90°, f) walking 45°, g) running 90°, h) running 45°; Group 4: i) walking - running 90°, j) walking - running 45°, k) running - walking 90°, l) running - walking 45° [10] © 2017 IEEE.

Walking is defined as the process of locomotion where at least one foot is always in contact with the ground [58]. In contrast during running both feet are up to 80% of the time in no contact with the ground [59].

Fig. 3.3 shows representative motion data of a test person during continuous locomotion. The left column of the figure shows the pitch angles of the upper legs, lower legs and the knees and the yaw angle of the chest during continuous walking. The right column represents the corresponding values during continuous running. The recorded extremities move periodically with a frequency of 1.17 Hz while walking and with a frequency of 1.66 Hz while running. One period is divided into a stance phase and a swing phase. During the change between stance and swing phase the knee angle is at its minimum. During the stance phase, the knee angle moves through his smaller maximum, while during the swing phase the knee angle reaches its maximum value. In contrast to walking, during running the swing phase is clearly longer than the stance phase, the maximum knee angle is significantly higher and the sinus like oscillation of the yaw angle of the chest is more intensive during running.

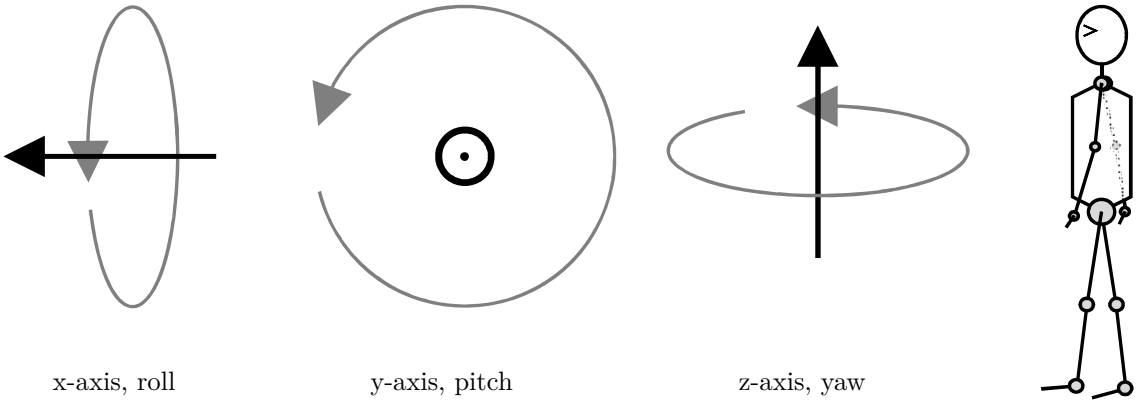

Fig. 3.2.: Definition of the coordinate system [10] © 2017 IEEE.

3.3. Group 2 - Gait Transitions

The second group of motion pattern are gait transitions between standing, walking and running in all possible combinations. In order to understand this kind of transitions the test subjects were asked to perform defined sequences of motion. Following transitions are included in the trajectory shown in Fig. 3.1(c):

C1: standing to walking

C2: walking to running

C3: running to standing

The trajectory shown in Fig. 3.1(d) includes:

D1: standing to running

D2: running to walking

D3: walking to standing

Fig. 3.4 and Fig. 3.5 show the motion data of the recorded gait transitions C1-C3 and D1-D3. Considered body parts are the upper legs, lower legs and the pitch angle of the chest. The chest pitch angle indicates the modification of the center of gravity during gait transitions. This modification can be an important indicator for pedestrian path prediction algorithms. The most significant modification of the chest angle in direction of locomotion can be measured during the gait transition from standing to running (D1). The modification of the chest pitch angle during

the gait transition from walking to running (D2) is smaller, but still significant and bigger than the modification during the transition from standing to walking (D3).

While the chest pitch angle modification during the transition from walking to standing (D3) is not significant, a strong modification against the direction of locomotion can be measured during the transitions from running to walking (D2) and running to standing (C3).

A significantly longer deflection of the upper leg in positive direction can be measured during the gait transition from walking to running (C2). Before and after this transition the measured values are smaller. This characteristic is marked by arrow 'A' in Fig. 3.4. Corresponding to this a similar effect can be seen during the gate transition from running to walking (D2). During the transition the negative deflection of the upper leg is significantly smaller than before and after the transition. This effect is part of the deceleration process and is marked by arrow 'B' in Fig. 3.5.

In general the range of the deflection of the legs changes during gait transitions as represented by the crossed lines in Fig. 3.4 and Fig. 3.5.

3.4. Group 3 - Direction Transitions

Beside the change of velocity the dynamic of a pedestrian is also characterised by sudden changes of direction. This path changes are visualised in Fig. 2.6 (c) in crossing pattern (2), (4) and (5).

In order to microscopically understand this transitions the sequences of motion pattern group 3 shown in Fig. 3.1 (e) - (h) are investigated:

E: walking 90° transition

F: walking 45° transition

G: running 90° transition

H: running 45° transition

With higher velocities and higher angles of the transition the measurable effects are more significant. The most significant effects within group 3 can be measured in transition 'G'. Representative values of the pitch and the roll angle of the chest are plotted relative to the yaw angle of the hip in Fig. 3.6. The 90° transition starts

with a hip yaw angle of 0° and is completed with an angle of 90°. In order to achieve more readable plots the pitch and roll angle of the chest are adjusted to zero with the beginning of the transition. The pitch angle of the chest is rising during the transition. This effect results from a deceleration of the initial speed shortly before the transition starts and then nearly continuous acceleration back to initial speed during the transition. The roll angle starts to decrease with the beginning of the transition and then goes back to its initial value until the end of transition. This effect results from leaning into the curve during direction changes.

3.5. Group 4 - Combined Transitions

This group of transitions are the most challenging in path prediction. A pedestrian walking at the curb who spontaneously decides to run across the street in a certain angle is one of the most dangerous examples in this group. Fig. 3.1 (i) - (l) illustrates a representative selection of velocity and direction transitions. This selection matches the pedestrian crossing paths in Fig. 2.6 (c):

I: walking to running 90° transition

J: walking to running 45° transition

K: running to walking 90° transition

L: running to walking 45° transition

With higher angles of the transition the measurable effects are more significant. The most significant effects within group 4 can be measured in transition 'I' and 'K'.

Representative values of the pitch and roll angle of the chest are plotted in the upper part of Fig. 3.7. The lower part shows the corresponding yaw angle of the chest which indicates the running direction. The transition starts with a yaw angle of 0° and is completed with a yaw angle of 90°.

Since transition 'I' is a combination of a 90° transition and a walking to running transition also the measured effects are a combination of a significant amplitude in the pitch angle of the chest due to the acceleration and the roll angle of the chest due to the 90° transition.

Transition 'K' is a combination of a 90° transition and a running to walking transition. The corresponding effects are also a combination of a negative amplitude of the pitch angle due to the deceleration and a significant amplitude of the roll angle due to the 90° transition.

3.6. Conclusion

In this chapter, representative motion capture data of continuous walking, continuous running, velocity transitions, direction transitions and combined velocity and direction transitions was analysed. It was shown, that the chest angle modification represents a significant pre-indicator for near-future pedestrian velocity changes and is usable for pedestrian path prediction.

The pitch angle of the chest, which is representing the trunk flexion/extension, can be used as pre-indicator for pedestrian velocity changes, especially for the transitions between walking to running (C2) and running to standing (C3), as can be seen in Fig. 3.4 and for the transitions between standing to running (D1) and running to walking (D2), as can be seen in Fig. 3.5.

The yaw angle of the chest, which is representing the trunk rotation to the left and right, can be used as indicator for a running person, since the sinus like oscillation is more intensive during running compared to walking, as can be seen in Fig. 3.3, which illustrates representative values for continuous walking and continuous running. Furthermore, it can also be seen in Fig. 3.7, which shows representative sensor data during combined velocity and direction transitions.

The roll angle of the chest, which is representing the trunk abduction/adduction, can be used as indicator for direction transitions during running, based on the leaning into the curve, as can be seen in Fig. 3.6.

Furthermore, the variation of the upper and lower leg motion shows significant characteristics for walking, running and the transitions in between.

In summary, this natural human motion pattern are significant characteristics of a dynamic pedestrian and must be considered in the test of advanced pedestrian detection algorithms. Therefore, the motion capture data recorded in this chapter is also used as input for the Pedestrian Dummy Device presented in the following Ch. 4 and Ch. 5.

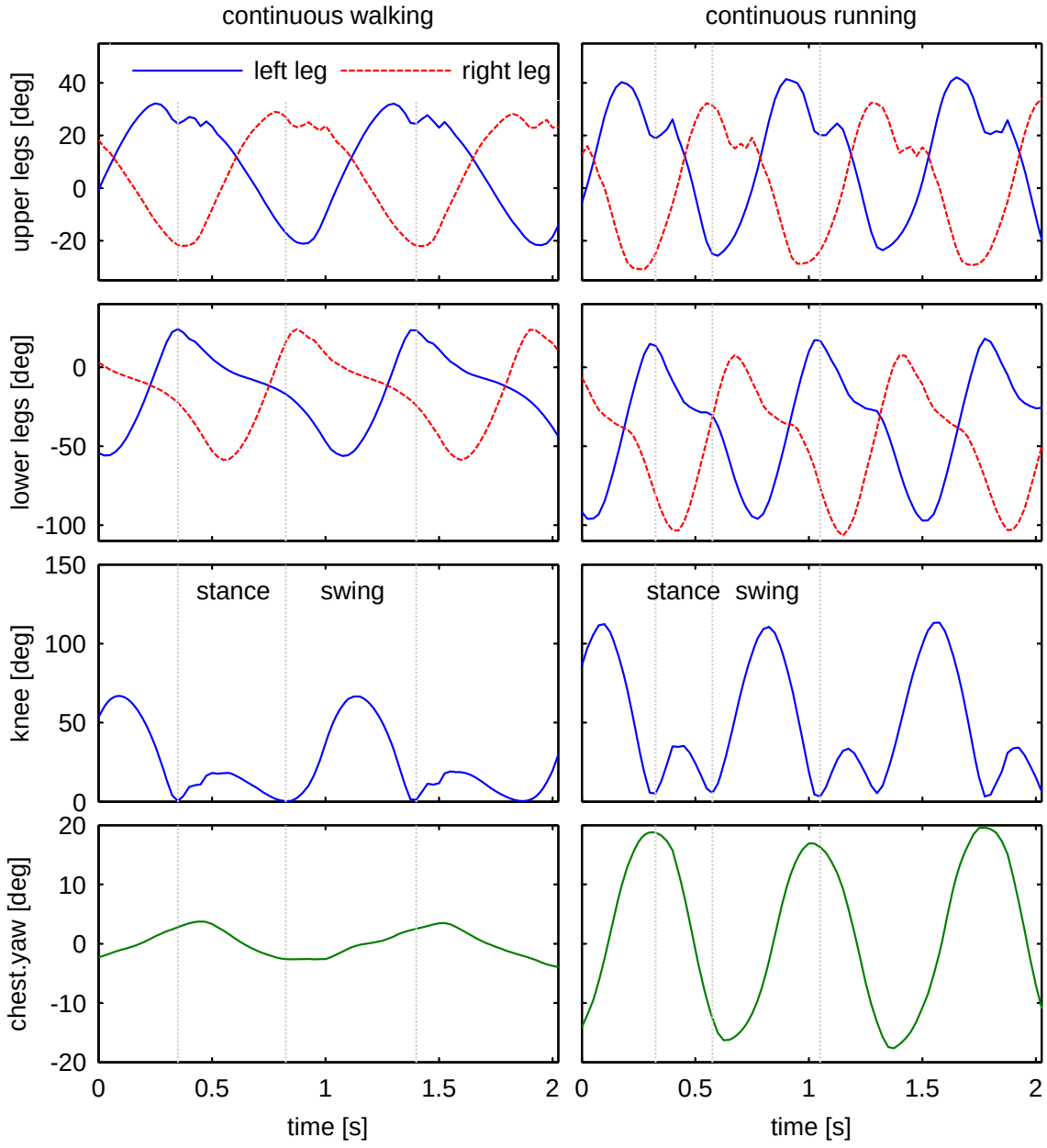

Fig. 3.3.: Representative sensor data during continuous locomotion [10]

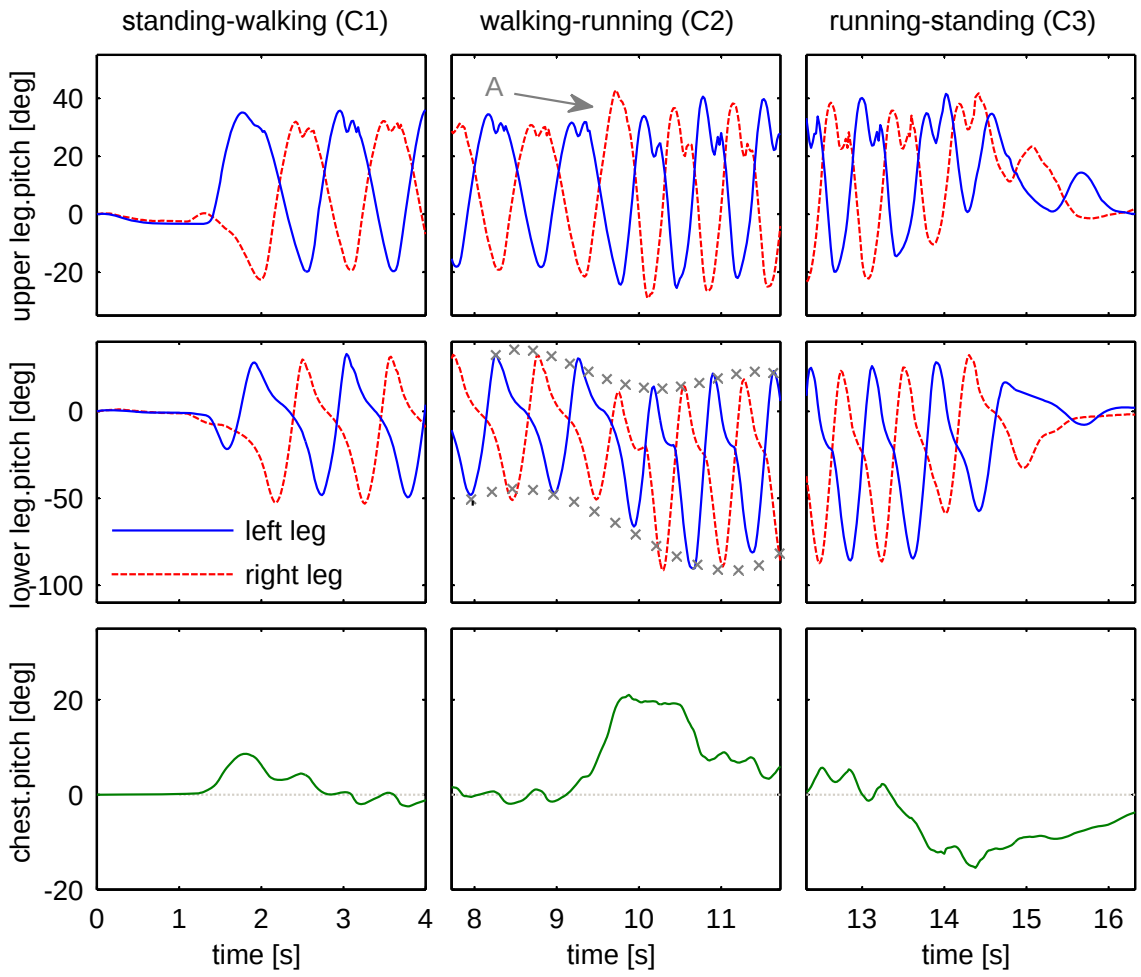

Fig. 3.4.: Representative sensor data during gait transitions C1, C2 and C3 [10] © 2017 IEEE.

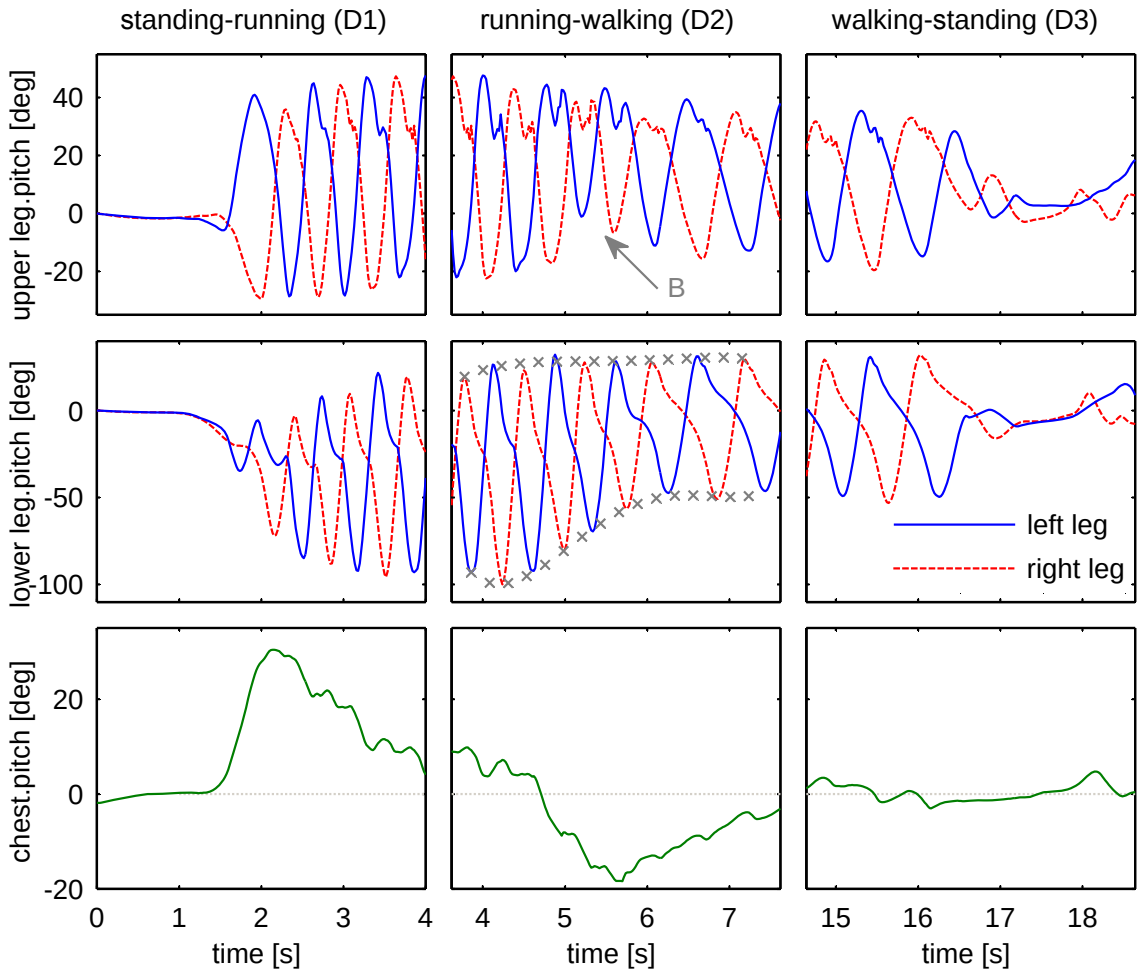

Fig. 3.5.: Representative sensor data during gait transitions D1, D2 and D3 [10] © 2017 IEEE.

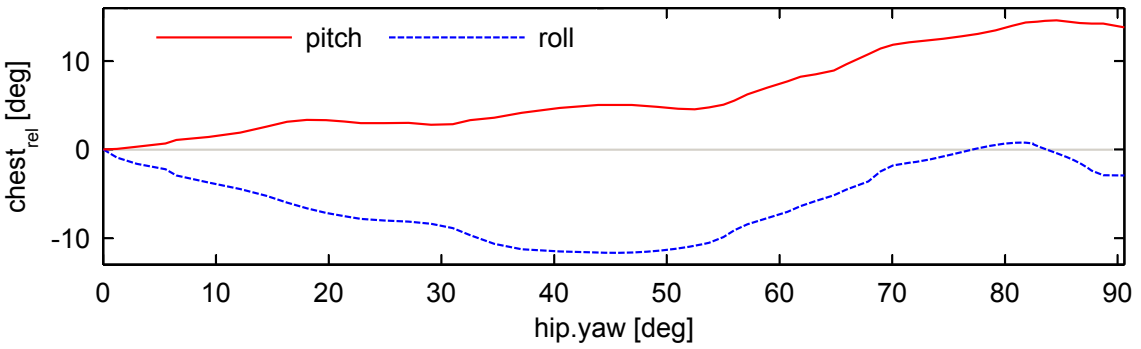

Fig. 3.6.: Representative sensor data of a test person during direction transition G: running 90° [10] © 2017 IEEE.

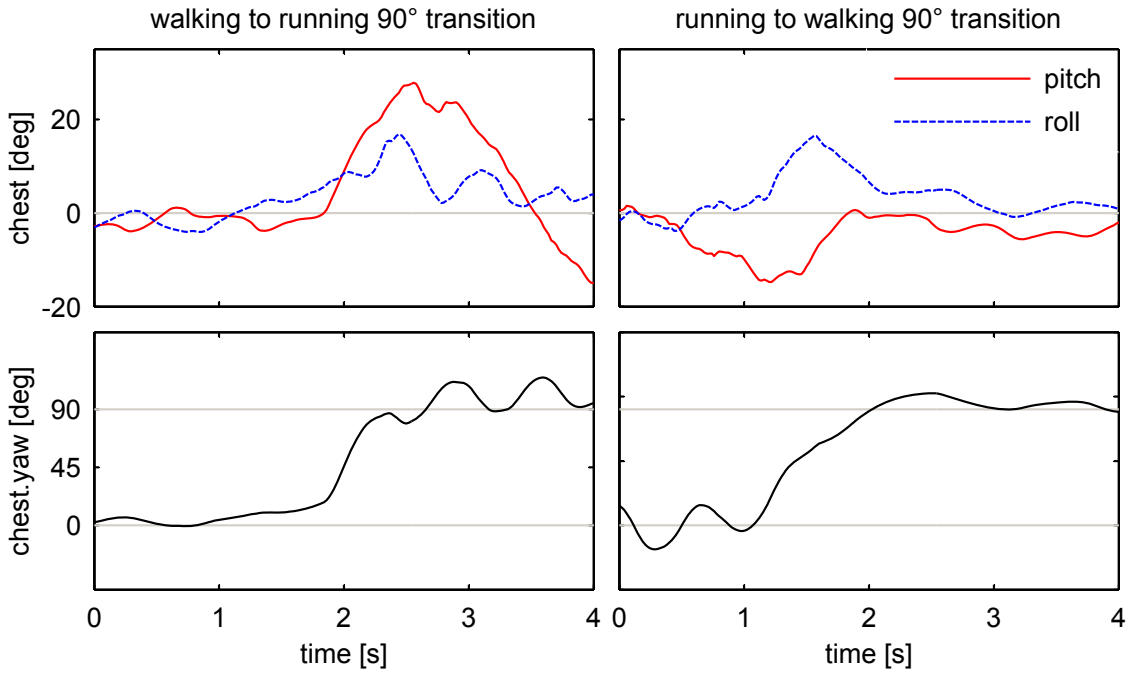

Fig. 3.7.: Representative sensor data of a test person during combined transition I:walking to running 90° and combined transition K: running to walking 90° [10] © 2017 IEEE.

4. Test System Approach

4.1. Introduction

In Ch. 2 it was shown that, based on studies in [8], 35% of pedestrian cross the street in a linear pattern, which corresponds to Fig. 2.6 (c) pattern (1) and (3), while 65 % cross the street in a more complex pattern, as illustrated in Fig. 2.6 (c) pattern (2), (4) and (5).

In Ch. 3 specific groups of pedestrian motion pattern were defined, including velocity and direction transitions. Based on this groups of motion pattern, pedestrian kinematics, especially focused on the leg and chest angles, were researched. It was shown, based on recorded motion capture data, that especially the modification of the chest angle is a significant pre-indicator and could be used for advanced pedestrian detection algorithms including pedestrian path prediction. Furthermore, as could be seen in Fig. 3.4 and Fig. 3.5, also the frequencies and amplitudes of the upper and lower legs have significant pedestrian characteristics and could be used in pedestrian detection algorithms.

This chapter introduces a novel pedestrian dummy and test system approach, focused on the replication of natural and dynamic human motion, including dynamic velocity and direction transitions for the test of advanced pedestrian detection systems.

The proposed test system is divded into two subsystems: A pedestrian dummy and a positioning apparatus. The positionioning apparatus enables the macroscopic motion of a pedestrian dummy, while the pedestrian dummy itself enables the replication of the microscopic motion of a pedestrian.

4.2. Positioning Apparatus

First design requirements for this application are multiaxial motion, high dynamic and level changes. A system which is designed for another purpuse but meets this three criteria is the Spider Cam system. The Spider Cam is originally designed for camera handling in larger areas like big stadiums [60]. The system consists of a camera which is held by four cables. Each cable is connected to a motor winch. The camera can be moved by synchronised control of the winches [61].

A similar principle to the Spider Cam was patented in 2009 for the test of advanced driver assistance systems. Hereby a test object can be moved by four ropes on any trajectory. In order to stabilise the test object a gyroscope is used [62]. However, gyroscopes could influence the vehicle sensor systems and the test results. Furthermore, gyroscopes are increasing the weight of the moved object and are very sensitive in case of collision.

As shown in Ch. 3 natural movements include a modification of the chest angle, especially during transitions. Usually a test objects itself can not replicate this modification, so this is an important requirement for the positioning apparatus. The positioning apparatus proposed in this thesis is based on six individual controlled ropes which are connected to a pole. Thereby three of the ropes are connected to the upper part of the pole and three ropes are connected to the lower part. Below the lower three ropes the pedestrian dummy is attached. This design enables beside to the translational modification also a rotational modification of the test object in pitch and roll angle. The ropes are connected to masts and redirected to the ground where they are actuated by electrical winches. In order to achieve a radar friendly test environment the electrical winches are placed outside the test area. The described concept is illustrated in Fig. 4.1 (a) and (b).

The concept of the positioning apparatus shown in Fig. 4.1 was developed within the context of this PhD research project and patented in [63] and [64]. A 1:10 scaled prototype of the positioning apparatus shown in Fig. 4.1 b) was built by the project partner MESSRING Systembau MSG GmbH.

Concept (a) is based on three masts. One mast has an upper and a lower rope connection. The lower part of the mast is connected to the lower part of the pole and the upper part of the mast to the upper part of the pole. The lower mast connection is below the pole connection and the upper mast connection is above the

pole connection. This configuration enables tensile forces to the pole and a torsional moment to the attached object.

Concept (b) is based on three high masts H_{1-3} and three lower masts or ground stations L_{1-3} in an alternating configuration. H_{1-3} are connected to the lower part of the pole and the ground stations L_{1-3} are connected to the upper part of the pole. This configuration enables compressive forces to the pole and a torsional moment to the attached object.

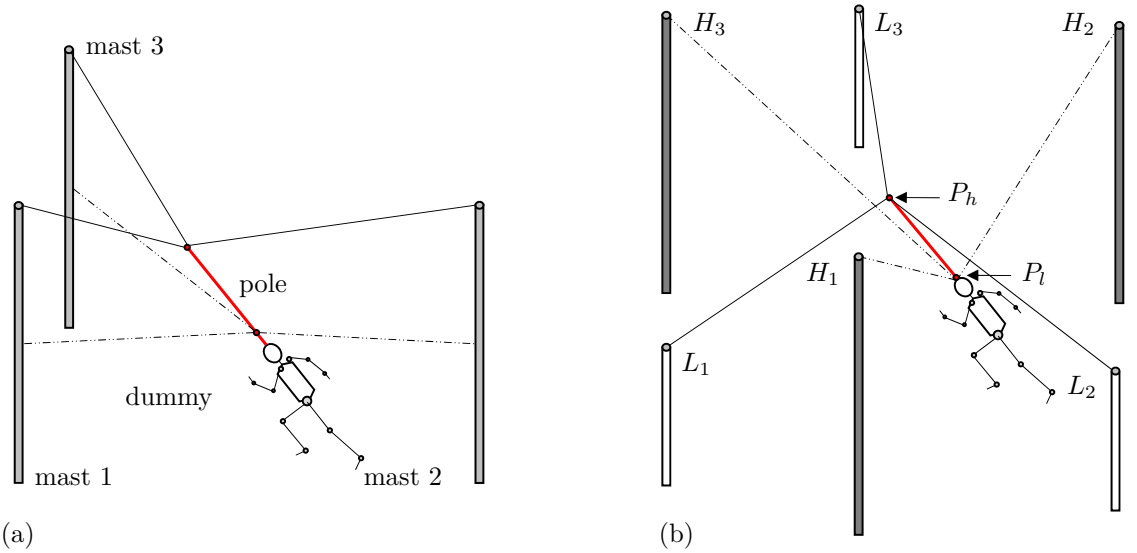

Fig. 4.1.: Concepts for the positioning apparatus: (a) basic model, (b) advanced model [10] © 2017 IEEE.

An advantage of the basic model (a) is the lower number of masts. Drawbacks are high tensile forces on the ropes to move the dummy upwards. This could lead to instabilities and a difficult control of the dummy in z direction and thus to the susceptibility to oscillate.

The advanced model (b) enables a larger range in the modification of the pitch and roll angle of the dummy. The angular configuration between the ropes and the pole leads to an optimised relation between the tensile rope forces and the pole forces in z direction. This enables a stiffer design and results in higher stability of the system. Also the length of the pole can be smaller in this configuration. In case of an detection error and an imminent collision this model enables to lift the dummy upwards in a safe position at comparatively lower height of the masts.

The applied torsional moment $\overrightarrow{M}$ for the modification of the pitch and roll angle of the dummy is defined as

$$\overrightarrow{M} = \overrightarrow{r} \times \overrightarrow{F} \tag{4.1}$$

whereby the displacement vector $\overrightarrow{r}$ is defined as

$$\overrightarrow{r}_{L_n} = \overrightarrow{P_l P_h} \quad and \quad \overrightarrow{r}_{H_n} = \overrightarrow{P_h P_l} \quad ; \quad n = 1, 2, 3; \tag{4.2}$$

and the corresponding force vectors are defined as

$$\overrightarrow{F}_{L_{n(t)}} = \frac{1}{|\overrightarrow{P_h L_{n(t)}}|} \cdot \overrightarrow{P_h L_{n(t)}} \cdot F_{L_{n(t)}} \tag{4.3}$$

and

$$\overrightarrow{F}_{H_{n(t)}} = \frac{1}{|\overrightarrow{P_l H_{n(t)}}|} \cdot \overrightarrow{P_l H_{n(t)}} \cdot F_{H_{n(t)}} \tag{4.4}$$

and can be described as the time variant unit vector of the discrete ropes multiplied with the time variant force applied by the corresponding drives.

The control of this system can be reduced on the individual drive forces $\overrightarrow{F}_{H_{n(t)}}$, $\overrightarrow{F}_{L_{n(t)}}$ and the corresponding lengths of the ropes which are defined as

$$l_{H_n(t)} = |\overrightarrow{P_l H_{n(t)}}| \tag{4.5}$$

and

$$l_{L_n(t)} = |\overrightarrow{P_h L_{n(t)}}|. \tag{4.6}$$

Since currently only a 1:10 scaled prototype of the positioning apparatus is available, the construction of a full scale positioning apparatus on a test track will be part of future work of the project partner MESSRING Systembau MSG GmbH.

In order to ensure that the positioning apparatus and its actuators are able to replicate the trajectories and dynamic of a real pedestrian, the project partner MESSRING Systembau MSG GmbH was provided with the dynamic trajectory data of combined direction and velocity transitions, which were recorded in Ch. 3. The corresponding trajectories can be seen in Fig. 3.1 (i), (j), (k) and (l).

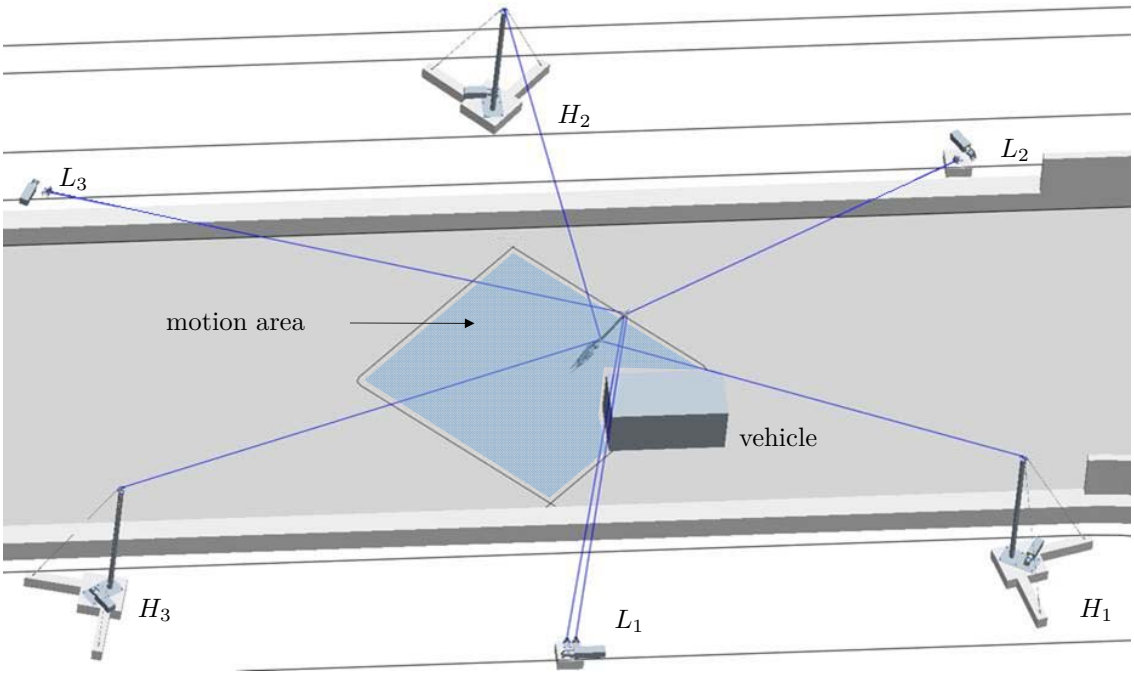

Fig. 4.2.: Model of the positioning apparatus installed on a test track (construction: MESSRING Systembau MSG GmbH) [10] © 2017 IEEE.

Fig. 4.2 shows a model of the positioning apparatus with a planned motion area width of 9 m, a maximum pedestrian running speed of 10 $\frac{m}{s}$ and a maximum pedestrian acceleration of 20 $\frac{m}{s^2}$, which enables the test of even complex pedestrian scenarios.

In complex scenarios the modification of the dummies yaw angle is mandatory for the replication of direction changes. Instead of using an electric motor attached or integrated in the pole, which would significantly increase the inertia and could be detected by automotive sensor systems, one more rope is installed parallel to an existing, as illustrated at mast L_1 in Fig. 4.2. Each rope is connected to a separate drive outside the test area and wound around the pole of the dummy. By counter-rotating winding and unwinding of the two ropes, the dummy is rotated around its vertical axis. If the ropes are simultaneously wound and unwound at the same speed no rotation of the dummy takes place. Hereby, all required actuators are placed outside the test area in order to reduce the visibility of the test configuration for the device under test.

4.3. Pedestrian Dummy Device

4.3.1. Necessary Degrees Of Freedom

For the classification of a pedestrian and for pedestrian path prediction advanced algorithms focus on indicators like the variation of the center of gravity, the variation of the motion of the arms and legs and the orientation of the pedestrians head [7]. The torso of the pedestrian dummy can be positioned by the positioning apparatus in 3 translational and 3 rotational DOF within the defined test area. The pedestrians position and variation of the center of gravity can be replicated by this DOF as illustrated in Fig. 4.3 by the central markings.

Although the motion of the legs is the only requirement for pedestrian locomotion as illustrated in Fig. 4.3 (a) also the counteracting swing of the arms is part of a natural gait and based on balance stabilisation but also on energy efficiency [65,66]. Hence the corresponding DOF for the motion of the arms should also be considered in order to replicate natural human motion as illustrated in Fig. 4.3 (b), especially during velocity transitions.

For the variation of the arms and legs during complex motion pattern, like very dynamic direction and velocity transitions, at least the following DOF per body side are necessary: shoulder: 3 DOF, elbow: 1 DOF, hip: 3 DOF, knee: 1 DOF

For the orientation of the pedestrians head at least one additional DOF is necessary. This results in a construction requirement of 17 DOF for the pedestrian dummy device itself. The rotation of the feet independent of the rotation of the leg (one DOF per body side) and the rotation of the hands independent on the rotation of the arm (one DOF per body side) have due to the lower size a lower significance compared to other body parts. Nevertheless they can be considered for complex motion pattern, especially if the dummy should be able to replicate related vulnerable road users, like skateboarder, roller skater, pedestrians with a baby buggy or nordic walker with metal sticks in their hands.

Ground contact of the feet is mandatory for some detection algorithm approaches [33]. Therefore the feet should be made of a flexible foam structure to ensure the required ground contact and prevent possible floating effects.

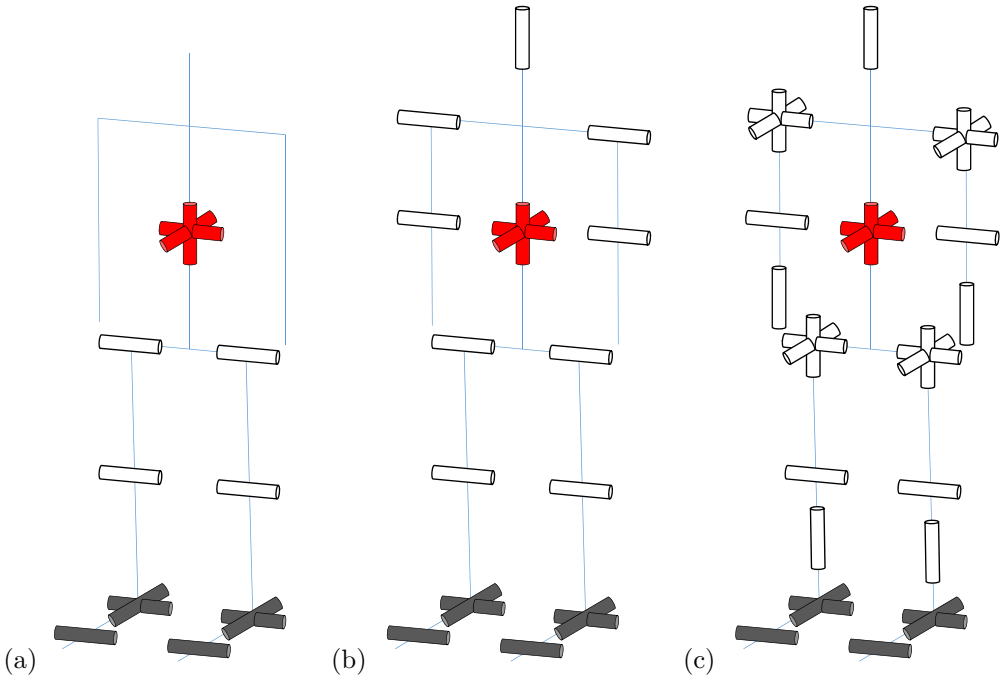

Fig. 4.3.: Simplified models of relevant DOF: (a) basic requirement for human locomotion: 4 + 6 DOF, (b) additional consideration of arm motion and orientation of the head 9 + 6 DOF, (c) replication of complex motion pattern: 21 + 6 DOF [10] © 2017 IEEE.

4.3.2. Comparison of Drive Principles

In order to find the most suitable drive concept for an advanced pedestrian dummy, possible technological drive concepts need to be evaluated and compared regarding relevant requirements.

To achieve a realistic radar signature, it is recommended to construct the dummy using low radar reflective materials and set the radar signature afterwards using radar reflective foil [18], [67]. Consequently, a low amount of metal components (M) is one important requirement in the selection of the drive concept for the pedestrian dummy. In case of a collision with a test vehicle, the weight (W) of the dummy should be as low as possible, which is also a requirement for the drive concept. Furthermore, as could be seen in Ch. 3, requirements for the replication of pedestrian motion sequences are the smoothness (S) and dynamic (D) of motion. In order to control the replication of these motion sequences, also the controllability (C) of the actuator concept must be considered. Since all actuators should fit within the average anthropometric measures of adult men, also the volume (V) is an important requirement.

Table 4.1.: Survey and evaluation of drive concepts for a pedestrian dummy. Evaluation: + positive, o neutral, - negative. Table published in [10] © 2017 IEEE

Actuator/Criteria	**M**	**W**	**S**	**V**	**D**	**C**
Stepper motor	-	o	-	+	+	+
Servomotor	-	o	+	+	+	+
Hydraulic cylinder	-	o	o	+	+	o
Hydraulic motor	-	o	+	+	+	o
Pneumatic cylinder	o	o	o	-	+	-
Pneumatic motor	-	o	+	o	+	-
Pneumatic artificial muscles (PAM)	+	+	+	-	+	-

In Table 4.1, which was published in [10], different technological drive concepts were evaluated regarding this criteria. Focused on the application, only available actuators providing the relevant power spectrum were considered [68].

In the table, electric, hydraulic and pneumatic actuators were considered. Electric actuators provide high dynamic and good controllability, but are made of a high amount of metal components.

Hydraulic cylinders and hydraulic motors consist based on the high pressure of metal components and have compared to electric actuators a lower controllability. Furthermore, using hydraulic or pneumatic cylinders at slow velocities the stick-slip effect can be observed, which is not acceptable for the replication of natural human motion pattern.

PAMs are pulling actuators. They can only transmit forces in one direction. Consequently one antagonistic pair of muscles is required to enable 1 DOF. Hence, they require much volume compared to other actuators. However, PAMs are lightweight, provide high dynamics and the motion is very smooth. Probably the biggest benefit of PAMs is the extremely low amount of metal components. Although the controllability of PAMs is due to their nonlinear behaviour and hysteresis worse compared to other systems it can be handled by an adequate muscle model and control concept.

In summary, PAMs show two main disadvantages compared to servomotors. First,

based on the antagonistic setup and the actuator design, they require more volume than servomotors. Second, based on their nonlinear behaviour and hysteresis, they have a worse controllability compared to servomotors.

Although, based on Table 4.1, servomotors achieve the best overall rating, they have some significant disadvantages compared to PAMs. First of all, they consist almost only of metal components, which could influence the radar signature of the pedestrian dummy. Furthermore, compared to PAMs, servomotors have a higher weight, which must be carried dynamically by a macroscopic positioning apparatus, e.g. shown in [63], [64] or an overrunable platform robot. Additionally, in case of collision, the higher weight would lead to higher damage, both on the vehicle and the pedestrian dummy.

Therefore, in the following, PAMs are used as actuators for the Pedestrian Dummy Device and it is shown in the next sections, that although servomotors are easier to control, also PAMs can be used for the replication of natural human motion, provided that an adequate muscle model and control concept is used. Furthermore, it will be shown, that although PAMs require more volume than servomotors, the average anthropometric measures of adult men provide enough space for 42 PAMs actuating 21 degrees of freedom.

4.3.3. Mechatronic Setup and Modeling

The setup is based on the bionic principle of muscles as actuators and tendons for the power transmission to the joints. Fig. 4.4 shows the antagonistic setup of two PAMs for the actuation of one DOF. P_n represents the pressure in muscle n which causes the force F_{PAMn} in the corresponding tendon.

The modeling of the drive system is based on the equilibrium of moments

$$\sum M_{PAM}(t) = \tau_i(q_{(t)}, \dot{q}_{(t)}, \ddot{q}_{(t)}) \tag{4.7}$$

where $\sum M_{PAM}$ represents the sum of torques that is generated by one antagonistic pair of muscles and τ_i represents the torque required to actuate the joint i of a robot manipulator to position q with the velocity $\dot{q}$ and the acceleration $\ddot{q}$. The vector of the generalised actuator torques $\boldsymbol{\tau}$ can be determined by the dynamic equation of motion

$$\boldsymbol{\tau} = \boldsymbol{M}(\boldsymbol{q})\ddot{\boldsymbol{q}} + \boldsymbol{C}(\boldsymbol{q}, \dot{\boldsymbol{q}})\dot{\boldsymbol{q}} + \boldsymbol{F}(\dot{\boldsymbol{q}}) + \boldsymbol{G}(\boldsymbol{q}) \tag{4.8}$$

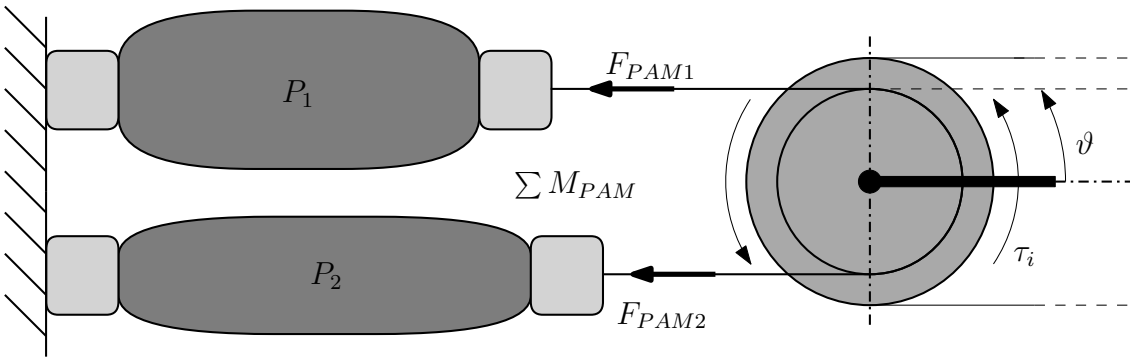

Fig. 4.4.: Antagonistic muscle setup for the actuation of one DOF [10]

where

- $\boldsymbol{q}$ is the $N \times 1$ vector of the generalised joint coordinates,
- $\boldsymbol{M}$ is the $N \times N$ joint-space inertia matrix,
- $\boldsymbol{C}$ is the $N \times N$ coriolis and centripetal coupling matrix,
- $\boldsymbol{F}$ is the $N \times 1$ friction vector, and
- $\boldsymbol{G}$ is the $N \times 1$ gravity loading vector,

while N represents the number of connected joints.

For the calculation of $\boldsymbol{\tau}$ the robotic model is implemented using the Robotics Toolbox [69] which is based on the recursive Newton-Euler algorithm. Therefore the kinematic structure is modeled using the Denavit-Hartenberg convention according to [70]. Input parameters for the calculation of the inverse dynamics are the generalised joint coordinates $\boldsymbol{q}, \dot{\boldsymbol{q}}$ and $\ddot{\boldsymbol{q}}$, for which real human motion data is used, while further relevant parameters are extracted from the construction data of the pedestrian dummy device.

Fig. 4.5 illustrates the relation between the muscle pressures P_1 and P_2, the tendon forces F_{PAM1} and F_{PAM2}, the corresponding contraction ε_1 and ε_2, and the resulting joint angle ϑ. The solid lines represent F_{PAM1} depending on the contraction rate ε_1 for pressure $P = \{100, 200, 300, 400, 500, 600\}$ kPa.

The dashed lines represent F_{PAM2} depending on the contraction ε_2. The joint angle ϑ increases with the contraction ε_1 and decreases with ε_2. The gray shaded area represents the operating area for one antagonistic configuration of PAMs. The figure can be used for approximation of required muscle pressures depending on ε and

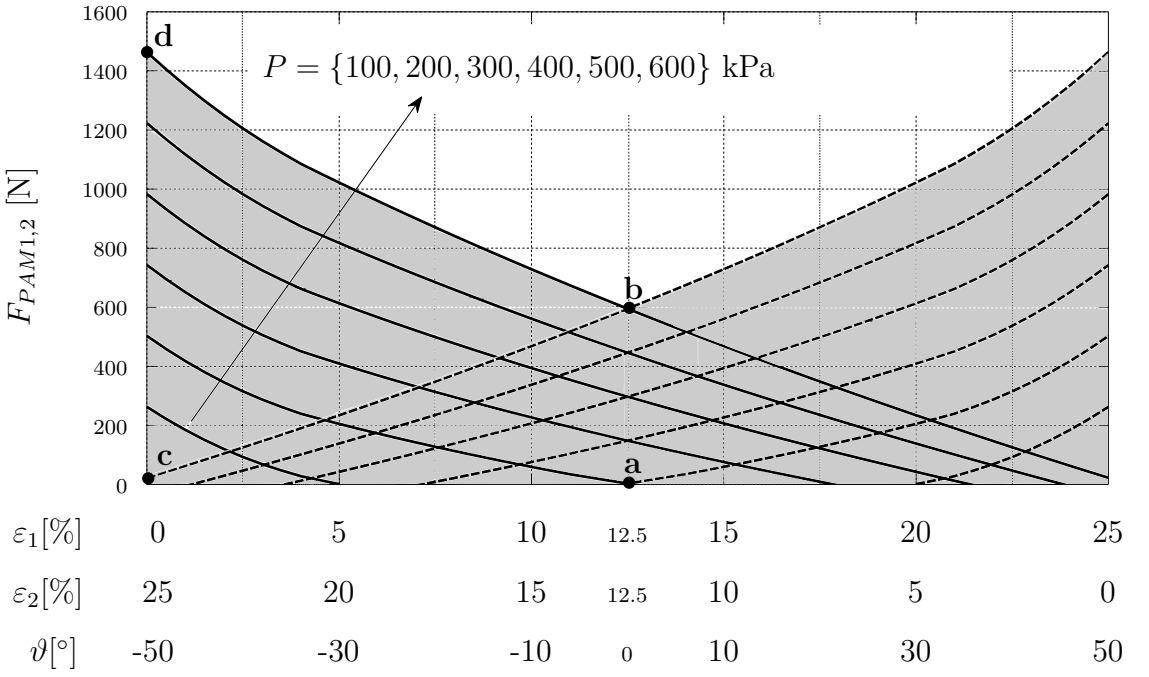

$\varepsilon_1[\%]$	0	5	10	12.5	15	20	25
$\varepsilon_2[\%]$	25	20	15	12.5	10	5	0
$\vartheta[°]$	-50	-30	-10	0	10	30	50

Fig. 4.5.: Relation between $F_{PAM1,2}$, $P_{1,2}$, $\varepsilon_{1,2}$ and ϑ in antagonistic configuration [10] © 2017 IEEE.

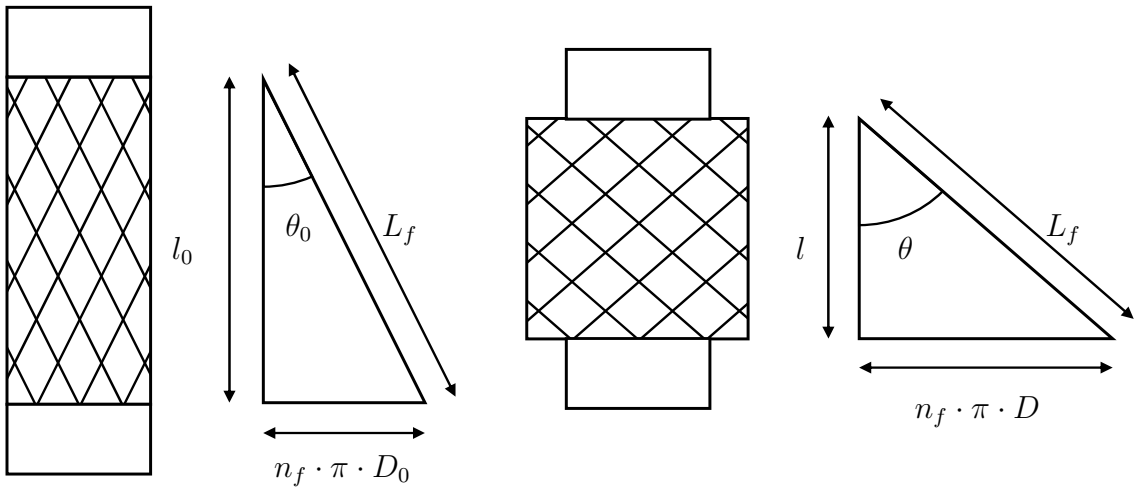

Fig. 4.6.: Functional principle of a McKibben PAM: (a) relaxed, (b) inflated [10] © 2017 IEEE.

the corresponding muscle forces. The angular zero position can be set by applying the same pressure to both PAMs while no external moments are applied. This corresponds to all pressures between **a** and **b**, while increasing pressure increases the stiffness of the joint. In **c** the minimum joint angle ϑ_{min} can be set by $P_1 = 0\ kPa$ and $P_2 = 600\ kPa$, if no external moment is applied. If an external force is applied

counteracting to F_{PAM1}, P_1 is increased and F_{PAM1} is adjusted between **c** and **d**.

In order to design a stable system the PAMs must be adequately modeled. The technical principle of PAMs is based on a contracting membrane which consists of an elastic tube with an integrated fiber structure. Inflated with compressed air, the diameter of the PAM increases while its length shortens [71], [72].

Fig. 4.6 illustrates the technical principle, where l and D are the length and diameter of the PAM, θ is the fiber angle, L_f and n_f are the length and the number of turns of a fiber around the PAM. The index 0 indicates the initial state of the PAM. The illustrated type of PAM is known as the McKibben muscle. It keeps a cylindric shape, while the angle between the opposing fibers varies. This leads to a maximum contraction up to $\varepsilon_{max} \approx 28\%$ of the inital length.

Based on [71], equation (4.9) and (4.10) result in (4.11), which describes the relation between the generated force of an ideal PAM $F_{PAM,ideal}$, the muscle pressure P and the contraction ε, where $L_{f(n_f=1)}$ represents the length of a fiber for $n_f = 1$.

$$F_{PAM,ideal} = -P \cdot \frac{dV}{dl} \tag{4.9}$$

$$V_{ideal} = \frac{1}{4} \cdot \pi \cdot D^2 \cdot l \tag{4.10}$$

$$F_{PAM,ideal} = \frac{P \cdot L^2_{f(n_f=1)}}{4 \cdot \pi} \cdot \left(3 \cdot \left(\frac{l_0}{L_f} \cdot (1 - \varepsilon) \right)^2 - 1 \right) \tag{4.11}$$

Fig. 4.7 compares this ideal model to the measured force depending on the contraction for both directions of hysteresis $F_{m,relax}$ and $F_{m,contract}$ at representative constant pressure of 300 kPa. It can be seen that in practice the McKibben PAM offers some drawbacks that influence the resulting force significantly [73], [74].

For a more realistic model $F_{PAM,real}$ the reducing forces based on the wall thickness of the membrane $F_{PAM,t}$, on the elasticity of the membrane $F_{PAM,e}$ and on the shape of the membrane $F_{PAM,s}$ must be considered.

$$F_{PAM,real} = F_{PAM,ideal} - (F_{PAM,t} + F_{PAM,e} + F_{PAM,s}) \tag{4.12}$$

Reducing forces based on the thickness of the membrane w_0 can be considered by

$$F_{PAM,t} = P \cdot \left(\frac{L_{f(n_f=1)} \cdot w_0}{2} \cdot \left(2 \cdot \sin\theta - \frac{1}{\sin\theta} \right) - \frac{\pi}{4} \cdot w_0^2 \right) \tag{4.13}$$

as also shown in [71]. For $P = 600\ kPa$, $w_0 = 2$ mm and $\theta_0 = 26°$ this results in a force reduction of $F_{PAM,t} = 131$ N. With increasing contraction, the wall thickness of the membrane decreases. However, this has only small influence on the volume reduction and is therefore not considered in (4.13).

However a significant effect can be seen based on the reducing forces $F_{PAM,e}$ which are necessary for the expansion of the elastic membrane. $F_{PAM,e}$ is proportional to $\left(1 - \frac{w}{w_0}\right)$:

$$F_{PAM,e} \sim \left(1 - \frac{w}{w_0} \right) \tag{4.14}$$

With a PAM specific and experimental determined elasticity factor $k_e = 1475\ N$ results

$$F_{PAM,e} = \left(1 - \frac{w}{w_0} \right) \cdot k_e. \tag{4.15}$$

This reaches a maximum of $F_{PAM,e} = 313$ N for $\theta = 45°$, which corresponds to a contraction of $\varepsilon \approx 21,3\ \%$.

The force reduction based on the form deviation of the membrane is linear to the pressure P and the contraction ε and inversely proportional to the initial length of the muscle l_0:

$$F_{PAM,s} \sim \frac{P \cdot \varepsilon}{l_0} \tag{4.16}$$

With a PAM specific and experimental determined form factor $k_s = 141 \cdot 10^3\ mm^3$ results

$$F_{PAM,s} = \frac{P \cdot \varepsilon}{l_0} \cdot k_s. \tag{4.17}$$

Fig. 4.7 visualises the modified model $F_{PAM,real}$, which fits in between the measured values and serves as the base for the control of the system.

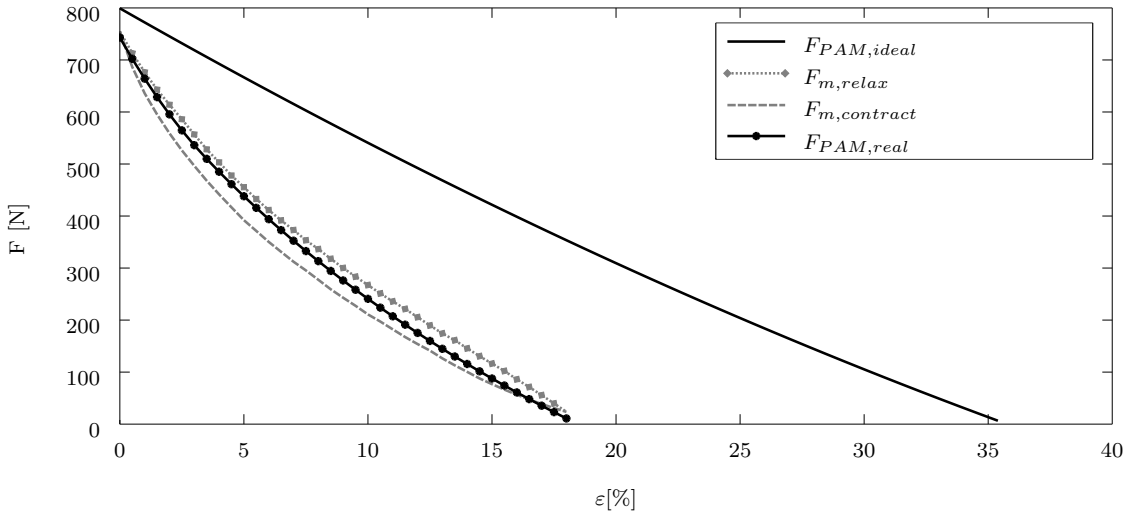

Fig. 4.7.: Comparison between the ideal model $F_{PAM,ideal}$ and measured values; Validation of $F_{PAM,real}$ at constant pressure of 300 kPa [10] © 2017 IEEE.

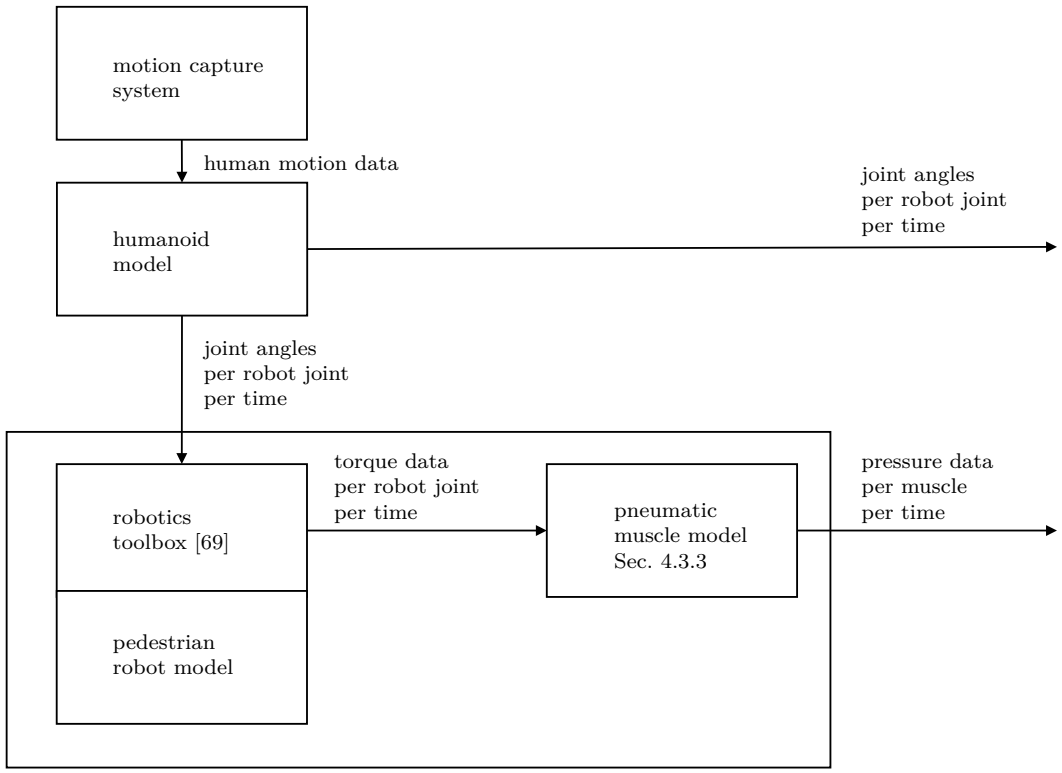

Fig. 4.8.: Preprocessing of motion capture data to joint angles per robot joint per time and pressure data per muscle per time.

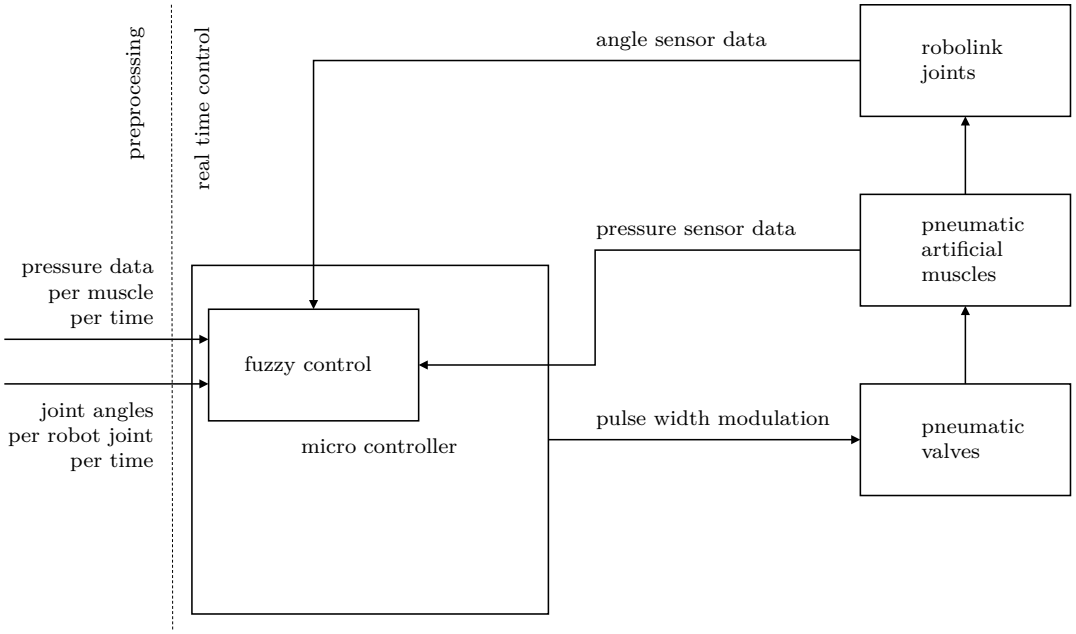

Fig. 4.9.: Real time control of the Pedestrian Dummy Device.

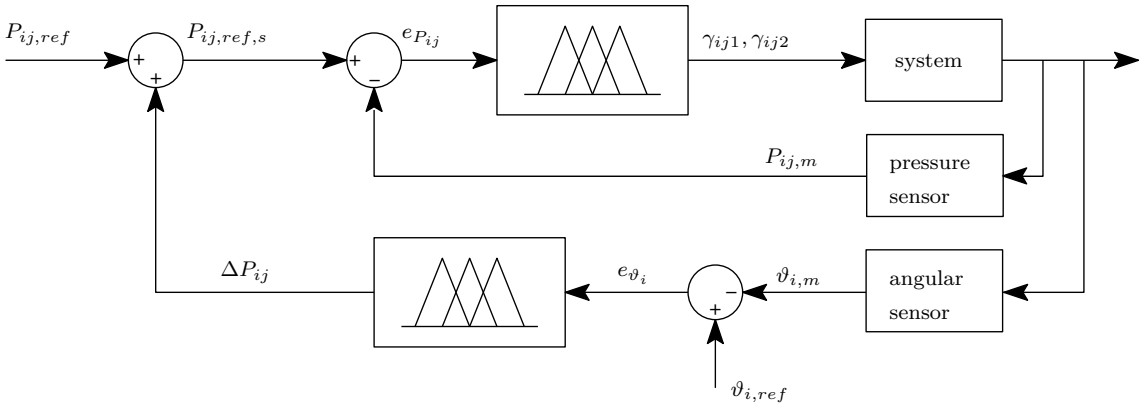

Fig. 4.10.: Structure of the fuzzy control circuit for PAM j of joint i [10] © 2017 IEEE.

4.3.4. Control

Fig. 4.8 visualises the preprocessing of the motion capture data while Fig. 4.9 shows the concept of the real time control (RTC) of the Pedestrian Dummy Device. The RTC is designed with one inner loop for the pressure control and one outer loop for the angular control, adding an offset to the pressure reference for the inner control loop. Hence, the RTC is based on two main parameters - motion capture data for the angular control which was also used in Ch. 3 for the research on pedestrian kinematics and pressure data for the pressure control which was preprocessed from the motion data based on the PAM model.

Fig. 4.10 visualises the structure of the fuzzy control circuit. $P_{ij,ref}$ are the preprocessed pressure reference values for robot joint i and joint muscle j. The angular reference for robot joint i is represented by $\vartheta_{i,ref}$.

Each PAM is actuated by two fast switching pneumatic jet valves - one high pressure supply valve and one low pressure exhaust valve. Each valve is actuated by a pulse width modulation (PWM). The generated PWM signals $\gamma_{ij1}, \gamma_{ij2}$ are the output of the control circuit. γ_{ij1} is the PWM signal for the high pressure supply valve of PAM j of robot joint i, while γ_{ij2} is the PWM signal of the corresponding exhaust valve. $P_{ij,m}$ are the measured pressure values, while $e_{P_{ij}}$ is the delta between the pressure reference and the measured values and also the input for the inner fuzzy control. e_{ϑ_i} is the delta between the measured angular values $\vartheta_{i,m}$ and the angular reference $\vartheta_{i,ref}$ and serves as input for the outer fuzzy control. The output of the outer fuzzy control is an additional pressure offset ΔP_{ij}, which is added to $P_{ij,ref}$ resulting in $P_{ij,ref,s}$.

Focus of the RTC was to generate PWM signals for the jet valves resulting in smooth and dynamic motion of the robot. For validation of the control concept a motion sequence composed of three phases was used. First the PAMs are initialised in angular zero position (phase 1), followed by a dynamic motion to $\vartheta = 60°$ (phase 2) and keeping that position (phase 3).

Fig. 4.11 shows the angular reference values $\vartheta_{2,ref}$ and the measured angular values $\vartheta_{2,m}$ as well as the reference values $P_{21,ref}$, $P_{22,ref}$ and measured values $P_{21,m}$, $P_{22,m}$ of the pressure in the corresponding PAMs during that sequence. After the PAM initialisation, where $\vartheta = 0°$, it may be expected an equal pressure in both PAMs based on Fig. 4.5. This is correct for joints which have the same angular range in

both directions. For joints which can only be moved in one direction, like knee or elbow joints, this angular scale is shifted in order to use the total range of motion. As soon as the initialisation is completed the motion sequence (phase 2) is started and completed by holding that static position (phase 3). The measured angular motion during phase 2 shows a dynamic and smooth behaviour. The measured steady-state error for the pressure ΔP is smaller than $5kPa$, which is negligible relative to the reference values. The measured angular steady-state error $\Delta\vartheta$ is smaller than 4° for the shoulder/hip joint and smaller than 5° for the elbow/knee joint. This control concept enables dynamic but also natural and smooth motion of the pedestrian dummy at acceptable angular deviation.

Fig. 4.12 visualises the design concept of the Pedestrian Dummy Device while Fig. 4.13 shows a photo of the assembled dummy in real size based on the presented results and considering human anthropometric measures. The illustrated pedestrian dummy has 21 DOF and is actuated by 42 PAMs, which were controlled by 84 pneumatic jet valves.

The PWM signal is generated by two micro controllers, placed in the head of the pedestrian dummy. One micro controller generates the PWM for the upper body and head rotation while the second micro controller generates the PWM for the lower body. Both micro controllers are connected via CAN bus to one host computer, so that commands can be transmitted via any device supporting the CAN protocol.

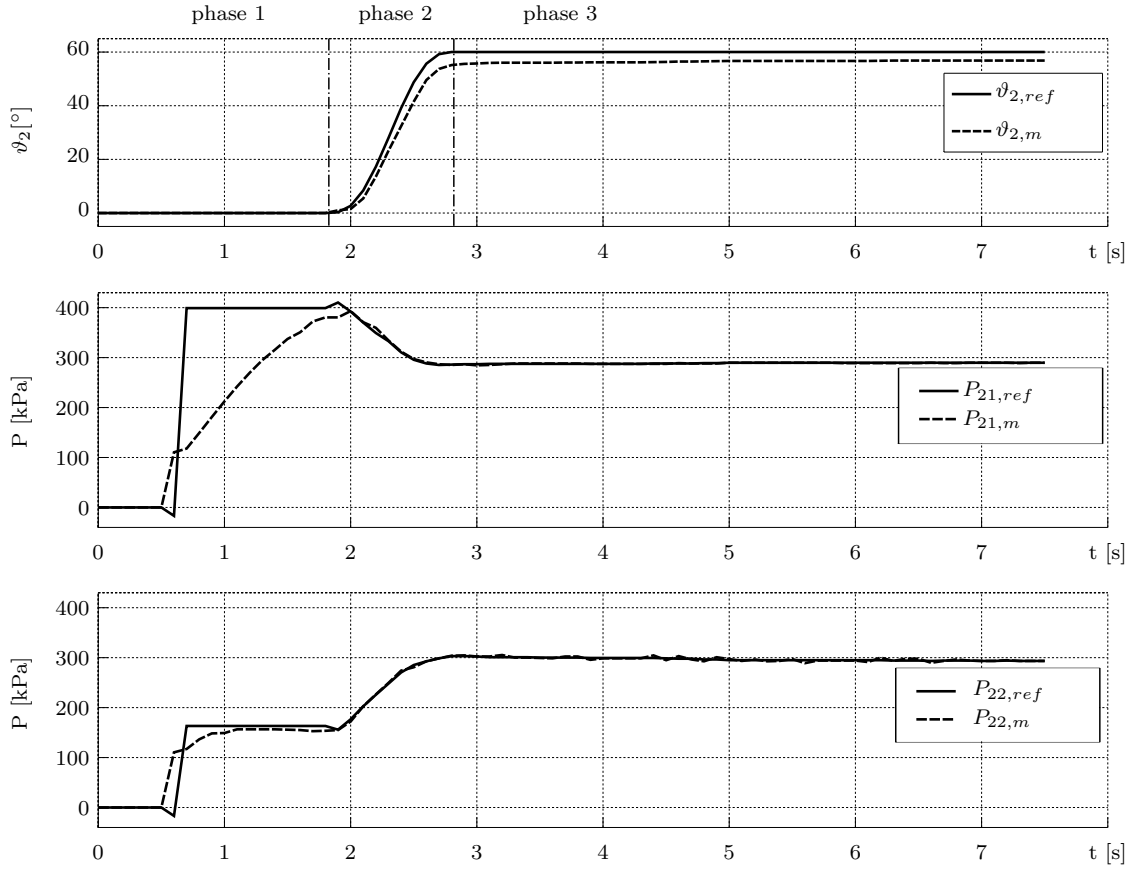

Fig. 4.11.: Validation of the fuzzy control algorithm - phase 1: initialisation; phase 2: smooth step from 0 to 60 degree; phase 3: keeping position [10] © 2017 IEEE.

4.3.5. Conclusion

Current test systems for pedestrian detection have limited suitability for the test of advanced detection algorithms especially considering pre-indicators and pedestrian path prediction. This chapter introduces a novel test system approach. The presented positioning apparatus enables the replication of complex crossing paths and the modification of the roll, pitch and yaw angle of a pedestrian dummy. The presented pedestrian dummy enables controlled motion of the arms, legs and head of the pedestrian dummy.

Pneumatic artificial muscles are most suitable for the actuation of a pedestrian dummy but require detailed modeling of the actuators and a robust control concept.

The positioning apparatus was constructed as 1:10 scaled model and patented in [63]. The pedestrian dummy was designed and assembled in real size and presented for the first time in May 2015 at the SafetyWeek in Aschaffenburg, Germany and in June 2015 at the PraxisConference on Autonomous Emergency Braking in Bicester, England. Furthermore, it was presented to the Bavarian Prime Minister Horst Seehofer at the 11th June 2015 in Ingolstadt, Germany.

The introduced test system enables the test of a huge variety of crossing paths and motion pattern, which is mandatory to prove the robustness of a system and necessary for the exploration of the limits of sensor systems. Furthermore it enables the comparison and rating of different detection algorithm approaches and can be used to support the review of software releases and test driven development. Fig. 4.13 shows a photo of the assembled skeleton and muscle apparatus of the Pedestrian Dummy Device in static and dynamic position with 21 degrees of freedom, where all actuators fit within the anthropometric measures of adult men.

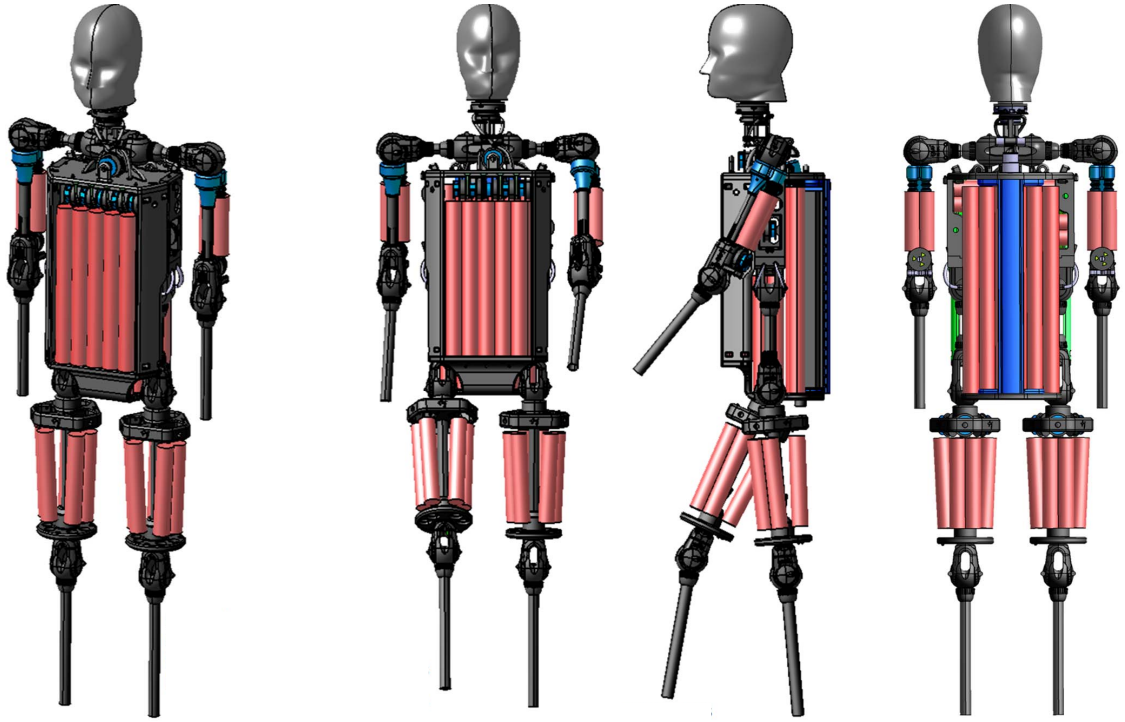

Fig. 4.12.: Skeleton and muscle apparatus of the Pedestrian Dummy Device (head: Human Solutions GmbH / RAMSIS model; joints: igus®robolink®) [10] © 2016 IEEE.

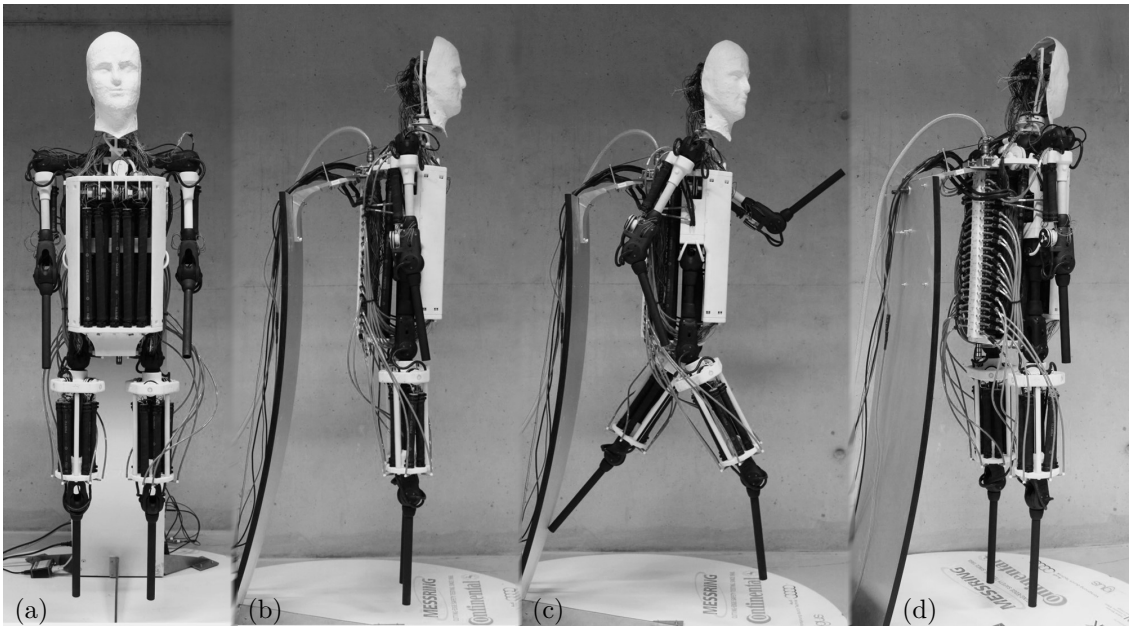

Fig. 4.13.: Photo of the skeleton and muscle apparatus of the Pedestrian Dummy Device: (a) front perspective static, (b) side perspective static, (c) side perspective running, (d) side/back perspective static [10] © 2017 IEEE.

5. Test System Optimisation

5.1. Introduction

The 21D Pedestrian Dummy Device, which was presented in the previous Ch. 4, was designed as laboratory setup and focused on the proof, that pneumatic artificial muscles in antagonistic configuration can be used as actuators for the replication of natural and dynamic human motion. Furthermore, it was shown, that average human anthropometric measures provide enough space for the integration of 42 pneumatic artificial muscles, actuating 21 degrees of freedom.

This chapter, introduces a second version of the pedestrian dummy, named 10D Pedestrian Dummy Device. Focus of this second version was to increase usability and robustness and transfer the 21D Pedestrian Dummy Device from a macroscopically static laboratory setup to a full working 10D Pedestrian Dummy Device on the test track, proving its usability in a full vehicle test run. Since it was already shown by the 21D Pedestrian Dummy Device that average anthropometric measures provide enough space for 42 pneumatic artificial muscles actuating 21 degrees of freedom, the amount of degrees of freedom integrated in the pedestrian dummy was reduced from 21 to 10 in the second version of the dummy. The developed 10D Pedestrian Dummy Device provides 10 degrees of freedom, each one degree of freedom for head rotation, upper arm motion, lower arm motion, upper leg motion and lower leg motion, as can be seen in Fig. 4.3 (b), with one additional integrated degree of freedom for the modification of the chest angle of the dummy. This amount of degrees of freedom enables controlled motion of the arms and legs, and a controlled modification of the chest angle.

Since the positioning apparatus is currently only available as 1:10 scaled model, an overrunable platform robot was used at the end of this chapter for the macroscopic motion of the 10D Pedestrian Dummy Device. However, the 10D Pedestrian Dummy

Device is designed to also be compatible with possible future macroscopic motion concept as they are presented in [63] or [64].

The development of the test system approach presented in Ch. 4 with special focus on the 21D Pedestrian Dummy Device in Sec. 4.3 was the first part of this PhD research project and showed that the approach is suitable for the test of advanced pedestrian detection systems. Ch. 5 shows the design and implentation of further improvements in a second version of the pedestrian dummy, which was mainly focused on enhanced usability and robustness, resulting in a test system demonstration where the pedestrian dummy runs in front of an approaching vehicle, proving that the presented approach is usable for real vehicle AEB tests.

The main contribution of Sec. 4.3 was showing that pneumatic artificial muscles (PAMs) are most suitable for the actuation of the Pedestrian Dummy Device and that all PAMs fit within the anthropometric measures of adult men. Furthermore it showed the design and the first prototype of a pedestrian dummy with 21 degrees of freedom based on the biomechanical principle of tendonds and muscles in antagonistic configuration.

In order to transfer this technology from the laboratory to the vehicle test track further design improvements were required. General design requirements for test equiment are usability and robustness. The required space on test tracks and the required amount of test engineers in usually scheduled in detail before vehicle functions are tested. Hence, it is mandatory that test equiment like the pedestrian dummy can be re-assembled fast and without expert knowledge even in case of an unplanned collision. Furthermore, parts of the pedestrian dummy can be damaged in case of a collision. Consequently, all parts of the dummy must be ether very robust or easily replaceable.

5.2. Usability and Robustness

In order to increase both, usability and robustness, a modular dummy concept was defined, which enables a fast assembly of the Pedestrian Dummy Device and rapid replacement of its individual modules.

Fig. 5.1 shows the design concept of an improved version of the Pedestrian Dummy Device with 10 degrees of freedom, divided into its eight main components:

1. a passive head unit,
2. an active torso unit,
3. two active arm units,
4. two active leg units and
5. two passive foot units.

Active units are defined as parts of the dummy with integrated PAMs or with an integreted microcontroller and pneumatic jet valves. Passive units contain no PAMs or control parts. Hence, the replacement of passive units is easier and more cost-efficient than the replacement of active units. Consequently, active units have to be designed more robust.

The main active module is a robust torso unit, which contains the only control unit and all 40 required pneumatic jet valves as well as integrated actuators for the head rotation (1 DOF, 2 PAMs) and the chest angle variation (1 DOF, 2 PAMs). The connected head unit is rotated by the actuators integrated in the torso, has itself no integrated actuators or sensors and is therefore, in case of an unplanned collision, very easy to be replaced. Furthermore, the torso is connected to two modular arm units, each providing 2 DOF by 4 integrated PAMs. Hereby, one pair of PAMs actuates the upper arm movement with 1 DOF while the other pair of PAMs actuates the lower arm with 1 DOF. The leg movement is enabled by two modular leg units, each providing 2 DOF actuated by 4 integrated PAMs. The foot units are connected to the leg units and designed flexible, ensuring ground contact during the process of walking, which is mandatory for some detection algorithms, as can be seen in [33].

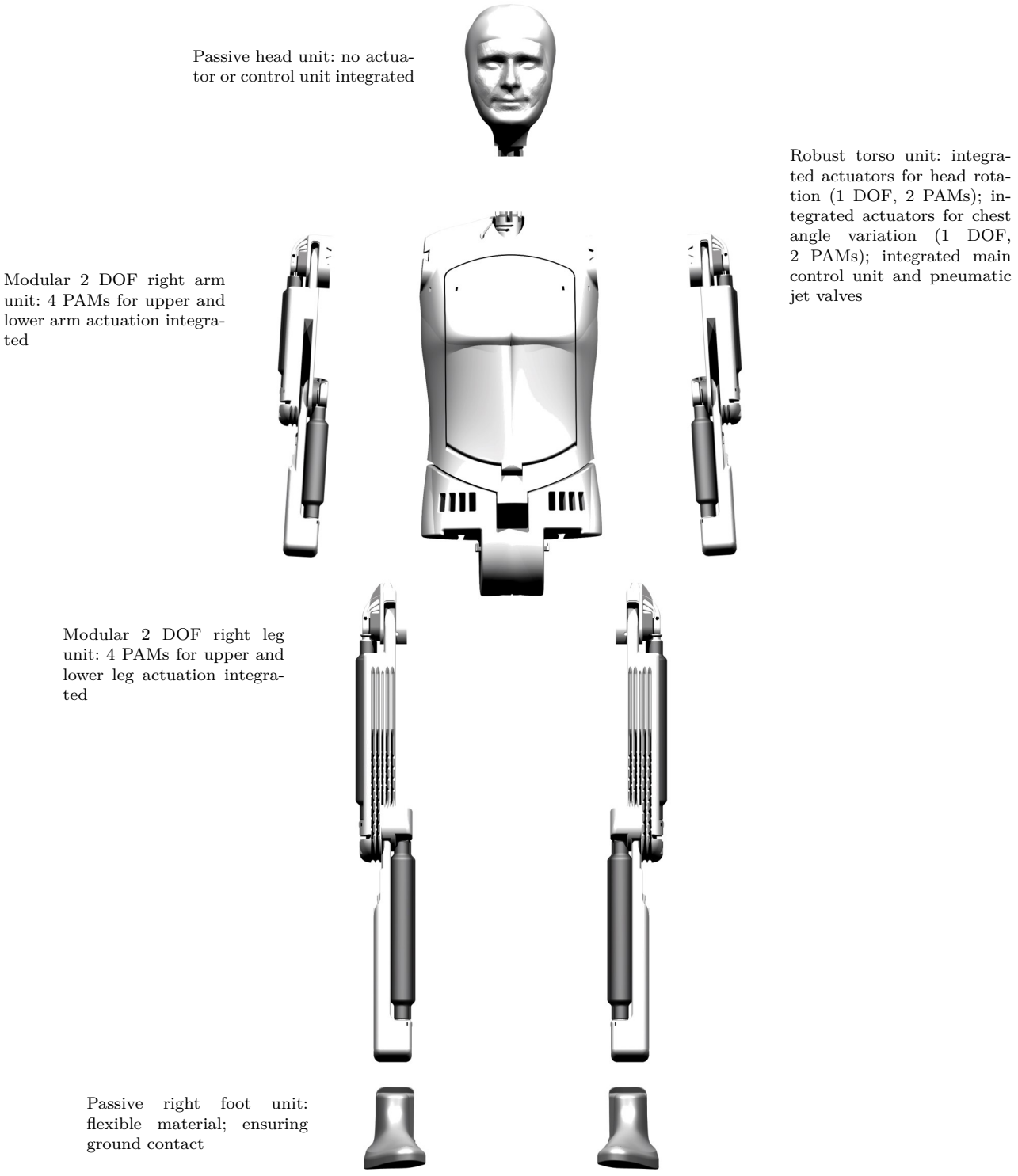

Fig. 5.1.: Modular concept of the 10D Pedestrian Dummy Device divided into its main components.

Since the torso provides enough volume and is suitable for a robust design, all pneumatic jet valves and the microcontroller are placed inside of it. For an easy access to the control components, a large service opening was designed over the complete breast and abdominal area of the dummy. In order to protect sensible components during testing the service opening can be closed and fixed in closed state with cable ties. The outline of the service opening can be clearly seen in Fig. 5.1 and Fig. 5.2. The torso unit itself consists of two main mechanical parts, one upper part which can be seen in Fig. 5.2 and one lower part which is illustrated in Fig. 5.3. Both are connected by an uniaxial joint, providing 1 DOF for the chest angle variation which is a significant pre-indicator for pedestrian path prediction during the acceleration process described in Ch. 3.

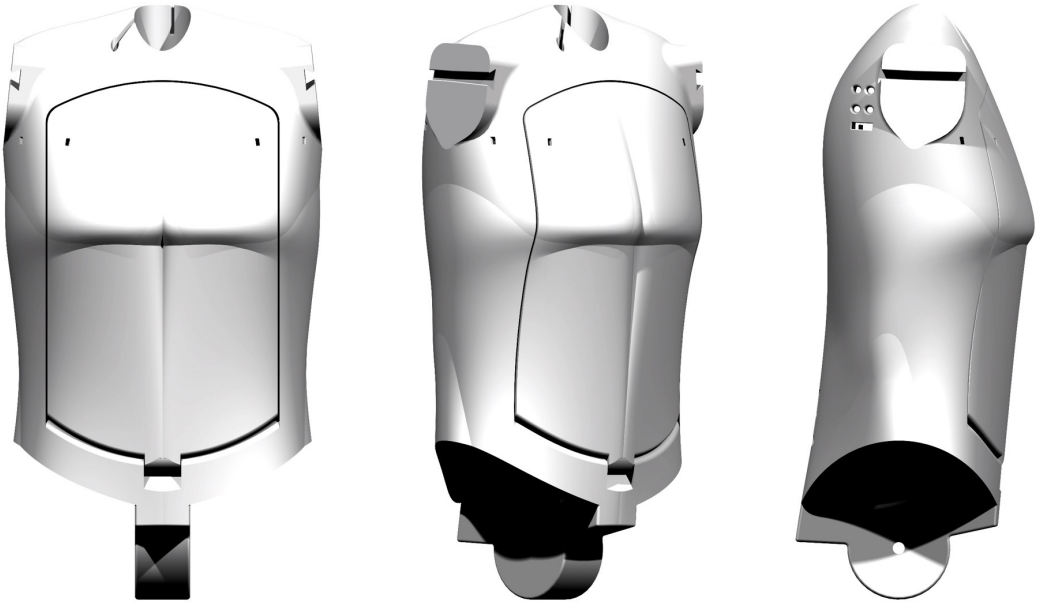

Fig. 5.2.: Upper part of the 10D torso a) front perspective, b) 45° perspective, c) 90° perspective.

Fig. 5.3.: Lower part of the 10D torso a) front perspective, b) 45° perspective, c) 90° perspective.

Fig. 5.4 shows the arm and leg units of the 10D Pedestrian Dummy Device in front, 45° and 90° perspective. In order to optimise the usability, the design concept of the arm and leg units is almost identical, except of the adapted lengths of the body parts, considering human anthropometric measures. Each unit consists of 4 PAMs enabling 2 DOF. Hereby, one DOF enables the motion of the upper arm/leg while the second DOF enables the motion of the lower arm/leg. The anthagonistic pair of PAMs is integrated directly in the corresponding body part and can be seen in Fig. 5.4 coloured in dark gray. Each PAM can be replaced separately within minutes and also the upper and lower part of the units can be separeted by removing the connecting axial bearing within minutes. To make sure that neither the PAMs nor the axial bearing are released accidentally or by mistake both are protected by a safety catch. Compared to the 21D Pedestrian Dummy Device, in the 10D concept all actuators are very easy to reach and maintain.

The upper part of the arm and leg units provides a defined groove to connect the units with the torso while the lower part of the arm and leg units provides the negative part of a sliding dovetail joint to attach passive hands or feet.

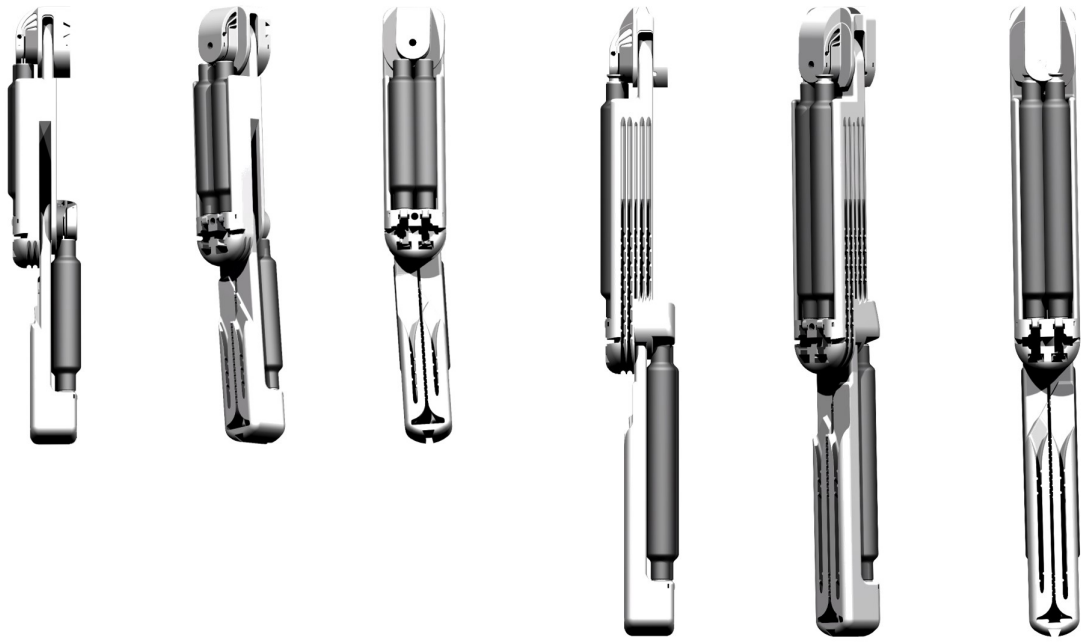

Fig. 5.4.: Arm and leg units of the 10D Pedestrian Dummy Device a) right arm front perspective, b) right arm 45° perspective, c) right arm 90° perspective, d) right leg front perspective, b) right leg 45° perspective, c) right leg 90° perspective.

Fig. 5.5 illustrates the model of the right foot of the 10D Pedestrian Dummy Device. In the upper part of the foot model the defined tail of the sliding dovetail joint can be seen, which enables to attach the passive foot to the leg unit. The dovetail joint is designed conical in sliding direction, which means that the foot unit can only be inserted from one sliding direction and is kept in position by the conical shape and the resulting friction. Additionally, the foot unit can also be secured by a safety catch.

The passive foot units are 3D printed from Thermoplastic Polyurethane (TPU 92A-1) which is a flexible material, while all other units are 3D printed from non-flexible Polyamide (PA), providing high mechanical resistance. The used Thermoplastic Polyurethane ensures durable elasticity of the passive foot units, which is mandatory for the replication of natural walking and running and enables ground contact of the feet.

For both materials the used 3D printing technology was laser sintering. In order to keep the weight low and the flexibility high, the feet units are printed mostly hollow, except of the tail of the dowetail joint and some integrated supporting structures. It must be considered, that using laser sintering as 3D printing technology, the raw material remains in closed hollow structures. This has positive effects on the stability of the 3D printed parts, but needs to be removed in order to achieve lightweight components. Therefore it is recommended to design openings in the components before printing and remove the raw material after printing.

Fig. 5.5.: Right foot model of the 10D Pedestrian Dummy Device a) front perspective, b) 45° perspective, c) 90° perspective.

The arm and leg units are connected to the torso by an easy exchangeable butterfly shaped component with predetermined breaking point. The design of this connecting component is similar to the sliding dovetail joint which was used to connect the passive foot units to the leg units and can be seen in Fig. 5.6.

The torso unit and the arm and leg units provide the corresponding openings, which can be seen in Fig. 5.1 and Fig. 5.2. In case of a collision, the connecting component breaks in its center and prevents the units from severe damage. The remaining halfs of the broken component can be removed from the units and exchanged. The breaking point can be set by the dimensions of the connecting component.

In order to assemble a prototype of the 10D Pedestrian Dummy Device, also the connecting components were 3D printed from Polyamide by laser sintering. To assemble an arm or leg unit to the torso unit, both are hold together so that the openings in both parts form the negative shape of the connecting component. Then, the connecting component is pushed in the opening and fixed using a pin and slight hammer taps. During testing, it could be seen that the designed component is suitable for the corresponding application. It did not brake by the test of various motion pattern of the Pedestrian Dummy Device itself, but breaks in half and releases the individual units if an external force, as it can be expected in case of a collision, is applied.

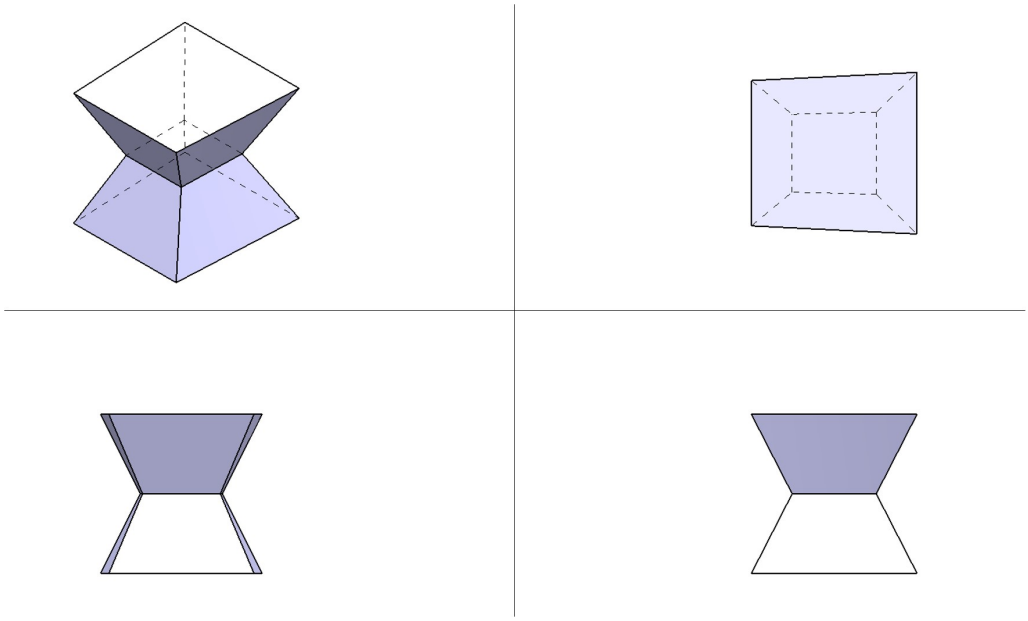

Fig. 5.6.: Perspective and three side view of the butterfly shaped connecting component with predetermined breaking point.

5.3. Shape Design and Variation

Beside the replication of natural human motion, another challenge in the design of humanoid robots is that, depending on the required degree of realism, individual parts can become very complex to design. An example for that is the head and in particular the face area. But also the design of realistic human hands or feet and detailed body proportions can become very time-consuming.

In the first version of the Pedestrian Dummy Device, presented in Ch. 4, simple structures were computer designed to fit inside the anthropometric measures of adult men. The result presented in Fig. 4.12 and Fig. 4.13 shows the skeleton and muscle apparatus of the 21D Pedestrian Dummy Device.

In order to improve the degree of realism in the second version of the Pedestrian Dummy Device, a 3D scan of a human test subject was taken and imported in the 3D computer design software CATIA, which can be seen in Fig. 5.7.

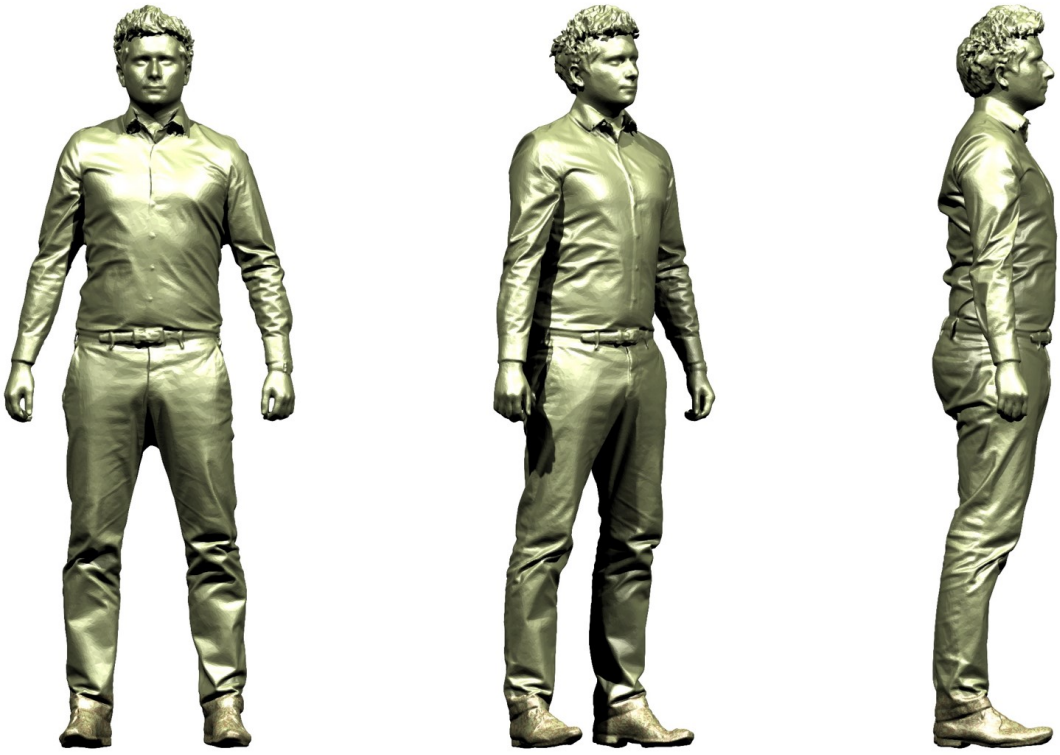

Fig. 5.7.: 3D scanned body of human test subject.

Complex parts of the 3D scan, like for example the face, were extracted and integrated in the model of the 10D Pedestrian Dummy Device. Fig. 5.8 shows the 3D scanned face of the test subject integrated in the head of the dummy. This method is very time-efficient, since only functional parts have to be designed in computer-aided design, while complex 3D structures can be scanned, imported and integrated.

This method was demonstrated on example of the face of the 10D Pedestrian Dummy Device, but can of course be used for the design of all complex 3D structures of the dummy. The functional body parts of the pedestrian dummy, were designed to fit within the outer shape of the 3D scan, which ensures realistic human proportions of the robot body.

In order to obtain a variety of differently shaped and sized pedestrian dummies, other test subjects can be 3D scanned and this procedure can be repeated very time-efficient.

While this methodology enables a huge variation of the shape and proportions of the Pedestrian Dummy Device, it is of course mandatory to also vary the colour and material of the clothing during testing.

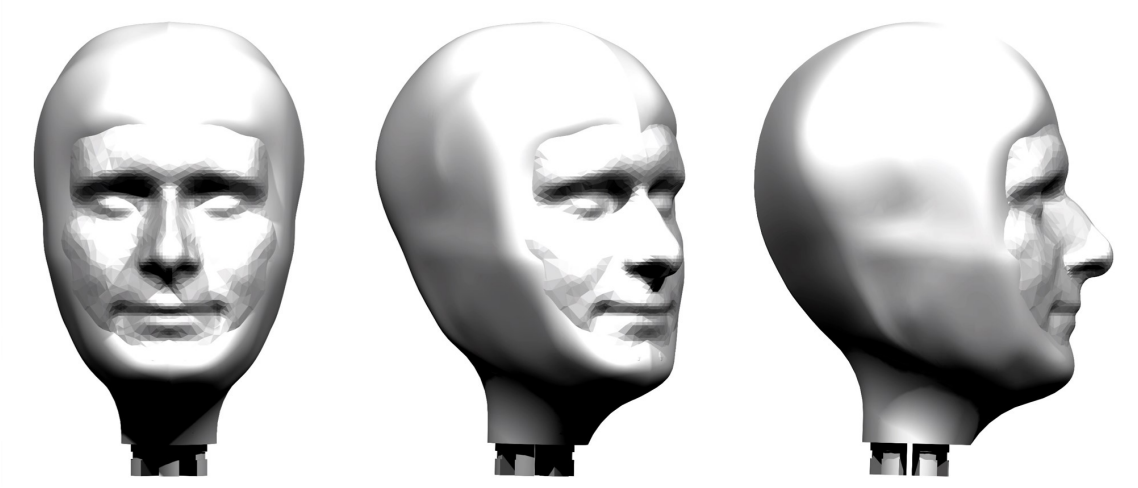

Fig. 5.8.: Shape of the test subject integrated in the head part of the dummy.

5.4. Replication of Thermal and Radar Signature

Although the replication of thermal and radar signature is not the main focus of this thesis, a variation of those signatures must be considered during testing.

An issue with existing pedestrian dummies is, that they only provide a fixed radar signature. This signature is usually set and fixed to an average human radar cross section (RCS). Therefore, developers and test engineers usually take radar shots of a number of human test subjects, and test the developed AEB systems with a pedestrian dummy which provides a fixed RCS, representing the average human. Although this is a good first step, this approach provides no variation of the radar signature, which is essential in order to test also the critical borders of the used radar based pedestrian detection algorithms and corresponding AEB systems.

Therefore, during testing, the RCS of the pedestrian dummy should be increased and minimised in order to test how the detection algorithm and the complete AEB system reacts if no standard test is performed.

It must be considered that, not only the minimisation of the RCS is important, which may lead to a non activated AEB, but also the maximisation of the RCS is important during testing, because if the RCS exceeds the value of an average human, the active pedestrian hood or pedestrian airbag may not be activated.

A novel technical concept for the varation of thermal and radar signature of pedestrian dummies was presented in [75]. The basic concept can be seen in Fig. 5.9 and is based on the design of a 3D printed double-walled and liquid-filled outer shape of the pedestrian dummy.

By variation of the temperature of the liquid the thermal signature of the dummy can be set to a defined setting but also simply and fast varied between AEB tests.

By variation of the radar reflectivity of the liquid the radar signature of the dummy can be changed. In application, different 3D printed channels could be responsible for different radar signatures. For example, three 3D printed channels in the outer shape of the dummy could be designed side by side, while one of the channels contains a highly conductive and radar reflective liquid, the second channel contains a medium reflective liquid and the third channel contains a low reflective liquid. Whether or not a channel is filled with radar reflective and tempered liquid can be set by a

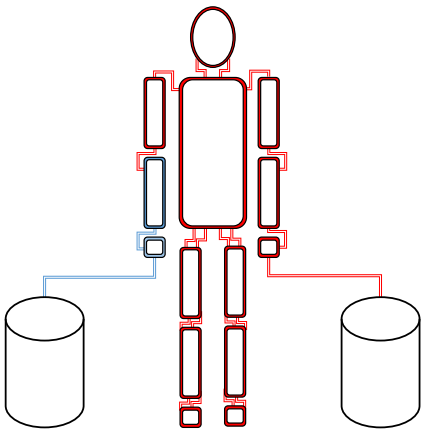

Fig. 5.9.: Technical concept for thermal and radar signature variation [75].

balance between the pressure of compressed air from one side of the channel and the pressure of the liquid from the other side. If the liquid is not used it can be stored in a reservoir. This reservoir could also be the base for the temperature control.

For a fast temperature change, also two reservoirs of the same liquid but different temperature setting could be used. Here, the liquid can be fast exchanged by different pressure settings between the two reservoirs.

An advantage of this approach is, that once the system is set up, the variation of the temperature and radar signature can be varied automatically inbetween tests, depending on the previous test results.

Another approach which is technically easier to implement would be to use temperature storing components which can be fitted to the outer shape, e.g. ceramics, and apply the temperatured elements before each test to the dummy. This parts coulds have integrated and uniformly distributed radar reflective components, e.g. aluminum, where based on the amount of aluminum the radar signature can be fixed for each part. This parts could also be designed flexible, by small distributed ceramic spheres and aluminum spheres integrated in e.g. cotton cases which can be applied via e.g. velcro closure like clothes to the body parts of the dummy. By the amount of radar reflective material the radar signature of the dummy can be set. For a variation of the radar signature during testing, a set of different components with fixed radar signature would be required. Furthermore, they would have to be exchanged manually in between the tests.

5.5. Conclusion

Fig. 5.10 shows the assembled 10D Pedestrian Dummy Device mounted on an ultraflat-overrunable platform. The photograph was taken right after an AEB test was successfully performed in the automotive research and test center CARISSMA in Ingolstadt, Germany on 6th June 2016. The test was performed live in front of more than 500 guests from the automotive industry, science and politics, including the German Federal Minister for Education and Research Dr. Johanna Wanka and the Bavarian Minister for Science Dr. Ludwig Spaenle.

A video which was recorded during the preparations for the live test is available here: `https://youtu.be/eF5IkqsknBE`

It can be seen that based on the optimisations described in Ch. 5 the prototype described in Ch. 4 was tranferred from a laboratory demonstrator to a working test system on the test track.

Although the test was performed using an ultraflat-overrunable platform the 10D Pedestrian Dummy Device is designed to be also compatible to possible future systems like they are described in [63] or [64].

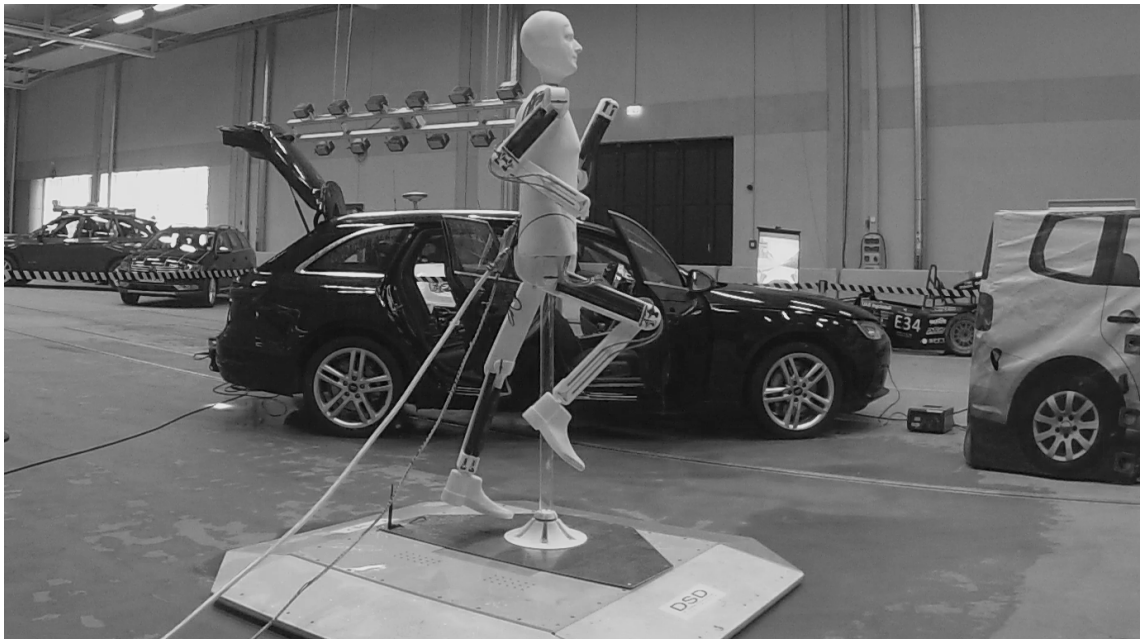

Fig. 5.10.: 10D Pedestrian Dummy Device mounted on an overrunable platform robot.

In the live performed test, the 10D Pedestrian Dummy Device was waiting in a side street for the vehicle to approach. When the vehicle, which was equipped with a driving robot, started to accelerate in direction of the dummy, a light barrier was activated which gave the initial signal to the 10D Pedestrian Dummy Device to activate the microscopic motion and to the ultraflat-overrunable platform to activate the macroscopic motion.

In order to make the test more challenging and realistic, the approaching vehicle had to pass through artificial rain and fog. The relevance of these external disturbances will be explained in detail in Ch. 6.

Right before the imminent collision automatic braking and steering was activated. The vehicle stopped beside the 10D Pedestrian Dummy Device and in front of a standardised European Vehicle Target (EVT). The final scene after the test was successfully completed can be seen in Fig. 5.10 with the 10D Pedestrian Dummy Device on the ultraflat-overrunable platform in the front, the vehicle under test with integrated driving robot in the back and the EVT on the right.

During testing the 10D Pedestrian Dummy Device showed increased usability and robustness compared to the laboratory setup presented in Ch. 4.

It was proved during a real vehicle test setup on an automotive test track that the developed pedestrian dummy is suitable for active pedestrian safety testing.

The developed 10D Pedestrian Dummy Device which is replicating the microscopic motion of a pedestrian in combination with the ultraflat-overrunable platform or any other system for the replication of the macroscopic motion, e.g. [63] or [64], enables a wide range of new test scenarios, including spontaneous velocity or direction transitions. An example for a challening scenario which could be tested with this system is introduced in Ch. 3 in the group of combined transitions, where a pedestrian is walking along the road and spontaneously accelerating in e.g. a 45° angle across the street in front of an approaching vehicle. Hereby, the 10D Pedestrian Dummy Device is replicating the motion of the arms and legs, including the chest angle variation and the optional head motion, while the macroscopic motion system to which the dummy is connected by e.g. a plexiglass tube, as it can be seen in Fig. 5.10, is responsible for the replication of the translational and rotational motion of the pedestrian dummy on the test track. This enables the reproducible test of advanced detection algorithm approaches at an early development stage.

6. Consideration of Athmospheric Disturbances

6.1. Introduction

In Ch. 4 a new developed Pedestrian Dummy Device was presented, which enables the realistic replication of natural and dynamic human motion sequences, actuated by pneumatic artificial muscles, based on previously recorded human motion capture data. In order to result in a low radar cross section, which can later be stepwise increased or decreased to initial value during testing by applying or removing radar reflective material, it was required that the Pedestrian Dummy Device consists of almost no metal components. In Ch. 5 further design improvements resulted in a new version of the Pedestrian Dummy Device, which was tested in a real vehicle test on the test track. In summary, until now this thesis was focused on the realistic replication and variation of target characteristics. However, environmental conditions, like athmosperic disturbances, can influence the detection as shown in this chapter based on [76], [77] and [78] and consequently also a variation of environmental conditions should be considered during testing. The variation of target characteristics, environmental conditions and driver behaviour will be summarised in a generalised active pedestrian safety test methodology in Ch. 8.

Pedestrian detection is based on sensor systems listed in Table 2.1. Sensor signals can be incfluenced by athmosperic disturbances, like rain or fog, between the sensor and the target, which could be a pedestrian, vehicle or any other object. This disturbances can have significant influence on the robustness and reliability of the object detection and hence must be considered during testing.

The following section shows based on [76] and [77] how environmental disturbances incluence standard automotive sensor systems like radar, lidar and camera and how they can be integrated in pedestrian testing.

6.2. Influence on Automotive Sensors

In order to show the influence of rain on standard automotive radar, lidar and camera, these sensor systems were tested in [77] under various rain conditions. A requirement to enable these tests are reproducible rain conditions. Therefore, natural rain was measured with a rain disdrometer and afterwards artificially generated by a novel indoor rain simulator [76].

In [77] a vehicle equipped with standard automotive sensors which provided a developer interface was placed at one end of the rain simulator. On the other side of the rain simulator a standardised European Vehicle Target (EVT) was placed. In the setup, the vehicle equipped with standard automotive sensors served as device under test (DUT) while the EVT served as target, providing a standardised sensor signature.

The space between the DUT and the EVT is divided into rain layers, which could be activated individually.

Fig. 6.1 shows the radar cross section (RCS) of a static EVT depending on the number of activated rain layers. The tested radar system operates at 77 GHz. Each box plot contains 200 single measurements. While the average measured RCS of the EVT without activated rain is approximately 12 dBsm it is reduced to lower than 8 dBsm with all four activated rain layers.

Fig. 6.2 shows the relative intensity of a laser signal reflected by the EVT depending on the number of activated rain layers. Each box plot contains 40 single measurements of the same angle. It can be seen that the relative reflection intensity is decreased with increased number of activated rain layers.

Fig. 6.3 shows the histogram of images of a static EVT recorded by a standard automotive camera sensor depending on the number of activated rain layers. It can be seen that with a higher number of activated rain layers the range of the intensity is getting smaller. This means that, since the total amount of pixels stays constant, with a higher number of activated rain layers more pixel have the same intensity. This consequently results in a lower contrast and a smoothing of gradients. Since visual object recognition algorithms are based on gradient detection, with increasing rain intensity it gets more difficult to detect other traffic participants.

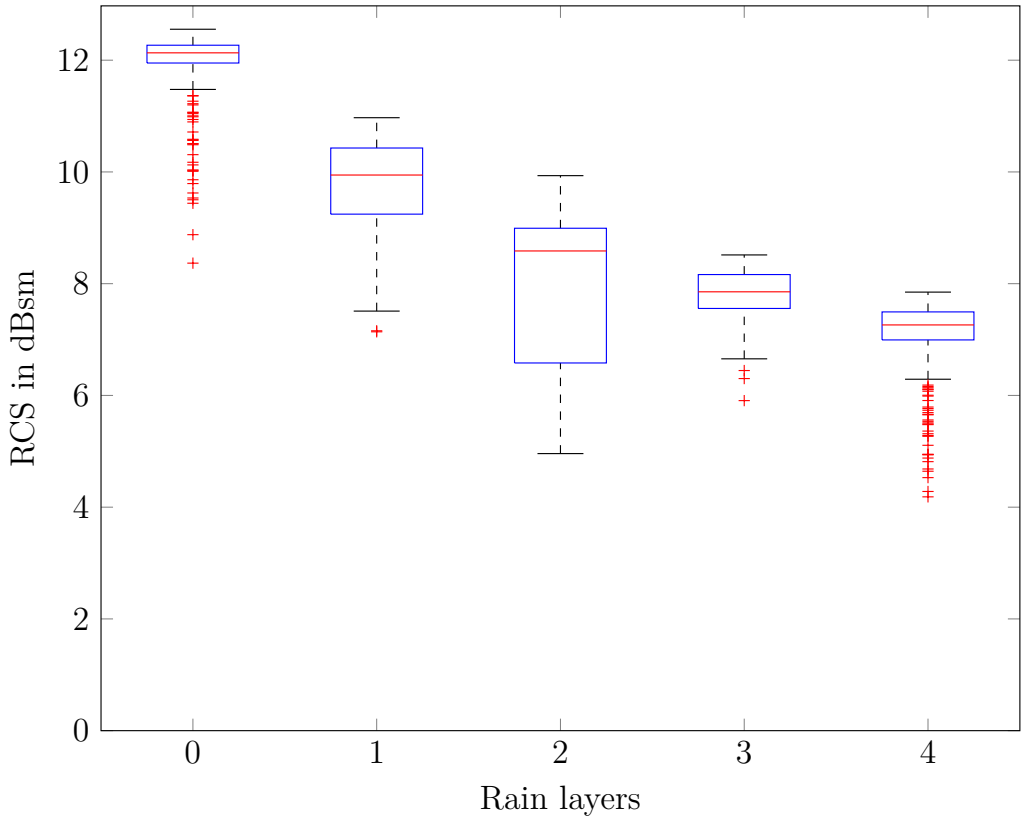

Fig. 6.1.: Radar cross section of a static EVT depending on the number of activated rain layers [77] © 2016 IEEE.

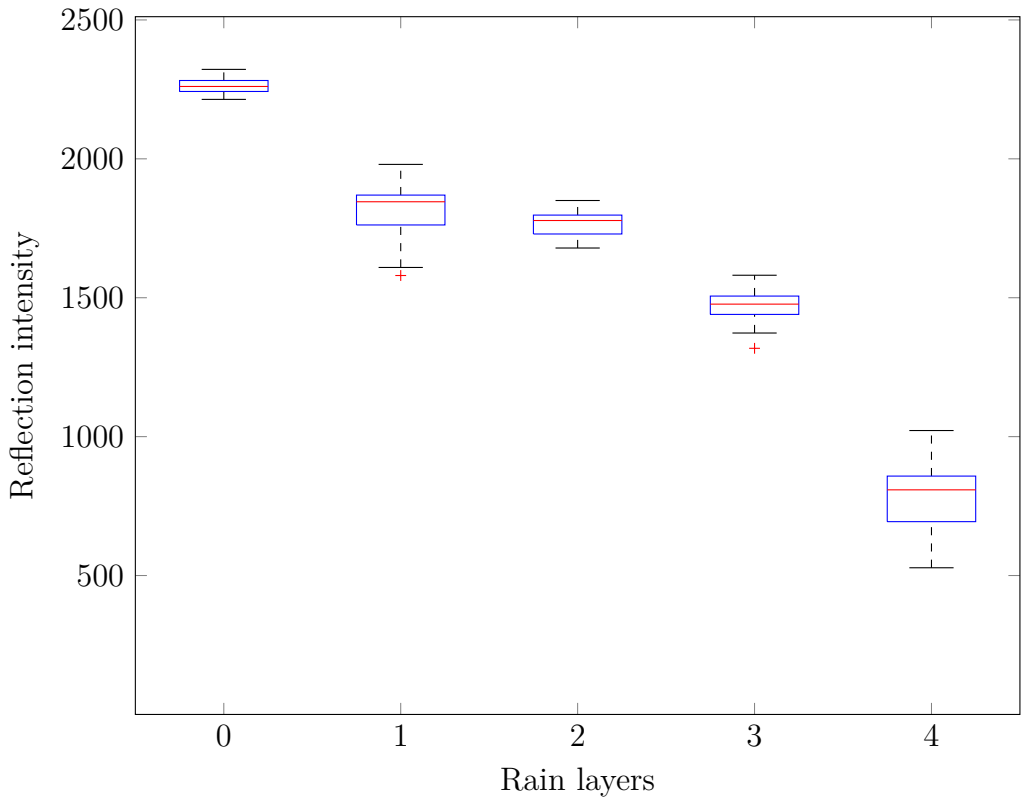

Fig. 6.2.: Relative intensity of a laser signal depending on the number of activated rain layers [77] © 2016 IEEE.

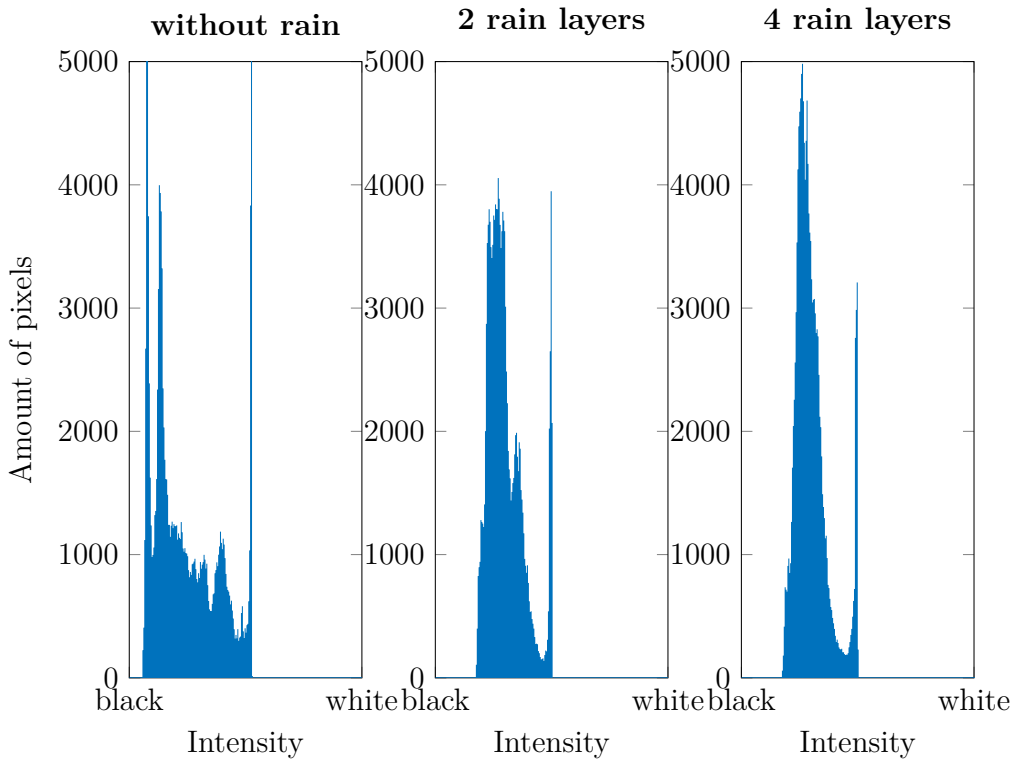

Fig. 6.3.: Histogram of images of a static EVT depending on the number of activated rain layers [77] © 2016 IEEE.

6.3. Conclusion

Sensor systems are based on electromagnetic waves which can be influenced by athmosperic disturbances like rain and fog based on multiple reflection, transmission and absorption of the signals. [77], [76], [78]

Consequently, this influences must be considered in the test of active pedestrian safety systems. A possible methodology for tests under reproducible and realistic rain influence was presented in [77] and applied to standard automotive radar, camera and lidar. The presented approach was adapted to reproducible fog influence and presented in [78] where it was also applied to standard automotive radar, camera and lidar. In order to adapt this approach to active pedestrian safety testing the artificial rain and fog setup can easily be integrated between the approaching vehicle and the pedestrian dummy and the test procedure can be repeated at different rain intensities. This enables the test of new detection algorithms under reproducible fog and rain conditions but also benchmark tests of different sensor system approaches.

7. Consideration of Natural Human Behaviour

7.1. Introduction

In Sec. 2.5.2 the crossing behaviour of pedestrians was defined as macroscopic motion and divided into three phases:

- Phase 1: Walking to the curb
- Phase 2: Waiting at the curb
- Phase 3: Crossing the street

Based on the macroscopic crossing pattern of phase 3 the pedestrian kinematics were defined as microscopic motion and analysed in detail in Ch. 3.

For the analysis specific groups of motion pattern were defined:

- Group 1 - Continuous motion pattern
- Group 2 - Gait transitions
- Group 3 - Direction transitions
- Group 4 - Combined transitions

The recorded human motion capture data was used as natural human input data for the 21D and 10D Pedestrian Dummy Device presented in Ch. 4 and Ch. 5. Based on the recorded motion capture data tests with natural human motion sequences can be performed, as shown in Sec. 5.5.

However, for further research on natural human crossing behaviour in a defined and safe environment, as well as for the research on pedestrian risk acceptance and

pedestrian to vehicle interaction a further tool, similar to a driving simulator but from the pedestrian perspective is required. In the following, the technical design of this tool, defined as Pedestrian Simulator, is presented.

The Pedestrian Simulator enables a test subject to enter a virtual traffic environment as a virtual pedestrian. Hereby, all motion capture data can be recorded using the same human motion capture system as used in Ch. 3. The recorded motion data can then be used for the analysis of pedestrian crossing behaviour and result in a selection of specific scenarios for real vehicle tests. Furthermore, in this selection of real vehicle tests, the motion capture data which was recorded while using the Pedestrian Simulator, could be used as base for the control of the Pedestrian Dummy Device.

While other Pedestrian Simulators, as for example [79], are often based on optical markers, which usually require a fixed installation inside a laboratory, the technical approach presented in this chapter is based on the Xsens human motion capture system, using small and leightweight intertial sensors. This system requires no fixed installation, is easy to transport and set up and calibrated within a few minutes. With regard to that, the motion area of a test subject can be moved very easily and expanded to the required space, depending on the virtual test scenario. Furthermore, the approach can be used indoor and outdoor.

Consequently, the Pedestrian Simulator represents a tool which enables the research of pedestrian behaviour, risk acceptance and pedestrian to vehicle interaction, and will be integrated in the generalised active pedestrian safety test methodology, which will be presented in Ch. 8.

7.2. Technical Design

The technical concept of the Pedestrian Simulator is based on the combination of virtual reality glasses, a small and leightweight human motion capture system and a virtual traffic environment and is illustrated in detail in Fig. 7.1.

17 small, leightweight and wireless Xsens motion capture trackers are applied to a human test subject. The motion capture sensors communicate synchronised and wireless with an output rate of 60 Hz with the motion capture base station (MVN Awinda). Based on a biomechanical model the current translational position ot the

test subject t_x, t_y, t_z is calculated and sent via User Datagram Protocol (UDP) to a developed C++ interface application. The head rotation of the test subject r_x, r_y, r_z is measured by the virtual reality glasses (Oculus Rift DK2) and also sent to the developed C++ interface application. Based on t_x, t_y, t_z and r_x, r_y, r_z a traffic object in IPG CarMaker is manipulated by Direct Variable Access (DVA). To this traffic object an IPG Movie camera perspective is fixed which is sent back as visual feedback to the test subject. This enables the test subject to move free in the virtual traffic environment as a pedestrian with direct visual feedback. This technical approach was implemented, tested and first published in [80].

The recorded crossing scenarios, respectively pedestrian motion capture data, can be saved in a pedestrian motion database. This data can be used for research on pedestrian crossing behaviour and risk acceptance and the extraction of relevant test scenarios. The corresponding natural human motion sequences can then be used as input data for the Pedestrian Dummy Device presented in Ch. 4 and Ch. 5.

A possible ego perspective of a test subject during a crossing scenario can be seen in Fig. 7.2. The test subject is standing on one side of the street while virtual friends of the test subjects are waiting on the other side of the street. In between them a traffic scenario with defined vehicle velocities and defined gaps between the vehicles is loaded. In Fig. 7.3 the same scenario can be seen from the bird view perspective. Hereby, the head of the test subject is visualised by a turquoise cube.

7.3. Conclusion

The presented technical approach of the Pedestrian Simulator opens a wide spectrum of new opportunities in pedestrian research and is suitable for

- research on pedestrian crossing behaviour,
- research on pedestrian risk acceptance, and
- research on pedestrian to vehicle interaction.

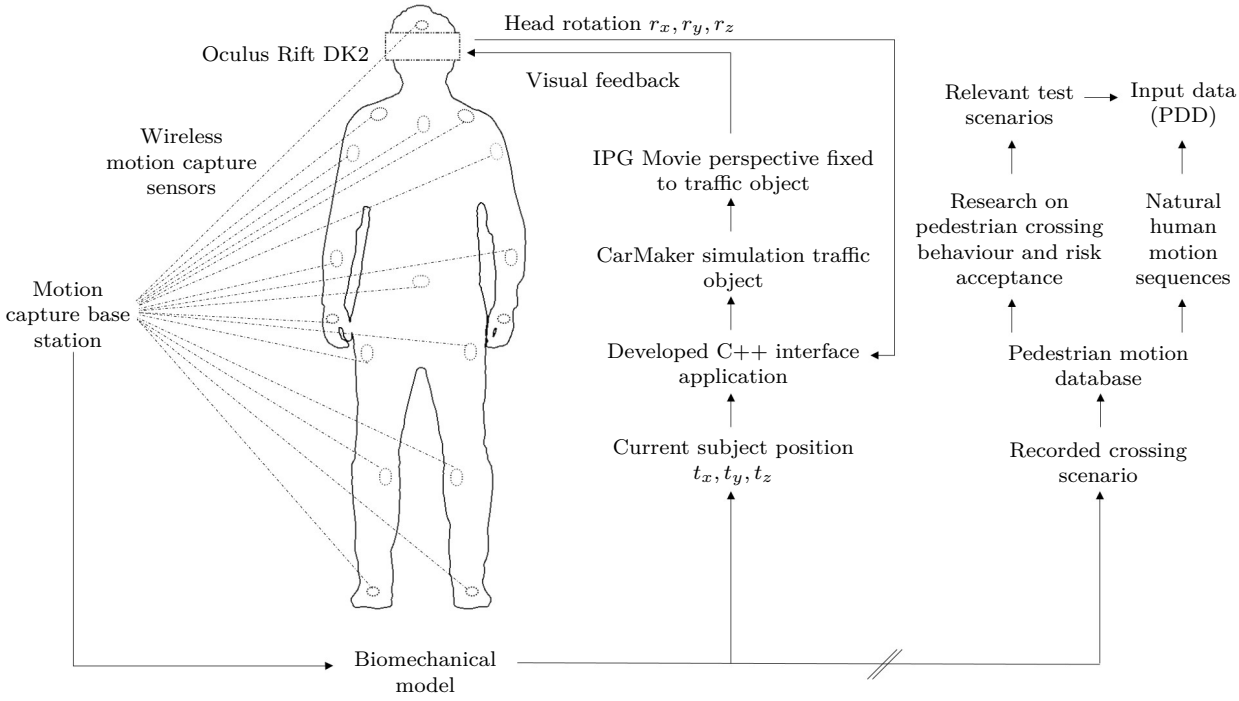

Fig. 7.1.: Technical design of the developed Pedestrian Simulator.

Furthermore, the recorded motion capture data can be used as input data for the PDD presented in Ch. 4 and Ch. 5.

Fig. 7.2.: Pedestrian Simulator ego perspective [80].

Fig. 7.3.: Birdview of the virtual scenario.

8. Generalised Active Pedestrian Safety Test Methodology

8.1. Introduction

Ch. 2 showed characteristic features of a pedestrian, like anthropometric measures and joint range of motion, crossing behaviour (macroscopic pedestrian motion) and relevant sensor characteristics. Ch. 3 focused on pedestrian kinematics (microscopic pedestrian motion) during continuous motion, gait transitions, direction transitions and combined transitions.

Ch. 4 showed the integration of those features to a test system approach based on a realistic articulated pedestrian dummy.

Ch. 5 optimised this approach and resulted in a novel pedestrian dummy focused on usability and robustness. Furthermore, it showed possibilities to consider a variation of the shape design and a technical approach for the replication and variation of thermal and radar signature.

Ch. 6 showed the influence of disturbances like rain and fog on automotive surround sensors and in Ch. 7 a novel technical approach for the research and consideration of natural human behaviour was introduced.

This chapter concentrates all these aspects of pedestrian safety testing in one combined general active pedestrian safety test methodology.

8.2. Active Pedestrian Safety Test Methodology

Fig. 8.1 illustrates the combination of the presented aspects of pedestrian safety testing in one generalised test methodology. In order to replicate the ADAS significant characteristics of the real world in a test setup the variation of three major parameters must be considered:

1. The variation of **Target characteristics**
2. The variation of **Environmental conditions**
3. The variation of **Driver behaviour**

The variation of the target characteristics can be achieved by replication and variation of natural human motion sequences, described in Ch. 3 and executed by an advanced pedestrian dummy, presented in Ch. 4 and Ch. 5. A variation of the shape of the target can be achieved as described in Sec. 5.3, while an approach for the variation of the sensor visibility of the target was presented in Sec. 5.4. Furthermore, the variation of natural human crossing behaviour, risk acceptance and interaction with approaching vehicles can be integrated based on research with the Pedestrian Simulator presented in Ch. 7.

The variation of environmental conditions can be achieved by consideration of athmosperic disturbances like rain and fog as can be seen in Ch. 6. Since [77] and [78] show that rain and fog can influence standard automotive sensors, like radar, lidar and camera, based on multiple reflection, transmission and absorption of the sensor signals, a reproducible and realistic variation of this influences should be considered during testing. In order to increase test efficiency, environmental disturbances could also be considered in virtual tests. However, this would require a realistic model of the multiple reflection, transmission and absorbtion effects of the sensor signals and consequently also a detailed model of the used sensor system and the implemented algorithms. For comparison of different approaches and for benchmark tests, however, the reproducible indoor test setup presented in [76], [77] and [78] is probably more suitable, since implemented algorithms are usually strictly confidential.

Furthermore, also the variation of light conditions, e.g. day or night, but also with fast changes, as they can appear in tunnel situations and also considering light directions, as for example when the sensor is blended by the sun or approaching traffic, must be considered during testing.

Test driven development and virtual variation of those parameters, can help to improve algorithms and individual systems, but requires realistic models of the athmospheric disturbances and light conditions, as well as a detailed model of the used sensors and the implemented algorithms. In regard of the test of real vehicles or vehicle prototypes, these two environmental aspects, athmosperic disturbances and light conditions, can be considered and tested inside a reproducible and defined indoor driving area.

Furthermore, also radar disturbances, like metal manhole covers or tram rails on the street can be replicated by aluminium foil on the test track and must be considered during testing.

In addition, also the variation of driver behaviour should be integrated in the test setup. Therefore, a range of driver reactions can be recorded in driving simulator studies and replicated by a driving robot during testing. Furthermore, also the variation of driver adaptive settings or parameters, as can be seen in [81], should be considered during testing.

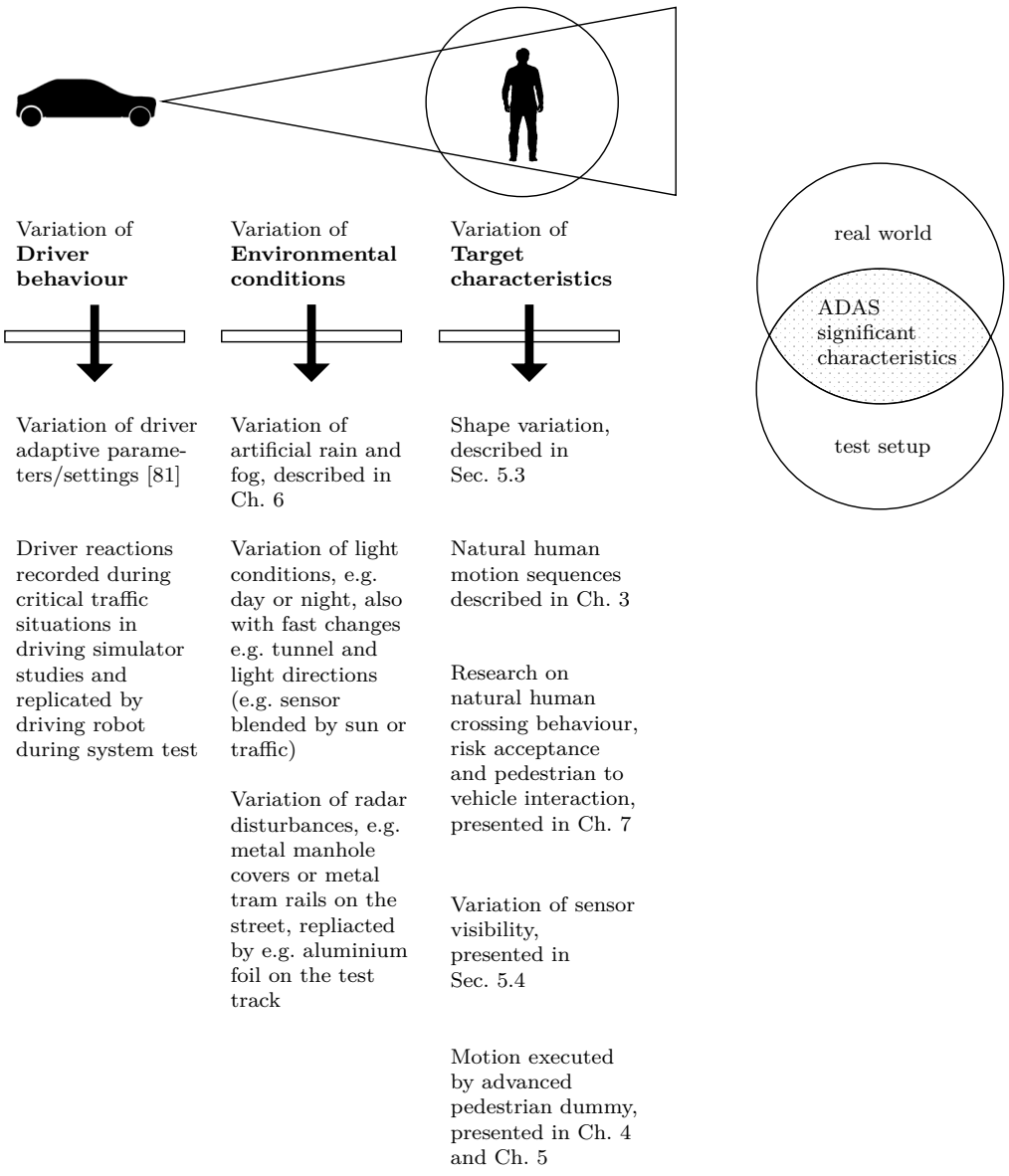

Fig. 8.1.: Generalised active pedestrian safety test methodology.

8.3. Conclusion

The various aspects of active pedestrian safety testing have been combined in a generalised active pedestrian safety test methodology and structured in three main parameters: the target characteristics, environmental conditions and driver behaviour. A variation of those parameters should be considered during testing, in order to replicate the real world in a test setup, focused on the ADAS significant characteristics.

The variation of the shape of the target can be achieved efficiently by 3D scanning and printing as presented in Sec. 5.3. This approach enables a fast and detailed replication of complex structures. Considering the key sensor systems presented in Table 2.1, also the thermal and radar signature must be considered. Therefore, Sec. 5.4 presented a novel technical concept for efficient thermal and radar signature variation of the target. This enables to increase and decrease the thermal and radar signature of the target between AEB tests, in order to test how the detection algorithm or sensor system reacts. Consideration of natural human motion sequences, like walking, running and direction or velocity transitions as described in Ch. 3 and executed by the Pedestrian Dummy Device presented in Ch. 4 and Ch. 5, enables a variation of the dynamically changing shape of the dummy based on pedestrian kinematics.

The developed Pedestrian Dummy Device enables the replication of complex human motion sequences, like velocity or direction changes, based on previously recorded human motion capture data. Furthermore, almost no metal components are used for the dummy, including the actuators, providing a low radar signature, which can based on the approach presented in Sec. 5.4 be stepwise increased during testing. Furthermore, the approach presented in Sec. 5.4 can be used to enable a variation of the thermal signature of the dummy. Enabling the test of advanced pedestrian detection algorithms, including path prediction algorithms considering pre-indicators and realistic pedestrian kinematics, the developed pedestrian dummy fullfills the requirements summarised in Ch. 2.

The influence of rain and fog on automotive surround sensors was shown in Ch. 6. Consequently, and based on [76], [77] and [78], a variation of these environmental disturbances should by considered by a reproducible indoor rain and fog setup during testing. Further external influences which must be considered are light conditions.

This means the consideration of day and night as well as tunnel effects with fast switches between light and dark. Additionally, the light direction should be considered since camera based sensors could be blended by sun or approaching vehicles. Considering radar sensor technology also disturbances based on radar reflective material on the road should be considered also on the test track.

In terms of non-fully autonomous vehicles also possible driver reactions during an activated AEB may influence the functionality. Consequently, also a variation of the driver reaction should be considered during testing and executed reproducible by a driving robot.

Fig. 8.1 summarises all these aspects of active pedestrian safety in one generalised active pedestrian safety test methodology.

9. Integrated Test Approach

9.1. Introduction

The number of tests which is resulting from the variation of target characteristics, environmental conditions and driver behaviour can only be handled efficiently by a combination of virtual tests and a reproducible indoor test setup.

Although the execution of single AEB tests takes usually only a few seconds to minutes, the preparation time, especially for non-standard tests, can become very time consuming. Furthermore, test equipment and time on test tracks is expensive and consequently only available in limited quantities.

Considering the variation of pedestrian crossing paths, pedestrian direction or velocity transitions, the variation of the shape and sensor visibility, the variation of light conditions and the variation of environmental disturbances like rain and fog, the variation of radar disturbances like metal tram rails on the street and the variation of the driver behaviour executed by a driving robot, the amount of tests for each software revision can not be handled only by full vehicle driving tests.

Virtual tests enable a fast and efficient variation of relevant parameters but are depending on the level of detail of the implemented models.

This chapter shows how test driven development of new detection algorithms considering a virtual variation of the relevant parameters in combination with AEB system tests in a reproducible indoor test environment can help to handle the challenges of autonomous driving.

9.2. Combination of Virtual and Indoor Tests

In Ch. 3 specific groups of pedestrian motion pattern were defined, where continuous motion like walking or running as well as velocity transitions, direction transitions and combined transitions were considered. The corresponding trajectories can be seen in Fig. 3.1.

Fig. 9.1 combines the resulting trajectories in one motion tree. This motion tree has a root, which is the inital position, a possible transition in the middle, which could be no transition, a velocity transition, a direction transition or a combined transition and five possible destinations. The circle represents standing in neutral position, the crossed circle represents a possible transition and the dashed lines represent walking and running.

Several motion trees can be attached to each other and combined to a more complex motion sequence. Hereby, each destination point becomes the root of another motion tree. Therefore, the root posture and destination posture must be identical, which in this case could be simple waiting in neutral position.

Fig. 9.2 shows a possible combination of two motion trees to each other. The gray circles show a possible trajectory. The lowest gray circle represents the first root, where the pedestrian stands in neutral position. Then the pedestrian starts walking or running followed by a 45° direction transition to the right and possible additional velocity transition from walking to running or running to walking. The first motion tree ends in neutral position, while the end of the first motion tree represents the root of the second motion tree. After a defined waiting time the pedestrian accelerates again from neutral standing to walking or running, continuing with the next 45° direction transition to the right and ending in neutral pose, while the end of the second motion tree corresponds to the possible root of another motion tree.

Based on this approach the motion sequences recorded in Ch. 3 can be used to automatically generate a wide range of pedestrian crossing scenarios in simulation. Automatic combination of motion trees and variation of the transition parameters helps to generate efficiently a wide range of virtual test scenarios. Furthermore, the initial position and initial direction relative to the virtual test track can be varied.

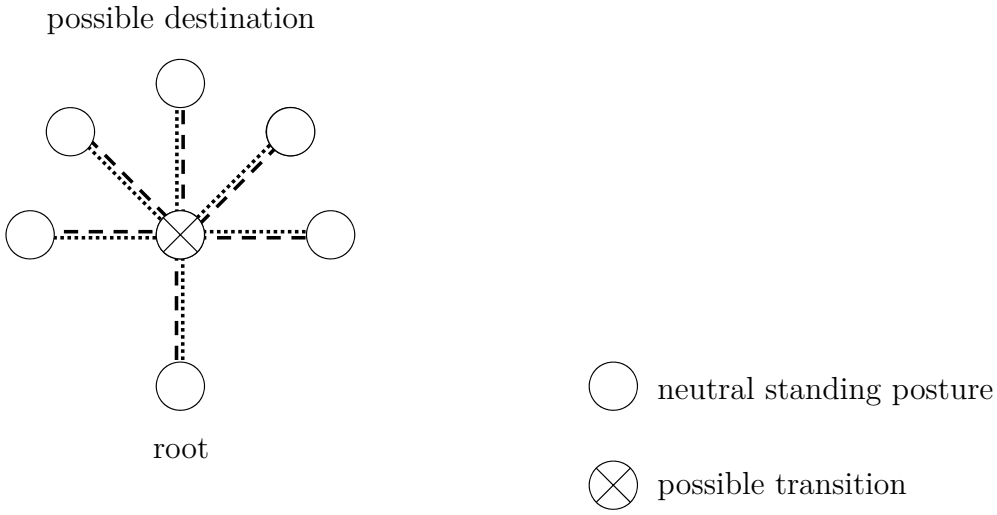

Fig. 9.1.: Combination of recorded motion capture trajectories to one motion tree.

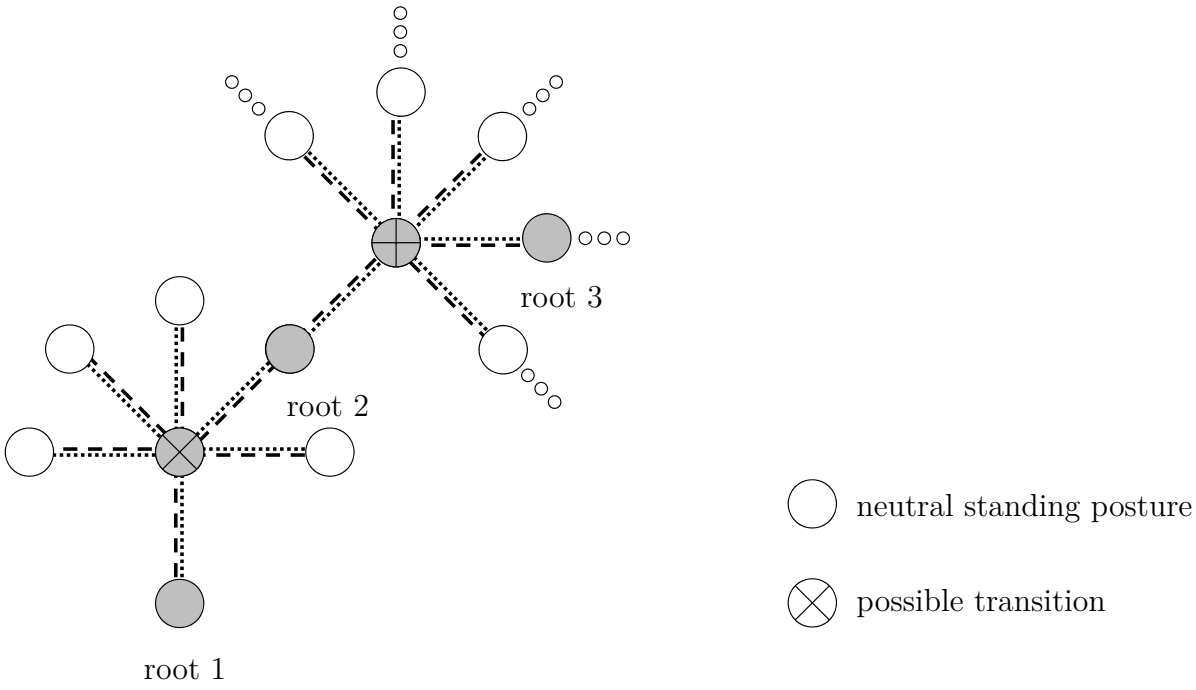

Fig. 9.2.: Possible combination of motion trees.

In Fig. 9.1 0°, 45° and 90° transitions were considered based on Ch. 3 and additionally mirrored to the right. This motion tree can of course be extended by recorded motion capture data of 135° transitions in both directions and also by an 180° turn, which can also be combined with a velocity transition. In Fig. 9.3 the gray coloured circles represent a composed trajectory of the extended motion tree. Starting with the first root in inital posture the pedestrian starts walking or running, changes direction by 135° to the right and stops at intital posture at the destination of the first motion tree which corresponds to the root of the second motion tree.

The extended motion tree consists of recorded motion capture data considering velocity and direction transitions in all possible combinations, covering 360° in 45° steps. By this approach a defined set of recorded motion capture data could be used to generate a wide range of virtual pedestrian crossing scenarios on a virtual test track. Beside the automatic variation of relevant parameters it also enables a test engineer to compose longer crossing sequences based on short motion capture data snippets.

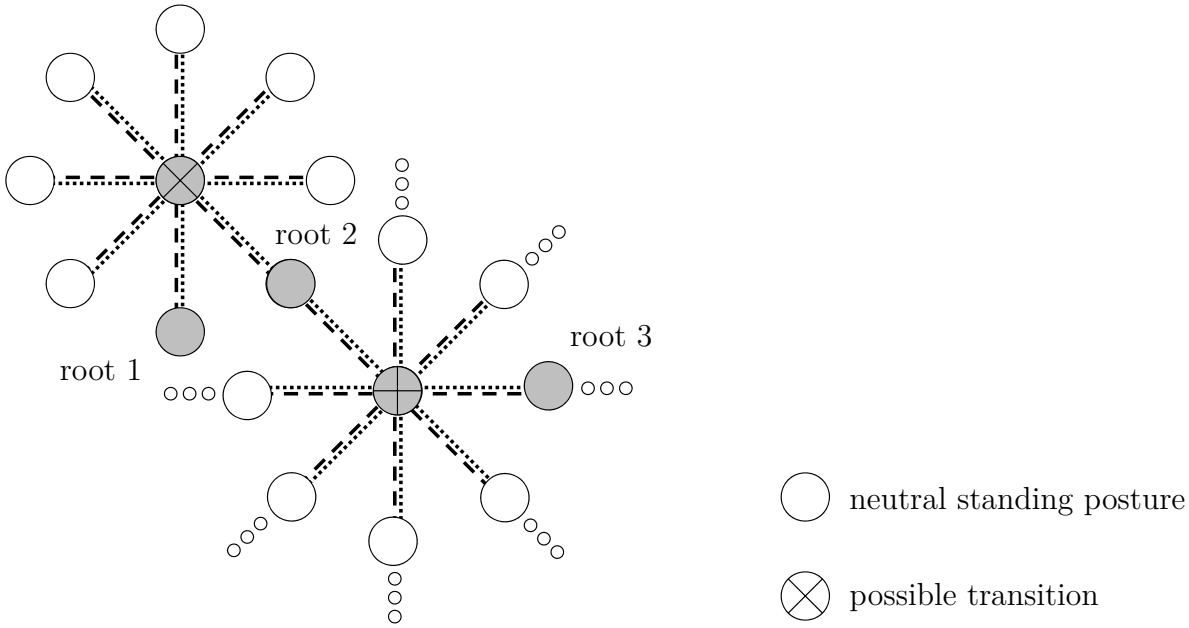

Fig. 9.3.: Combination of extended motion trees to a more complex motion sequence.

In Fig. 9.4 standing rotation motion capture snippets were added. This means in detail, that test subjects wearing the motion capture suite were ask to stand in neutral posture, then rotate a certain degree to another direction and stop the sequence again in neutral posture heading the new direction. Adding this new motion capture snippets to the motion tree, virtual pedestrians can rotate in standing position and then continue their motion with the root of another motion tree. This can be seen in Fig. 9.4 where the gray circles represent a possible trajectory. Hereby, the virtual pedestrian rotates after the first motion tree to the left and then continues with the second motion tree. After the second motion tree, the virtual pedestrian rotates again to the left and continues with the third motion tree.

Furthermore, also a variation of the path lenghts can be considered in the motion capture recordings, resulting in different sizes of motion trees, as can be seen in Fig. 9.5. In addition, also the waiting times in neutral standing posture can be varied.

This approach shows, how based on the variation of a comparable small amount of recorded motion capture snippets, a wide range of test scenarios can be generated in simulation. Applying this approach to a virtual test environment, a new pedestrian detection algorithm can be tested by a virtual vehicle driving in a round course through a virtual city, while virtual pedestrians cross the street based on a variation of recorded motion capture snippets.

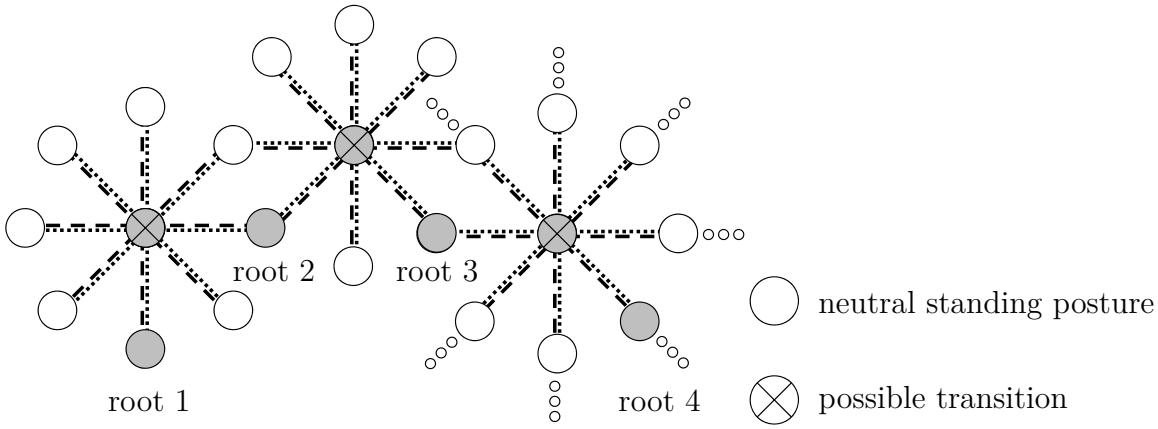

Fig. 9.4.: Combination of extended motion trees considering standing rotation.

This approach enables the time efficient design of new pedestrian test scenarios in simulation, either by automatic variation of parameters or by a test engineer designing a specific pedestrian crossing scenario. Further motion capture recordings like a waving pedestrian or recordings based on the Pedestrian Simulator presented in Ch. 7 can be used to extend the current database in future. In addition, researching crossing behaviour, risk acceptance and pedestrian to vehicle interaction with the Pedestrian Simulator, can be used as base for parameter variation in virtual testing.

Considering also a variation of the shape of the pedestrian, as for example the variation between an adult pedestrian and a child, and a variation of the sensor visibility, as for example the visibility of the clothing, it becomes clear that this amount of tests, especially considering more frequent software updates, can only be handled, when full vehicle test runs are supported by simulation.

Beside the variation of pedestrian crossing paths and the corresponding pedestrian kinematics, also the variation of further parameters, like environmental conditions and driver behaviour must be considered in simulation.

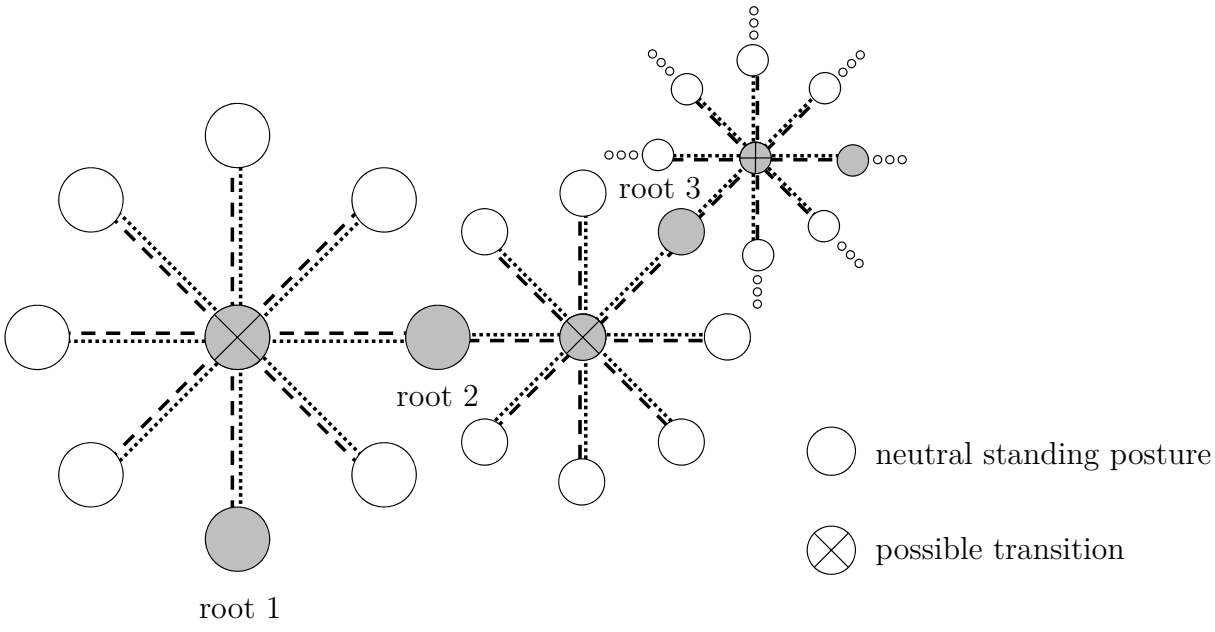

Fig. 9.5.: Combination of extended motion trees considering a variable path length of motion capture recordings and variation of waiting times.

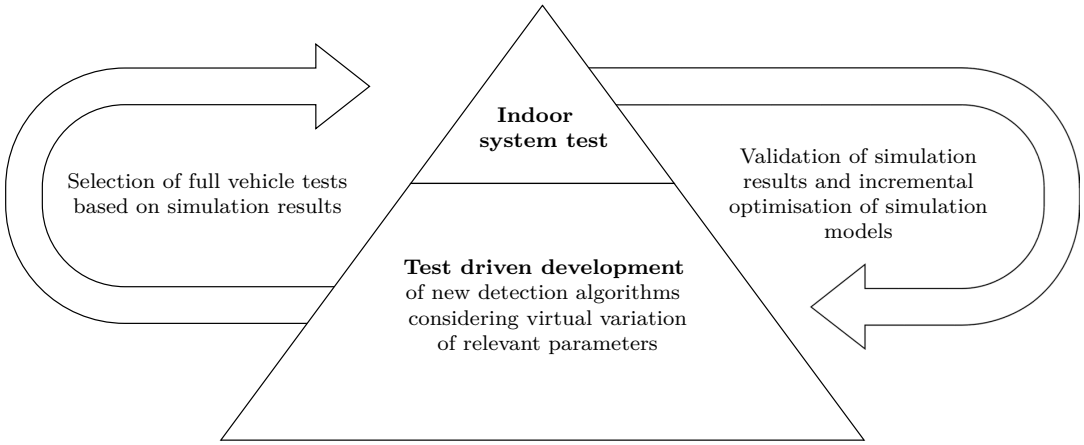

Fig. 9.6.: Combination of virtual variation of relevant parameters and reproducible full vehicle indoor tests.

Simulation, however, always depends on the degree of detail of the implemented models. In order to test the complete AEB system integrated in a real vehicle and also to validate simulation results, reproducible indoor driving tests are performed, as can be seen in Sec. 5.5.

A huge advantage of simulation is that it can be used for test driven development and the time-efficient virtual tests of a high number of scenarios considering a wide variation of relevant parameters. The disadvantage is that simulation is based on a simplified model of reality and the quality of the results always depends on the level of detail of the integrated models. Full vehicle tests, especially considering non-standard tests, usually require much preparation time. But combining both approaches with each other, virtual tests can help to find a selection of relevant test scenarios for full vehicle indoor tests, while the full vehicle indoor tests help to validate simulation results and incrementally optimise the used simulation models.

Based on test driven development of new detection algorithms and simulation considering virtual variation of relevant parameters, a selection of full vehicle test scenarios can be made. The results of these full vehicle tests performed in a defined and reproducible indoor test environment can be used to validate the corresponding simulation results and incrementally optimise the simulation models. In summary, test driven development, respective virtual testing considering the variation of relevant parameters and reproducible full vehicle indoor tests complement each other, as illustrated in Fig. 9.6.

9.3. Conclusion

In order to ensure robustness and reliability of active pedestrian safety systems, a variation of relevant parameters, summarised in Ch. 8, like target characteristics, environmental conditions and driver behaviour, must be considered in testing.

Virtual tests enable the efficient variation of parameters but simulation results always depend on the level of detail of the integrated models. Full vehicle indoor driving tests, as shown in Sec. 5.5, bring the test setup closer to the real world, but especially non-standard tests require much preparation time for each single test run.

Test driven development and simulation results considering virtual variation of relevant parameters, can help to find a selection of relevant test scenarios for full vehicle indoor driving tests. In return, the results of the full vehicle indoor driving tests can be used to validate simulation results and incrementally optimise simulation models.

Consequently, as can be seen in Fig. 9.6, the combination of virtual variation of relevant parameters and reproducible full vehicle indoor driving tests complement each other and can be used to test a wide range of test scenarios virtually, arrange based on the simulation results a set of full vehicle indoor driving tests, and optimise based on the full vehicle indoor driving tests the used models for simulation.

10. Conclusions and Recommendations for Further Work

10.1. Scientific Contributions

Sec. 2.5 summarises characteristic features of a pedestrian, like anthropometric measures, joint range of motion, sensor characteristics and pedestrian crossing behaviour (macroscopic motion).

Based on the macroscopic motion specific groups of motion pattern were defined in Ch. 3 and the corresponding pedestrian kinematics (microscopic motion) were researched using a human motion capture system. As can be seen in Fig. 3.1, the first group of motion pattern considers coninuous walking and continous running. The second group considers velocity transitions between standing, walking and running in all possible combinations. The third group considers direction transitions and the fourth group considers combined velocity and direction transitions. Based on the motion capture measurements it was shown that pedestrian kninematics and pre-indicators like the chest angle modification are significant pedestrian characteristics and can be used for pedestrian path prediction and consequently must also be considered in the test of advanced pedestrian detection systems. Furthermore, it was shown that current test systems have limited suitability for the test of advanced pedestrian detection algorithms, especially considering pre-indicators and pedestrian path prediction.

Ch. 4 presented a novel test system approach, considering the replication of macroscopic pedestrian motion by a positioning apparatus presented in Sec. 4.2 and the

replication of natural human motion by a novel Pedestrian Dummy Device presented in Sec. 4.3.

The 21D Pedestrian Dummy Device was realised as full scale prototype and can be seen in Fig. 4.13. The design of the novel positioning apparatus was patented in [63] and [64] and built by the project partner MESSRING Systembau MSG GmbH as a 1:10 scaled prototype.

The necessary degrees of freedom were presented and compared in Fig. 4.3 and resulted in the amount and position of joints of the Pedestrian Dummy Device. Hereby, the 21D Pedestrian Dummy Device was designed based on Fig. 4.3 (c) with 21 degrees of freedom, enabling also the replication of complex human motion pattern.

Furthermore, Table 4.1 showed the evaluation of different actuator concepts based on relevant criteria, which are a low amount of metal components, low weight, smoothness of motion, volume, dynamic of motion and controllability. Based on the low amount of metal components, the low weight, the smoothness and dynamic of motion, pneumatic artificial muscles (PAM) are most suitable for the actuation of an articulated pedestrian dummy, but require due to their nonlinear behaviour, hysteresis and memory effect an adequate PAM model and control concept. Based on the mechatronic setup and PAM model showed in Subsection 4.3.3, the preprocessing, real time control and successfull validation of the control concept was shown in Subsection 4.3.4. Although PAMs require more installation space than other actuators, the anthropometric measures of an average adult man provide enough volume for 42 PAMs in anthagonistic configuration actuating 21 degrees of freedom. This does not mean that the presented approach is only suitable for a Pedestrian Dummy Device representing adult men, since also PAMs with a smaller diameter are available which could be used in future work for the design of a Pedestrian Dummy Device with measures representing a female pedestrian or a child. The design of the novel pedestrian dummy can be seen in Fig. 4.12. A photo of the skeleton and muscle apparatus of the corresponding laboratory prototype can be seen in Fig. 4.13.

Based on the 21D Pedestrian Dummy Device it was shown that PAMs can be used as actuators for the replication of natural human motion sequences in a pedestrian dummy and that they fit within the average anthropometric measures of adult men. However, the 21D Pedestrian Dummy Device is a laboratory setup and should not be used on the vehicle test track. Therefore, a second version of the pedestrian dummy,

named 10D Pedestrian Dummy Device was designed. Focus of this second version was to increase usability and robustness of the system, and to prove its functionality in a real vehicle test. Since the 21D Pedestrian Dummy Device already proved that anthropometric measures provide enough space for 42 PAMs actuating 21 degrees of freedom, the degrees of freedom of the 10D Pedestrian Dummy Device were reduced to 10, providing a controlled motion of the upper legs, lower legs, upper arms, lower arms and head rotation, as can be seen in Fig. 4.3 (b), with one additional degree of freedom, which was integrated for the controlled chest angle modification.

In Ch. 5 the usability and robustness of the first prototype were improved by a modular design concept, resulting in the second version of the pedestrian dummy. The functionality of the 10D Pedestrian Dummy Device was proven by a full vehicle indoor AEB test. Since the positioning apparatus, which was presented in Sec. 4.2, is currently only available as 1:10 scaled prototype, the test was performed using an overrunable platform robot for the macroscopic motion of the 10D Pedestrian Dummy Device. However, the 10D Pedestrian Dummy Device is also compatible with possible future systems, as presented in [63] and [64]. In the test setup, the dummy was waiting in a side street for the approaching test vehicle, which was equipped with a driving robot. When the driving robot accelerated, a light barrier was activated, which gave the inital signal to the 10D Pedestrian Dummy Device and the overrunable platform robot, which was responsible for the macroscopic motion of the dummy. Right before the imminent collision the crash was avoided by automatic braking and steering. A photograph of the developed 10D Pedestrian Dummy Device right after the full vehicle AEB test can be seen in Fig. 5.10. A video of the full vehicle AEB test, which was recorded during the preparations of the final test, is available online: `https://youtu.be/eF5IkqsknBE`

Furthermore, in Ch. 5 a novel technical concept for thermal and radar signature variation was presented, which was patented in [75].

In Ch. 7 an approach for researching pedestrian crossing behaviour, risk acceptance and pedestrian to vehicle interaction, named Pedestrian Simulator, was presented. The technical approach allows a person to enter a virtual traffic environment as a pedestrian, while the persons behaviour is recorded by a human motion capture system. The motion capture data can be used for research on pedestrian crossing behaviour, for research on relevant test scenarios and also as input data for the Pedestrian Dummy Device presented in Ch. 4 and Ch. 5. Furthermore, also virtual

tests can be performed based on the Pedestrian Simulator. The technical design of the Pedestrian Simulator can be seen in Fig. 7.1.

Ch. 8 summarises the variation of target characteristics, the variation of environmental conditions and the variation of driver behaviour in a generalised active pedestrian safety test methodology. The variation of target characteristics includes the variation of the target shape, the variation of natural human motion sequences, the consideration and variation of pedestrian crossing behaviour and the variation of the sensor visibility of the target. The variation of environmental conditions includes the variation of artificial rain, fog and light conditions and the variation of radar disturbances. The consideration of driver behaviour includes the variation of driver adaptive parameters as well as the integration of driver reactions. The combination of the presented aspects is illustrated in Fig. 8.1, showing the generalised active pedestrian safety test methodology.

Ch. 9 shows the virtual variation of relevant parameters in combination with reproducible full vehicle indoor tests, complementing each other. As shown in Fig. 9.6 virtual tests can be used to handle a wide range of test scenarios considering virtual variation of target characteristics, environmental conditions and driver behaviour and furthermore also help to define a selection of full vehicle test scenarios. Reproducible full vehicle indoor tests can in return help to incrementally optimise the used simulation models.

Summary and conclusions:

1. Considering pedestrian path prediction, pre-indicators and the variation of test parameters, currently available test systems have limited suitability for the test of advanced pedestrian detection algorithms.

2. Pre-indicators, like the chest angle modification or the variation of the arm and leg frequency, are significant pedestrian characteristics for near future velocity and direction changes and must be considered in the test of autonomous emergency brake systems for pedestrians.

3. Pneumatic artificial muscles (PAM) are most suitable for the actuation of an articulated pedestrian dummy but require due to their nonlinear behaviour, hysteresis and memory effect an adequate PAM model and control concept.

4. The resulting 21D Pedestrian Dummy Device showed that the average measures of an adult man provide enough volume for 42 PAMs actuating 21 degrees

of freedom based on the biomechanical principle of tendons and muscles in antagonistic configuration.

5. Based on the first prototype an optimised 10D Pedestrian Dummy Device focused on usability and robustness was developed.

6. The 10D Pedestrian Dummy Device proved its functionality in a successfully performed full vehicle indoor AEB test.

7. Furthermore, an approach for researching pedestrian crossing behaviour, risk acceptance and pedestrian to vehicle interaction, named Pedestrian Simulator, was presented.

8. In order to ensure reliability and robustness of future pedestrian detection systems, a variation of relevant parameters must be considered during testing.

9. The variation of target characteristics, environmental conditions and driver behaviour was summarised in a generalised active pedestrian safety test methodology.

10. Virtual variation of relevant parameters can be used to define a selection of full vehicle test scenarios. In return, reproducible full vehicle indoor tests can help to incrementally optimise the used simulation models.

10.2. Recommendations for Further Work

The 10D Pedestrian Dummy Device, which was presented in Ch. 5, showed based on the modular concept, increased usability and robustness compared to the 21D Pedestrian Dummy Device presented in Ch. 4. Although the functionality of the 10D Pedestrian Dummy Device was shown in a full vehicle indoor AEB test, the crash ability of the 10D Pedestrian Dummy Device has not yet been evaluated. Therefore, in future work, the computer model of the 10D Pedestrian Dummy Device could be used to simulate the crash of individual components and the complete 10D Pedestrian Dummy Device at different vehicle velocities. Based on the simulation results, the design and crash ability of individual components could be further optimised. Furthermore, a future version of the dummy could be designed of lighter or elastic material.

The Pedestrian Simulator presented in Ch. 7 opens a wide spectrum of research possibilities in the area of pedestrian to vehicle interaction, providing a safe and reproducible environment for pedestrian behaviour studies.

Currently, the Pedestrian Simulator enables a person to enter the traffic simulation as a pedestrian while all motion capture data is recorded by a human motion capture system. The recorded motion capture data can then be used as input data for the Pedestrian Dummy Device, presented in Ch. 4 and Ch. 5, or as input data for virtual tests showed in Ch. 9. Currently no real time manipulation of the virtual pedestrian model based on a real time motion capture data stream of the Pedestrian Simulator is implemented. In future, real time manipulation of the virtual pedestrian could be used by a test engineer wearing the Pedestrian Simulator while interacting in the simulation environment with virtual vehicles and performing virtual real time autonomous emergency brake tests in a safe and reproducible environment, while all motion capture data and test results are recorded for documentation.

Furthermore, the virtual variation of pedestrian crossing paths, based on motion trees presented in Ch. 9, could be used in simulation to train camera based detection algorithms. Starting with a self training detection algorithm, integrated in a virtual vehicle driving in a traffic simulation, virtual pedestrians could cross the street, varying their crossing paths, shapes and clothing. In case of a non-detected pedestrian the simulation could inform the self training algorithm about the need for improvement and provide information about the pedestrian position in the camera image. But also in case of a detected pedestrian, the simulation could provide

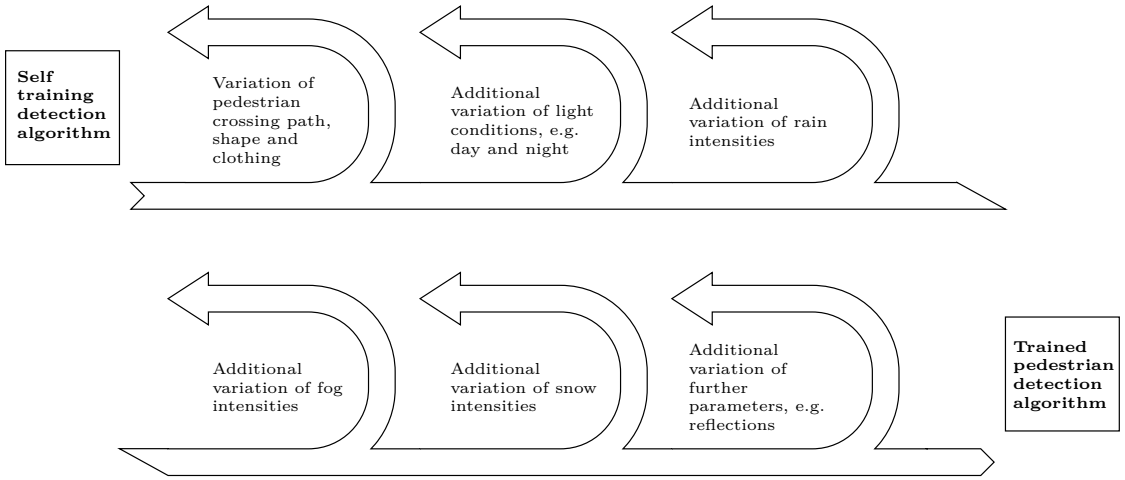

Fig. 10.1.: Self training algorithm in virtual AEB training considering variation of target characteristics and environmental conditions.

additional data for training, like the exact distance between the sensor and the pedestrian, the walking or running velocity and the walking or running direction. When the self training algorithm achieves a sufficient score, additional variation of light conditions could be added in simulation and the training process could be repeated. In the following optimisation cycles, additional variation of rain, fog and snow intensities, and also further parameters, like disturbing reflections, could be added in simulation. This approach requires a realistic graphical simulation of the traffic environment, including a realistic pedestrian model considering variation of the target characteristics and a realistic model of environmental disturbances like rain, fog and snow.

Fig. 10.1 illustrates the idea of virtual AEB training of a self training detection algorithm, resulting in a virtual trained pedestrian detection algorithm.

Focus of the self training algorithm, should be to result in a fast and reliable pedestrian detection under consideration of maximum possible code size. After virtual training and optimisation, the resulting pedestrian detection algorithms could be validated by recorded and labeled real camera data and subsequently tested in full vehicle indoor driving tests, using the 10D Pedestrian Dummy Device, shown in Ch. 5.

Appendix

A. List of IEEE Journal Publications

1. I. Doric, A. Reitberger, S. Wittmann, R. Harrison and T. Brandmeier, *A Novel Approach for the Test of Active Pedestrian Safety Systems*, in IEEE Transactions on Intelligent Transportation Systems, doi: 10.1109/TITS.2016.2606439, © 2017 IEEE

   URL: `http://ieeexplore.ieee.org/document/7581089/`

2. F. Muehlfeld, I. Doric, R. Ertlmeier and T. Brandmeier, *Statistical Behavior Modeling for Driver-Adaptive Precrash Systems*, in IEEE Transactions on Intelligent Transportation Systems, doi: 10.1109/TITS.2013.2267799, © 2013 IEEE

   URL: `http://ieeexplore.ieee.org/document/6553235/`

B. List of Conference Publications (Peer Reviewed)

1. I. Doric, A. Frison, P. Wintersberger, A. Riener, S. Wittmann, M. Zimmermann and T. Brandmeier, *A Novel Approach for Researching Crossing Behavior and Risk Acceptance: The Pedestrian Simulator*, in Adjunct Proceedings of the 8th International Conference on Automotive User Interfaces and Interactive Vehicular Applications (AutomotiveUI '16), 2016, Ann Arbor, USA. ACM Digital Library 978-1-4503-4654-2/16/10

   URL: `http://dl.acm.org/citation.cfm?doid=3004323.3004324`

2. S. Hasirlioglu, I. Doric, C. Lauerer and T. Brandmeier, *Modeling and simulation of rain for the test of automotive sensor systems*, in 2016 IEEE Intelligent Vehicles Symposium (IV), 2016, Gothenburg, Sweden.
   doi: 10.1109/TITS.2016.2606439, © 2016 IEEE

   URL: `http://ieeexplore.ieee.org/document/7535399/`

3. S. Hasirlioglu, A. Riener, and I. Doric, *Rain Simulation for the Test of Automotive Surround Sensors*, in Geophysical Research Abstracts Vol. 19, EGU2017-7951, EGU General Assembly, 23–28 April 2017, Vienna, Austria.

   URL: `http://meetingorganizer.copernicus.org/EGU2017/EGU2017-7951.pdf`

4. S. Hasirlioglu, A. Kamann, I. Doric and T. Brandmeier, *Test methodology for rain influence on automotive surround sensors*, in 2016 IEEE 19th International Conference on Intelligent Transportation Systems (ITSC), 2016, Rio de Janeiro, Brazil. doi: 10.1109/ITSC.2016.7795918, © 2016 IEEE

   URL: `http://ieeexplore.ieee.org/document/7795918/`

5. A. Kamann, S. Hasirlioglu, I. Doric, T. Speth, T. Brandmeier and U. Schwarz, *Test Methodology for Automotive Surround Sensors in Dynamic Driving Situations*, in 2017 IEEE 85th Vehicular Technology Conference (VTC), 2017, Sydney, Australia. © 2017 IEEE

6. S. Hasirlioglu, I. Doric, A. Kamann and A. Riener, *Reproducible Fog Simulation for Testing Automotive Surround Sensors*, in 2017 IEEE 85th Vehicular Technology Conference (VTC), 2017, Sydney, Australia.

7. T. Speth, I. Doric, H. Riedel, T. Brandmeier and U. Jumar, *Dynamic position calibration by road structure detection*, 2015 IEEE International Conference on Vehicular Electronics and Safety (ICVES), Yokohama, 2015.
doi:10.1109/ICVES.2015.7396902,

   URL: `http://ieeexplore.ieee.org/document/7396902/`

8. D. Böhmländer, I. Doric, E. Appel and T. Brandmeier, *Video camera and capacitive sensor data fusion for pedestrian protection systems*, 2013 Proceedings of the 11th Workshop on Intelligent Solutions in Embedded Systems (WISES), 2013, Pilsen, Czech Republic.

   URL: `http://ieeexplore.ieee.org/document/6664948/`

C. List of Conference Presentations

1. I. Doric and L. Wech, *Indoor Testing of active Systems*, CARHS PraxisConference Autonomous Emergency Braking, 28th - 29th September 2017, Ingolstadt, Germany

2. I. Doric, *Test of Active Pedestrian Safety Systems in Automated Vehicles*, 2017 WMG Doctoral Research and Innovation Conference, 28th June 2017, Coventry, England

3. I. Doric, *Test of Active Pedestrian Safety Systems*, Munich RE Motor Future Lab, 9.-11. May 2017, Munich, Germany

4. I. Doric and S. Hasirlioglu, *Artificial Rain, Fog, and Night - Indoor Active Safety Testing in CARISSMA*, CARHS SafetyWeek / SafetyUpdate, 16th - 17th May 2017, Aschaffenburg, Germany

5. I. Doric, *Pedestrian to Vehicle Interaction and the Virtual Test of Active Pedestrian Safety Systems*, Automated Driving Conference: Road Safety & the Human Factor, 8th - 9th March 2017, Kuratorium für Verkehrssicherheit (KFV), Vienna, Austria

6. I. Doric, *Test of active pedestrian safety systems in CARISSMA*, Automotive Test and Development Symposium, 31st May - 2nd June 2016, Stuttgart, Germany

7. I. Doric, T. Brandmeier, *Pedestrian Safety Research in CARISSMA*, TÜV SÜD crash.tech, 19th - 20th April 2016, Munich, Germany

8. I. Doric, *Dynamic pedestrian target for the test of active safety systems*, CARHS PraxisConference Autonomous Emergency Braking, 14th - 15th July 2015, Bicester, England

9. I. Doric, W. Rohleder, *Test of Active Pedestrian Safety Systems*, CARHS SafetyWeek / SafetyAssist, 19th - 21st May 2015, Aschaffenburg, Germany

D. List of Automotive Patents

1. I. Doric, T. Brandmeier, D. Arp, *Dummy und Vorrichtung sowie Verfahren zur Nachahmung menschlicher Thermo- und Radarsignatur*, DE102016124240.3
2. I. Doric, T. Speth, T. Brandmeier, H. Riedel, *Verfahren zum Betrieb eines Kraftfahrzeugs*, DE102016002232A1
3. I. Doric, T. Brandmeier, C. Lauerer, T. Speth, D. Arp, S. Zecha, M. Schulte, H. Riedel, *Vorrichtung zum Bewegen einer Verkehrsteilnehmer-Attrappe*, DE102015005471A1
4. I. Doric, T. Speth, T. Brandmeier, H. Riedel, *Ermitteln einer Relativposition eines Verkehrsobjekts bezüglich eines Kraftfahrzeugs*, DE102015014048B4
5. I. Doric, T. Brandmeier, C. Lauerer, T. Speth, D. Arp, H. Riedel, S. Zecha, M. Schulte, *Vorrichtung zum Test eines Systems zur Fußgängerdetektion und automatischen Kollisionsvermeidung*, DE102014002304B3
6. I. Doric, T. Brandmeier, T. Speth, H. Riedel, *Method for correcting position data and motor vehicle*, DE102013016435B4, EP000003052963A1, WO002015049044A1

References

[1] World Health Organization, "Global status report on road safety 2013: Supporting a decade of action," Geneva and Switzerland, 2013. [Online]. Available: www.who.int/iris/bitstream/10665/78256/1/9789241564564_eng.pdf 1

[2] D. Xu, X. Zhu, Q. Miao, Z. Ma, and B. Wu, "The research of reversible pop-up Hood for pedestrian protection," in *2010 IEEE International Conference on Vehicular Electronics and Safety (ICVES)*, 2010, pp. 42 –47. 1, 6

[3] C. M. Kang, Y. Son, Y. O. Lee, C. C. Chung, and S. H. Lee, "Collision prediction system for external airbag using an interacting multiple model estimation with multirate kalman filter," in *2012 12th International Conference on Control, Automation and Systems*, Oct 2012, pp. 878–882. 1, 6

[4] European Road Safety Observatory, DaCoTa, Traffic Safety Basic Facts 2012 - Pedestrians, Source: SafetyNet Accident Causation Database 2005 to 2008 / EC Date of query: 2010. 1

[5] "Test protocol - aeb vru systems, version 2.0," in *European New Car Assessment Programme (Euro NCAP)*, Mar March 2017. 2, 3

[6] "Articulated pedestrian target specifications," in *European Automobile Manufacturers Association*, Oct 2015. 3

[7] G. Bauer, R. D. Rasshofer, O. D. Scherf, and S. Zecha, "Evaluation unit for evaluating information related to creature i.e. pedestrian, in environment of car, has determination component determining future movement path of creature by considering recognized indicator," Patent DE102 007 052 093A1, 2007. 3, 12, 22, 24, 40

[8] X. Zhuang and C. Wu, "Modeling pedestrian crossing paths at unmarked roadways," *IEEE Transactions on Intelligent Transportation Systems*, vol. 14, no. 3, pp. 1438–1448, 2013. 3, 20, 22, 35

[9] S. Zecha, G. Jürgens, and P. Quittenbaum, "Innovative test methods and facilities for predictive pedestrian protection," in *The 23rd International Technical Conference on the Enhanced Safety of Vehicle (ESV)*, Seoul, 2013. 3

[10] I. Doric, A. Reitberger, S. Wittmann, R. Harrison, and T. Brandmeier, "A novel approach for the test of active pedestrian safety systems," *IEEE Transactions on Intelligent Transportation Systems*, vol. 18, no. 5, pp. 1299–1312, May 2017. 4, 8, 10, 16, 18, 19, 21, 26, 27, 31, 32, 33, 34, 37, 39, 41, 42, 44, 45, 48, 49, 52, 54

[11] "Traffic Safety Basic Facts 2016 - Seasonality." [Online]. Available: https://ec.europa.eu/transport/road_safety/sites/roadsafety/files/pdf/statistics/dacota/bfs2016_seasonality.pdf 6

[12] B. Wu, X. Zhu, D. Wang, Z. Ma, and J. Liu, "Research on design method regarding pedestrian head protection," in *2010 IEEE International Conference on Vehicular Electronics and Safety (ICVES)*, 2010, pp. 24 –29. 6

[13] I. Doric, T. Speth, T. Brandmeier, and H. Riedel, "Verfahren zum betrieb eines kraftfahrzeugs," Patent DE102 016 002 232A1, 2016. 7, 13

[14] M. Kühn, R. Fröming, and V. Schindler, *Fussgängerschutz: Unfallgeschehen, Fahrzeuggestaltung, Testverfahren*, ser. VDI-Buch. Berlin and New York: Springer, 2007. 9

[15] D. T. Linzmeier, M. Skutek, M. Mekhaiel, and K. C. J. Dietmayer, "A pedestrian detection system based on thermopile and radar sensor data fusion," in *2005 7th International Conference on Information Fusion*, vol. 2, July 2005, pp. 8 pp.–. 9

[16] T. Gandhi and M. M. Trivedi, "Pedestrian protection systems: Issues, survey, and challenges," *IEEE Transactions on Intelligent Transportation Systems*, vol. 8, no. 3, pp. 413–430, 2007. 9

[17] D. Gerónimo, A. M. López, A. D. Sappa, and T. Graf, "Survey of pedestrian detection for advanced driver assistance systems," *IEEE Transactions on Pattern Analysis and Machine Intelligence*, vol. 32, no. 7, pp. 1239–1258, 2010. 9, 11

[18] P. Lemmen, J. Stoll, U. Bergelt, P. Seiniger, M. Wisch, O. Bartels, Schubert, Eugen / Kunert, Martin, I. Knight, D. Brookes, M. Ranovona, T. Okawa, C. Domsch, and T. Schaller, "Evaluation of pedestrian targets used in aeb testing: A report from harmonistion platform 2 dealing with test equipment," in *The 23rd International Technical Conference on the Enhanced Safety of Vehicle (ESV)*, Seoul, 2013. 10, 41

[19] P. Lemmen, P. Seiniger, J. Stoll, T. Schaller, and E. Schubert, *ASPECSS D2.1: Test target specification document, including sensor response requirements*, 2012. 10, 14, 16

[20] T. Gandhi and M. M. Trivedi, "Pedestrian collision avoidance systems: a survey of computer vision based recent studies," in *2006 IEEE Intelligent Transportation Systems Conference*, Toronto, ON, Canada, pp. 976–981. 10

[21] B. Fardi, J. Dousa, G. Wanielik, B. Elias, and A. Barke, "Obstacle detection and pedestrian recognition using a 3d pmd camera," in *2006 IEEE Intelligent Vehicles Symposium*, Meguro-Ku, Japan, 13-15 June 2006, pp. 225–230. 10

[22] Y. Luo, J. Remillard, and D. Hoetzer, "Pedestrian detection in near-infrared night vision system," in *2010 IEEE Intelligent Vehicles Symposium (IV)*, La Jolla, CA, USA, pp. 51–58. 9

[23] E. F. Knott, J. Shaeffer, and M. Tuley, *Radar Cross Section, Second Edition.* Institution of Engineering and Technology, 2004. 9

[24] A. Bole, B. Dineley, and A. Wall, *Radar and ARPA Manual: Radar and Target Tracking for Professional Mariners, Yachtsmen and Users of Marine Radar*, second edition ed. Elsevier Science, 2005. 9, 23

[25] M. Enzweiler and D. Gavrila, "Monocular Pedestrian Detection: Survey and Experiments," *IEEE Transactions on Pattern Analysis and Machine Intelligence*, vol. 31, no. 12, pp. 2179 –2195, 2009. 9

[26] C. Keller, T. Dang, H. Fritz, A. Joos, C. Rabe, and D. Gavrila, "Active Pedestrian Safety by Automatic Braking and Evasive Steering," *IEEE Transactions on Intelligent Transportation Systems*, vol. 12, no. 4, pp. 1292 –1304, 2011. 11

[27] K. Doman, D. Deguchi, T. Takahashi, Y. Mekada, I. Ide, H. Murase, and Y. Tamatsu, "Estimation of traffic sign visibility considering temporal environmental

changes for smart driver assistance," in *2011 IEEE Intelligent Vehicles Symposium (IV)*, 2011, pp. 667 –672. 11

[28] H. Ritter and H. Rohling, Eds., *Pedestrian detection based on automotive radar: Radar Systems, 2007 IET International Conference on*, 2007. 11, 22

[29] M. Heuer, A. Al-Hamadi, M. Meinecke, and R. Mende, "Requirements on automotive radar systems for enhanced pedestrian protection," in *Radar Symposium (IRS), 2012 13th International*, 2012, pp. 45 –48. 11

[30] T. Gandhi and M. Trivedi, "Pedestrian collision avoidance systems: a survey of computer vision based recent studies," in *IEEE Intelligent Transportation Systems Conference, 2006. ITSC '06*, 2006, pp. 976 –981. 11

[31] K. Fuerstenberg, "Pedestrian protection using laserscanners," in *2005 IEEE Intelligent Transportation Systems, 2005. Proceedings*, 2005, pp. 437 – 442. 11

[32] R. O'Malley, M. Glavin, and E. Jones, "A review of automotive infrared pedestrian detection techniques," in *Signals and Systems Conference, 208. (ISSC 2008). IET Irish*, Jun. 2008, pp. 168 –173. 11

[33] J. Martinez-Carballido and M. Morales-Velazquez, "Using adaptive threshold to detect pedestrians crossing on a street for advanced driver assistance systems," in *Electrical Communications and Computers (CONIELECOMP), 2012 22nd International Conference on*, 2012, pp. 179–182. 11, 23, 40, 57

[34] I. Kallfass, "Remote detection of heart and breath rate," Fraunhofer Institute for Applied Solid State Physics, Annual Report, 2011. [Online]. Available: http://www.iaf.fraunhofer.de/content/dam/iaf/documents/geschaeftsfelder/Jahresbericht_AnnualReport_2011_MWC_Projekt4.pdf 12

[35] H. H. Tadjine, K. Schulze, R. Roellig, and H. Daniel, Eds., *New methods and tools for the development and verification of safety functions during development of pedestrian detection systems: Computing Technology and Information Management (ICCM), 2012 8th International Conference on*, vol. 1, 2012. 13

[36] S. Khastgir, S. Birrell, G. Dhadyalla, and P. Jennings, "Identifying a gap in existing validation methodologies for intelligent automotive systems: Introducing the 3xd simulator," in *2015 IEEE Intelligent Vehicles Symposium (IV)*, June 2015, pp. 648–653. 13

[37] "Fahrerassistenzsysteme - Notbremssystem mit Personenerkennung," ADAC, Tech. Rep. [Online]. Available: http://www.adac.de/infotestrat/tests/assistenzsysteme/fussgaengererkennung/default.aspx 14, 15

[38] M. Fritz, R. Holze, M.-M. Meinecke, H. Riedel, J. Ringswirth, and D. Vieth, "Driver assistance system's e.g. night-view system, functionality testing system for e.g. car, has dummy element movable for simulating real traffic situation on track and held in surrounding area detected by assistance system to test system," Patent DE102 007 035 474A1, 26.07.2007. 16

[39] M. G. Carpenter, M. T. Moury, J. R. Skvarce, M. Struck, T. D. Zwicky, and S. M. Kiger, "Objective tests for forward looking pedestrian crash avoidance/-mitigation systems," 2014. 16, 17

[40] H. W. Jürgens, *Erhebung anthropometrischer Maße zur Aktualisierung der DIN 33 402 - Teil 2*, ser. Schriftenreihe der Bundesanstalt für Arbeitsschutz und Arbeitsmedizin : Forschung. Bremerhaven: Wirtschaftsverl. NW, 2004, vol. 1023. 18

[41] M. Schuenke, *Thieme atlas of anatomy: General anatomy and musculoskeletal system : 1694 Illustrations, 100 Tables*. Stuttgart and New York: Thieme, op. 2010. 19

[42] D. R. Geruschat, S. E. Hassan, and K. A. Turano, "Gaze behavior while crossing complex intersections," *optometry and vision science*, vol. 80. 20

[43] D. Helbing, "A mathematical model for the behavior of pedestrians," *Behavioral Science*, vol. 36, no. 4, pp. 298–310, 1991. 20

[44] D. Helbing and P. Molnár, "Social force model for pedestrian dynamics," *Physical Review E*, vol. 51, no. 5, pp. 4282–4286, 1995. [Online]. Available: http://link.aps.org/doi/10.1103/PhysRevE.51.4282 20

[45] G. Antonini, "A discrete choice modeling framework for pedestrian walking behavior with application to human tracking in video sequences," Ph.D. dissertation, EPFL, 2005. [Online]. Available: http://infoscience.epfl.ch/record/55416 20

[46] G. Antonini, M. Bierlaire, and M. Weber, "Discrete choice models of pedestrian walking behavior," *Transportation Research Part B: Methodological*, vol. 40, no. 8, pp. 667–687, 2006. 20

[47] A. Makarenko, D. Krushinsky, and B. Goldengorin, *Anticipation and delocalization in cellular models of pedestrian traffic*, 2008. 20

[48] L. Yang, W. Fang, J. Li, R. Huang, and W. Fan, "Cellular automata pedestrian movement model considering human behavior," *Chinese Science Bulletin*, vol. 48, no. 16, pp. 1695–1699, 2003. [Online]. Available: http://dx.doi.org/10.1360/02ww0271 20

[49] C. Burstedde, K. Klauck, A. Schadschneider, and J. Zittartz, "Simulation of pedestrian dynamics using a two-dimensional cellular automaton," *Physica A: Statistical Mechanics and its Applications*, vol. 295, no. 3–4, pp. 507–525, 2001. [Online]. Available: http://www.sciencedirect.com/science/article/pii/S0378437101001418 20

[50] S. Chandra, R. Rastogi, and V. R. Das, "Descriptive and parametric analysis of pedestrian gap acceptance in mixed traffic conditions," *KSCE Journal of Civil Engineering*, vol. 18, no. 1, pp. 284–293, 2014. 20

[51] P. P. Koh and Y. D. Wong, "Gap acceptance of violators at signalised pedestrian crossings," *Accident Analysis & Prevention*, vol. 62, no. 0, pp. 178–185, 2014. [Online]. Available: http://www.sciencedirect.com/science/article/pii/S0001457513003746 20

[52] R. L. Moore, "Pedestrian choice and judgment," *Journal of the Operational Research Society*, vol. 4, no. 1, pp. 3–10, 1953. 20

[53] T. Wang, J. Wu, P. Zheng, and M. McDonald, "Study of pedestrians' gap acceptance behavior when they jaywalk outside crossing facilities," in *2010 13th International IEEE Conference on Intelligent Transportation Systems - (ITSC 2010)*, pp. 1295–1300. 20

[54] R. Knoblauch, M. Pietrucha, and M. Nitzburg, "Field studies of pedestrian walking speed and start-up time," *Transportation Research Record*, vol. 1538, no. 1, pp. 27–38, 1996. 21

[55] Kramers-de Quervain, Inès A, E. Stüssi, and A. Stacoff, "Ganganalyse beim gehen und laufen," *Schweiz Z. Sportmed. Sporttraum*, vol. 56, pp. 35–42, 2008. 21

[56] D. Chang, *National Pedestrian Crash Report*. Washington and D.C: U.S. Dept. of Transportation, National Highway Traffic Safety Administration, 2008. 21, 22

[57] R. A. Mann and J. Hagy, "Biomechanics of walking, running, and sprinting," *The American journal of sports medicine*, vol. 8, no. 5, pp. 345–350, 1980. 21

[58] V. T. Inman, H. J. Ralston, F. Todd, and J. C. Lieberman, *Human walking*. Baltimore: Williams & Wilkins, 1981. 26

[59] C. L. Vaughan, G. N. Murphy, and Du Toit, Leon L, *Biomechanics of human gait: An annotated bibliography*, 2nd ed. Champaign and Ill.: Human Kinetics Publishers, 1987. 26

[60] J. Peters, "Cable-controlled device," Patent WO002 001 077 571A1, 11.04.2001. 36

[61] "Spidercam." [Online]. Available: http://dev.spidercam.org/en/products 36

[62] T. Bleier and H. Riedel, "Vorrichtung zum bewegen eines prüfkörpers sowie verfahren zum prüfen oder charakterisieren von fahrerassisenzsystemen," Patent DE102 009 012 281B4, 09.03.2009. 36

[63] I. Doric, T. Brandmeier, C. Lauerer, T. Speth, D. Arp, S. Zecha, M. Schulte, and H. Riedel, "Vorrichtung zum test eines systems zur fußgängerdetektion und automatischen kollisionsvermeidung," Patent DE102 014 002 304B3, 2014. 36, 43, 53, 56, 67, 68, 95, 96

[64] ——, "Vorrichtung zum bewegen einer verkehrsteilnehmer-attrappe," Patent DE102 015 005 471A1, 2015. 36, 43, 56, 67, 68, 95, 96

[65] B. R. Umberger, "Effects of suppressing arm swing on kinematics, kinetics, and energetics of human walking," *Journal of biomechanics*, vol. 41, no. 11, pp. 2575–2580, 2008. 40

[66] C. J. Arellano and R. Kram, "The effects of step width and arm swing on energetic cost and lateral balance during running," *Journal of biomechanics*, vol. 44, no. 7, pp. 1291–1295, 2011. 40

[67] H. Yuasa, M. Nakanishi, and Mochida, Tsutomu, Yamada, Naoyuki, Nakai, Makoto, "Research into evaluation method for pedestrian pre-collision system," in *The 23rd International Technical Conference on the Enhanced Safety of Vehicle (ESV)*, Seoul, 2013. 41

[68] H. Janocha, *Actuators: Basics and applications*. Berlin and New York: Springer, 2004. 42

[69] P. I. Corke, *Robotics, vision and control: Fundamental algorithms in MATLAB*, ser. Springer tracts in advanced robotics. Berlin: Springer, ©2013, vol. v. 73. 44, 48

[70] L. Sciavicco and B. Siciliano, *Modelling and control of robot manipulators*, 2nd ed. London: Springer, 2004. 44

[71] Ching-Ping Chou and B. Hannaford, "Measurement and modeling of mckibben pneumatic artificial muscles," *IEEE Transactions on Robotics and Automation*, vol. 12, no. 1, pp. 90–102, 1996. 46, 47

[72] F. Daerden, "Conception and realization of pleated pneumatic artificial muscles and their use as compliant actuation elements," Ph.D. dissertation, Vrije Universiteit Brussel, Brüssel, 1999. 46

[73] F. Daerden and D. Lefeber, "The concept and design of pleated pneumatic artificial muscles," *International Journal of Fluid Power*, no. 2(3), pp. 41–50, 2001. 46

[74] B. Tondu, "Modelling of the mckibben artificial muscle: A review," *Journal of Intelligent Material Systems and Structures*, vol. 23, no. 3, pp. 225–253, 2012. 46

[75] I. Doric, T. Brandmeier, and D. Arp, "Dummy und vorrichtung sowie verfahren zur nachahmung menschlicher thermo- und radarsignatur," Patent DE102 016 124 240.3, 2016. 65, 66, 96

[76] S. Hasirlioglu, I. Doric, C. Lauerer, and T. Brandmeier, "Modeling and simulation of rain for the test of automotive sensor systems," in *2016 IEEE Intelligent Vehicles Symposium (IV)*, June 2016, pp. 286–291. 69, 70, 74, 81, 84

[77] S. Hasirlioglu, A. Kamann, I. Doric, and T. Brandmeier, "Test methodology for rain influence on automotive surround sensors," in *2016 IEEE 19th International Conference on Intelligent Transportation Systems (ITSC)*, Nov 2016, pp. 2242–2247. 69, 70, 71, 72, 73, 74, 81, 84

[78] S. Hasirlioglu, I. Doric, A. Kamann, and A. Riener, "Reproducible fog simulation for testing automotive surround sensors," in *2017 IEEE 85th Vehicular Technology Conference (VTC)*, June 2017. 69, 74, 81, 84

[79] C. Lehsing, I. Feldstein, and A. Dietrich, "Fußgängersimulation am lehrstuhl für ergonomie - bits und bytes lernen laufen," in *Ergonomie Aktuell*, vol. 16, 2015. 76

[80] I. Doric, A.-K. Frison, P. Wintersberger, A. Riener, S. Wittmann, M. Zimmermann, and T. Brandmeier, "A novel approach for researching crossing behavior and risk acceptance: The pedestrian simulator," in *Adjunct Proceedings of the 8th International Conference on Automotive User Interfaces and Interactive Vehicular Applications*, ser. AutomotiveUI '16 Adjunct. New York, NY, USA: ACM, 2016, pp. 39–44. [Online]. Available: http://doi.acm.org/10.1145/3004323.3004324 77, 79

[81] F. Muehlfeld, I. Doric, R. Ertlmeier, and T. Brandmeier, "Statistical behavior modeling for driver-adaptive precrash systems," *IEEE Transactions on Intelligent Transportation Systems*, vol. 14, no. 4, pp. 1764–1772, Dec 2013. 82, 83